

**Identification of regulators modulating ECM
expression
and their downstream effects on aging in
*C. elegans***

A thesis submitted to attain the degree of
DOCTOR OF SCIENCES of ETH ZURICH
(Dr. sc. ETH Zurich)

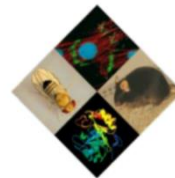
presented by

Alina Carolin Teuscher

M.Sc. in Biology, University of Cologne, Germany
born 09.06.1991 in Bergisch Gladbach, DE

DHEST
Department of Health Sciences and Technology

ITM Institute of
Translational
Medicine



uzh | eth | zürich
Zurich Ph.D. Program
in Molecular Life Sciences

Prof. Dr. Collin Y. Ewald
Prof. Dr. Katrien De Bock
Prof. Dr. Alex Hajnal
Prof. Dr. Michael Raghunath
Chair: Prof. Dr. Dr. Viola Vogel

22.03.2021

To my family:
Ina Volpp, Ulrich Teuscher and Nils Teuscher

and all the kind hearts in science

“A straight line may be the shortest distance between two points, but it is by no means the most interesting.”

- Robert Holmes, Doctor Who

Acknowledgment

First of all, I thank my supervisor Prof. Dr. Collin Y. Ewald. He provided me with this project and introduced me to Switzerland. Through all the difficulties, but I am immensely proud how we steered the project to a successful finish. Thank you!

Next, I thank my committee Prof. Dr. Alex Hajnal and Prof. Dr. Michael Raghunath for their scientific input and open discussions over the last 4 years. Prof. Dr. Katrien De Bock for helping me bringing this project over the finish line and Prof. Dr. Viola Vogel for being the chair of my defense.

I cannot express enough how grateful I am that I could be part of the “fantastic four” of the Ewald lab PhD students. I did not only find great colleagues, but also fantastic friends that helped me also through difficult times. Therefore, I want to thank Cyril Statzer for being such a positive force that motivated me to push my boundaries, but also for being ready to carry me down mountains if needed. Eline Jongsma, my du(t)chess, for listening, caring and showing me puppy pictures whenever I needed it. Richard Venz for his critical input, strong support and for creating wonderful worlds, in which I could escape from lab life and plunge into medieval quests. I want to thank my fellow Cologne expat Jasmin Mantl for keeping the lab running, being a great friend and horse-riding buddy. I am also grateful to Desirée Dürr for supporting me by organizing the lab. Dr. Anita Goyala for the long talks about science and her wisdom about life in academia. And all my students I had the privilege to supervise throughout the years: Andrea Thurnheer, Vira Chea, Mariam Baghdady, Katharina Tarnutzer and Kieran Toms. Thank you, for doing an amazing job helping me to push forward the screening project.

Our lab is located in a small ETH building far away from the two main campuses. The more remote the more important good neighbors are. Therefore, I want to thank all the groups in the SLA building that helped me and the group by providing us with access to machines, their scientific input and their good spirit especially during the Corona time. I would like to mention specifically our direct neighbors, the Ristow lab: I want to thank you for a fantastic time, your patience with such a young lab, your scientific input in and outside our lab meetings and the great coffee! Thank you, Meenakshi Ravichandran, Doris Pöhlmann and Beate Laube for listening and for providing such great scientifically and personal support. Thank you, Giovanna Grigolon for being one of my first flat mates in Switzerland.

Thanks also goes to the facility management that was always ready to help with input to fix freezers, microscopes, climate systems or with administrative problems!

I also thank the group of Alex Hajnal at UZH for their scientific input and for providing help with the RNAi clones and sending us important *C. elegans* strains for my research. Here, I would like to mention especially Dr. Michael Walser and Michael Daube. The Werner and Bordoli

groups for helping me establishing the Herovici staining in *C. elegans*, particularly I want to thank Salome Brütsch, Sophia Pantasis and the fantastic Hayley Hiebert. I also want to thank the MLS graduate school from UZH and ETH. I had a great time in this graduate school meeting a lot of different students and always feel supported.

Furthermore, I would like to mention my great collaborators: For their input and encouragement in the Matrisome project I would like to thank Prof. Alexandra Naba (UIC) and Dr. Jan Gebauer (University of Cologne). For his expertise and help in the computational analysis of my collagen turnover experiments I want to thank Prof. Dr. Orcun Goksel (ETH Zurich, University of Uppsalla). I thank Dr. Jeliaskov Jeliasko for his help in programming a R script that could remove the *C. elegans* autofluorescence and allowed me to measure the GFP signal in isolation.

I had the great luck to be spotted by Dr. Nina Ripin after the ETH introduction day: she introduced me to AVETH and especially the AVETH Counseling Team. You guys are fantastic and are doing such an amazing job helping students! It was an honor to be part of the team and doing my bit to help. Of this highly dedicated people, I want to especially thank again, Dr. Nina Ripin, but also Florentine Veenstra, Anne Jomard, Linda Wehner, Michael Ferguson and Dr. Betty Friedrich-Grube.

For their help escaping so many rooms that I struggle to remember and their friendship during my time here in Switzerland, I also want to thank Nathalie Vonrüti, Nadine Peneder und Janine Burren. I would also like to thank all my study friends for their advice, personal and scientifically during my doctorate studies. Thank you, Leona Bergheim (thank you for listening to me for hours and for taking me with you on your travels), Matthias Uthoff (the Anubis high priest), Tobias Romankiewicz (where is my picture?), Jessica Pietsch and Christian Burberg (we still have to write our book).

Another special person is my old school friend Annika Jahns, my Holmson. I met her relatively late during my school time, but we immediately became partners in crime, until this day. Like Leona, she is a fantastic travel buddy and a fantastic emotional support. With her I can talk the whole day, without it ever getting boring. I hope we will never stop solving crimes and riddles together! Oh Organoon...

At last I would like to mention the people that I have the fortune, not only to know since the first day of my life, but to also be loved by them: my mother Ina Volpp, my father Ulrich Teuscher and my dear brother Nils Teuscher. Thank you, for bearing such a stubborn daughter and sister, for saving me from drowning in swimming pools, or near death by falling from slides and that you always encouraged my curiosity! Thank you, I love you!

Summary

Aging is defined by the decline of molecular and cellular functions and the accumulation of cellular damage over time. Genetic and environmental influences can extend the lifespan by activating protective mechanisms to prevent or repair cellular damage. A key signature of aging is the decline in the biosynthesis of extracellular matrix (ECM) proteins, the accumulation of damage and crosslinking of ECMs. During development, ECMs are dynamic, but whether ECMs are still remodeled during life is still unknown, as well as the importance of ECM integrity for healthy aging. Previous studies have shown that longevity interventions are upregulating ECM proteins. Furthermore, some cuticular collagens in the model organism *C. elegans* are sufficient to increase the lifespan and are required for full lifespan extension in long-lived animals. However, the detailed mechanism remains unknown.

To investigate this question, I had to deal with several challenges.

- 1) To examine the ECM in *C. elegans*, we needed to know which proteins form, are localized in, and remodel the ECM. We quickly realized that such a list was not available. Therefore, we joined forces with Alexandra Naba (UCI) and Jan Gebauer (University of Cologne) to define the *in-silico* *C. elegans* matrisome. The matrisome is a compendium of all proteins that are part of the extracellular matrix or contribute to it. We found that 719 (~4%) genes of the *C. elegans* genome encode for matrisome proteins, including 181 collagens, 35 glycoproteins, 10 proteoglycans, and 493 matrisome-associated proteins. 173 out of the 181 collagens are nematodes specific and are predicted to encode cuticular collagens. In our paper, we also propose a new classification of these cuticular collagens, which is accessible in a novel database of all *C. elegans* collagens (CeCoIDB), and developed an automated annotation tool to identify ECM components in large datasets (Teuscher et al., 2019a).
- 2) Next, I faced the problem that the signal from weakly expressed GFP fusion proteins, such as collagen tagged with GFP, is masked in *C. elegans* by autofluorescence emitted from the intestinal lysosome-related gut granules that accumulate with aging. To solve this problem, we came up with a novel triple-band GFP filter setup that separates the GFP signal from autofluorescence, displaying GFP in green and autofluorescence in yellow. We described and tested the setup in a method paper (Teuscher and Ewald, 2018).
- 3) In our next paper, we extended the toolbox to examine collagen deposition during aging. We adapted two methods to assess collagen levels in *Caenorhabditis elegans*.

We present a method to determine the concentration of hydroxyproline as a substitute measurement for collagen, as it is highly enriched in collagens. The other method we established in *C. elegans*, the polychrome Herovici's staining, is useful to visualize collagen structures and potential collagen turnovers (Teuscher et al., 2019a).

- 4) Finally, in the experimental chapter, we employ all these novel developed tools and methods to examine the role of the ECM during aging and search for regulators. We systematically examined the ECM composition of *C. elegans in-vivo* during development and aging. We observed that the abundance of cuticular collagens progressively declines during aging, but that they were replenished or stabilized by longevity-promoting interventions, while basement membrane components stayed stable or increased during aging. We performed a targeted RNAi screen for regulators of cuticular collagen during aging. In this screen, we found that most molecular components that connect the muscles via integrins to the basement membrane and the hemidesmosome—like structures that anchor the basement membrane through the hypodermis to the cuticular exoskeleton are involved in collagen regulation. We demonstrated a potential age-dependent dissociation of integrins with basement membrane-localized collagen and perlecan, a proteoglycan known to bind to and crosslinks many extracellular matrix components, leading to an uncoupling of mechanotransduction. Thus, mechanical coupling to cells across tissues is important to promote cuticular collagen expression, which was previously shown to increase the lifespan of *C. elegans*.

Taken together, we present evidence that the ECM composition of two major ECM (basement membrane and cuticle) of *C. elegans* behave differently during aging, but that their dynamic composition is linked in part via a mechanotransduction system, and we shine a light on the importance of mechanotransduction for longevity.

Zusammenfassung

Altern wird durch den Abbau der molekularen und zellulären Funktionen und die Anhäufung von Zellschäden im Laufe der Zeit definiert. Genetische und Umwelteinflüsse können die Lebensdauer durch die Aktivierung von Schutzmechanismen verlängern, indem sie Zellschäden verhindern oder reparieren. Ein Hauptmerkmal des Alterns ist der Rückgang der Biosynthese von Proteinen der extrazellulären Matrix (ECM) zusammen mit der Anhäufung von Schäden und der Vernetzung von ECMs. Während der Entwicklung sind ECMs dynamisch, aber ob ECMs über die Lebensdauer hinweg weiterhin umgebaut werden, ist ebenso wie die Bedeutung der ECM-Integrität für das gesunde Altern noch unbekannt. Frühere Studien haben gezeigt, dass Langlebigkeitsinterventionen ECM-Proteine hochregulieren. Im Modellorganismus *C. elegans* reichen einige cuticuläre Kollagene bereits aus, um die Lebensdauer der Tiere zu verlängern. Dieselben Kollagene waren notwendig, um die vollständige Verlängerung der Lebensdauer von langlebigen Tieren zu erreichen. Der genaue Mechanismus, wie diese Kollagene zur Lebensverlängerung beitragen, blieb jedoch unbekannt.

Um die Frage nach einem potenziellen Mechanismus zu untersuchen zu können, musste ich mich mehreren Herausforderungen stellen.

- 1) Um die ECM in *C. elegans* zu untersuchen, mussten wir wissen, welche Proteine tatsächlich die ECM bilden, in ihr lokalisiert sind oder zu ihrem Umbau beitragen. Wir haben schnell festgestellt, dass es eine solche Liste bisher nicht gibt. Deshalb haben wir uns mit Alexandra Naba (UCI) und Jan Gebauer (Universität zu Köln) zusammengetan, um das *in-silico* *C. elegans*-Matrisom zu definieren. Das Matrisom ist eine Zusammenstellung aller Proteine, die Teil der extrazellulären Matrix sind oder zu ihr beitragen. Wir fanden heraus, dass 719 (~ 4%) Gene des *C. elegans*-Genoms für Matrisom-Proteine kodieren, darunter 181 Kollagene, 35 Glykoproteine, 10 Proteoglycane und 493 Matrisom-assoziierte Proteine. 173 der 181 Kollagene sind Nematoden-spezifisch und codieren für prognostizierte cuticuläre Kollagene. In unserer Arbeit schlagen wir auch eine neue Klassifizierung dieser cuticulären Kollagene vor, die in einer neuartigen Datenbank aller *C. elegans*-Kollagene (CeCoIDB) verfügbar ist. Ausserdem wurde in der Veröffentlichung ein automatisiertes Annotationstool zur Identifizierung von ECM-Komponenten in großen Datensätzen entwickelt (Teuscher et al., 2019a).

-
- 2) Als nächstes stand ich vor dem Problem, dass das Signal von schwach exprimierten GFP-Fusionsproteinen, wie unseren GFP markierten Kollagenen, in *C. elegans* durch Autofluoreszenz leicht überstrahlt wird. Die zu den Darm-Lysosomen zugehörigen Darmkörner emittieren diese Fluoreszenz, die mit zunehmendem Alter stärker wird. Um dieses Problem zu lösen, haben wir ein neuartiges Triple-Band-GFP-Filterset zusammengestellt, das das GFP-Signal von der Autofluoreszenz trennt und GFP in Grün und Autofluoreszenz in Gelb anzeigt. Wir haben den Aufbau in einem Methodenpapier beschrieben und getestet (Teuscher und Ewald, 2018).

 - 3) In unserem nächsten Artikel haben wir unsere Methodensammlung erweitert, um die Kollagenablagerungen während des Alterns zu untersuchen. Wir haben zwei Methoden für unsere Zwecke angepasst, um das Kollagenniveau bei *Caenorhabditis elegans* zu bestimmen. Zum einen präsentieren wir eine Methode zur Bestimmung der Hydroxyprolinkonzentration als Ersatzmessung für Kollagen, da es stark in Kollagenen angereichert ist. Zum anderen haben wir neu für *C. elegans* die Methode der polychromen Herovici-Färbung eingeführt. Sie ist nützlich, um Kollagenstrukturen und mögliche Kollagenumsätze sichtbar zu machen (Teuscher et al., 2019a).

 - 4) Schließlich verwenden wir im letzten, experimentellen Kapitel all diese neu entwickelten Werkzeuge und Methoden, um die Rolle der ECM während des Alterns zu untersuchen und nach Regulatoren der ECM zu suchen. Dafür haben wir zunächst systematisch *in-vivo* die ECM-Zusammensetzung von *C. elegans* während der Entwicklung und des Alterns untersucht. Wir beobachteten, dass die Häufigkeit von cutikulären Kollagenen während des Alterns abnimmt, diese jedoch durch langlebigkeitsfördernde Maßnahmen wieder aufgefüllt oder stabilisiert wurden. Die Basalmembran-Komponenten blieben währenddessen auch im Alter stabil oder nahmen sogar von der Menge her zu. Anschliessend führten wir ein gezieltes RNAi-Screening auf Regulatoren cutikulärer Kollagens während des Alterns durch. In diesem Screen fanden wir heraus, dass die meisten molekularen Komponenten, die an der Kollagenregulation beteiligt sind, diejenigen sind, die die Muskeln über Integrine mit der Basalmembran sowie die Basalmembran über die Hypodermis mit dem cutikulären Exoskelett verankern. Wir konnten zeigen, dass wahrscheinlich eine altersabhängige Dissoziation von Integrinen mit sich in der Basalmembran befindlichem Kollagen und Perlecan stattfindet. Perlecan ist ein Proteoglycan, von dem bekannt ist, dass es an viele extrazelluläre Matrixkomponenten bindet und diese vernetzt. Unser Experiment zeigt, wie diese wahrscheinliche Dissoziation zu einer Entkopplung der

Mechanotransduktion führt. Diese mechanische Kopplung von Zellen über Gewebe hinweg ist wichtig, um die cutikuläre Kollagenexpression zu fördern, von der zuvor gezeigt wurde, dass sie die Lebensdauer von *C. elegans* verlängert.

Zusammengefasst legen wir Beweise dafür vor, dass sich die ECM-Zusammensetzung von zwei Haupt-ECMs (Basalmembran und Cuticula) von *C. elegans* während des Alterns unterschiedlich verhält und dass ihre dynamische Zusammensetzung teilweise über ein Mechanotransduktionssystem verbunden ist, was neues Licht auf die Bedeutung von Mechanotransduktion für Langlebigkeit wirft.

Contents

1. Introduction.....	11
1.1. Aging	11
1.2. The extracellular matrix	12
1.3. The model organism <i>C. elegans</i>	12
1.4. Matrisome during aging	18
1.5. ECM and longevity	19
1.6. Matrisome, Adhesome and Mechano-transduction.....	20
1.7. References	21
2. Scope of the thesis.....	29
3. Paper: The <i>in-silico</i> characterization of the <i>Caenorhabditis elegans</i> matrisome and proposal of a novel collagen classification	30
4. Paper: Overcoming autofluorescence to assess GFP expression during normal physiology and aging in <i>Caenorhabditis elegans</i>	44
5. Paper: Assessing collagen deposition during aging in mammalian tissue and in <i>Caenorhabditis elegans</i>	68
6. Mechanotransduction regulates extracellular matrix dynamics across tissue boundaries and influences longevity in <i>C. elegans</i>	69
6.1. Introduction	69
6.2. Results	70
6.3. Discussion	91
6.4. Material and Methods	98
6.5. References	104
7. Conclusion and Outlook	110
8. Supplements.....	112
9. Curriculum vitae.....	131

1. Introduction

1.1. Aging

For about 200 years, life expectancy has been increasing. The number of people over 60 years today is twice as high as forty years ago (1980). The number of people aged 80 years is expected almost quadruple to 395 million between now and 2050. (World Health Organization, 2018). Higher life expectancy can be generally considered to be a positive development, although age is the main risk factor for several diseases (Thomas B. L. Kirkwood, 2008). Old age is actually considered the single greatest risk factor to succumb to diseases. However, removing a single age-dependent disease like cancer would merely increase the population lifespan by approximately 5 years, since other age-dependent diseases would occur instead (Olshansky et al., 1990). This underlines the importance of better understanding the aging process, with the ultimate goal to treat aging itself.

Aging is a complex multifactorial process of the decline of molecular and cellular function. Aging is defined by this decline of molecular and cellular functions and the accumulation of cellular damage over time. While cells are able to cope with this damage when the organism is still young, the efficiency of the maintaining mechanisms decrease with age, leading to damage accumulation (López-Otín et al., 2013). Interestingly, humans that live longer than 100 years, appear to be living mostly disease free with a late onset of age-related diseases (Andersen et al., 2012). In the early 1990s, it was shown that aging can be regulated genetically: a single mutation in the *daf-2* gene, a homolog to the human Insulin/IGF-1 receptor, was sufficient to double the lifespan of the model organism *Caenorhabditis elegans* (Kenyon et al., 1993). After this first gene and pathway was found to influence aging and longevity, several other fundamental mechanisms, like the TOR-pathway, were discovered in *C. elegans* and have been shown to promote longevity also for higher organisms such as mice (Driscoll and Gerstbrein, 2003; Harrison et al., 2009; Houtkooper et al., 2012; Mannick et al., 2014; Onken and Driscoll, 2010; Vellai et al., 2003). Aging is also plastic in humans. Non-genetic factors like diet, caloric restriction, exercise and psychosocial factors, and good medical care were shown to be important factors (López-Otín et al., 2013; Passarino et al., 2016). Genetic polymorphisms were shown to be responsible for approximately 25% of the differences in human lifespans (Budovsky et al., 2013; Christensen et al., 2006; Chung et al., 2010).

Until now aging research focused mainly on the damage accumulated inside the cells. However, also their surroundings, the extracellular matrix (ECM), undergoes progressive deterioration. The ECM is also associated with several age-dependent diseases and conditions like fibrosis, arthritis, osteoporosis and skin aging, including wrinkles, pigmentation, and a weakened wound healing ability (Herrera et al., 2018; Mei Xiong et al., 2017; Shi et al.,

1.2. The extracellular matrix

Some specific collagens in the eye lens or cartilage are only synthesized once and remain in the ECM for life. This implies that the half-lives of these collagens can be over 117 years (Birch, 2018; Toyama and Hetzer, 2013). However most extracellular matrices, especially during development are dynamic networks of secreted macromolecules. In general matrices provide structural support, but also play a role in intercellular signaling by controlling proliferation, adhesion, migration, polarity, differentiation, and apoptosis (Yue, 2014). The matrix does so by serving as an anchor for cells, by signaling to cells through adhesion receptors, as reservoir of growth factors and bioactive molecules, and as coreceptor (Lu et al., 2011). Furthermore, evidence suggest that its biomechanical properties, including stiffness or deformability, can influence cell behavior (Hynes, 2009). In mammals, the ECM consists of around 300 proteins, mainly fibrous proteins like collagens, elastins, fibronectins, laminins, proteoglycans, and glycoproteins. The compendium of all these proteins that are part of the extracellular matrix or contribute to it are called the matrisome (Hynes and Naba, 2012).

Cells constantly reorganize their ECM through deposition, degradation, reassembly, modification, and other processes. These highly dynamic and tightly regulated changes are necessary for tissue homeostasis and, if deregulated, can lead to pathological conditions or aggravate disease progression like cancer and tissue fibrosis (Bonnans et al., 2014; Lu et al., 2011).

1.3. The model organism *C. elegans*

1.3.1. *C. elegans* and its role as an aging model

C. elegans is a free-living, transparent nematode of about 1 mm in length. The animal was introduced in 1973 by Sydney Brenner as a new model organism to study development and neurobiology (Brenner, 1973). During their short life cycle of about 3 days (Fig. 1), they can be maintained on Nematode Growth Media (NGM) agar plates together with the *Escherichia coli* (*E. coli*) strain OP50 as food source (Edgar and Wood, 1977). A special feature of *C. elegans* is its invariant cell number of 959 somatic cells in hermaphrodites and 1031 in males (Sulston et al., 1983). Since its introduction to science, *C. elegans* became a popular model organism to study apoptosis, cell signaling, cell cycle, cell polarity, gene regulation, metabolism, and aging. Its easy maintenance, short lifespan of three weeks, and ease for genetic manipulation, combined with a high evolutionary conservation of genes involved in human diseases make

C. elegans a good pioneer model to understand the molecular mechanisms of aging (Shaye and Greenwald, 2011; Tissenbaum, 2015). An additional advantage of *C. elegans* is its transparency, allowing the monitoring of many processes and proteins *in vivo*, for example by using fluorescent reporter proteins. A further advantages are fast genotype crossings by mating male *C. elegans* (abundance < 1%) with hermaphrodites.

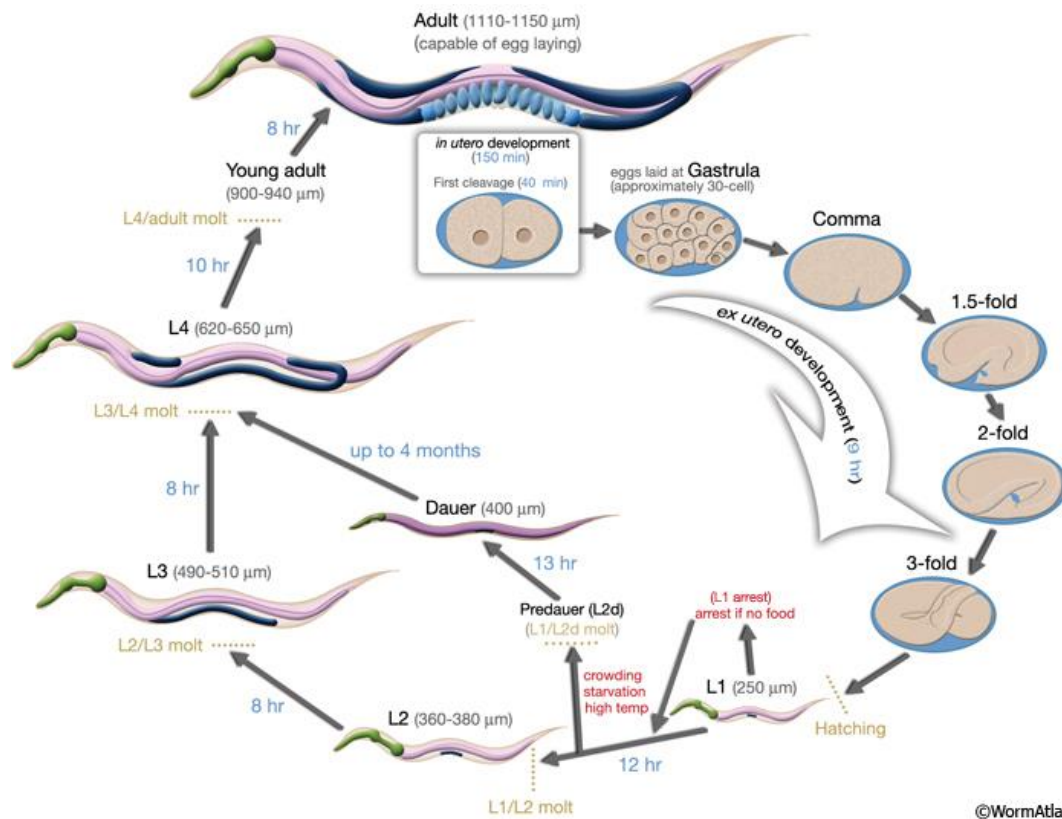


Figure 1: The lifecycle of *C. elegans*.

C. elegans undergo four larval stages (L1-L4) during development before it reaches adulthood. At 20°C it needs approximately 60h to close the cycle starting with the first cleavage inside the uterus. If the conditions are not feasible for further development, the L1 larvae are able to enter the so called dauer stage, a type of stasis. In this form it can survive harsh conditions and stay like this for months. When the condition become better the worm directly molt into L4 stage and goes on with the normal development. (Figure from Altun and Hall, 2006)

Lifespan measurements play an important role in aging research in order to find age-related genes. *C. elegans* is particularly suitable for this kind of measurements as they can be genetically inbred, making them genetically identical. They also can be age-synchronized and can be kept under standard lab conditions (Sánchez-Blanco and Kim, 2011). In order to keep the culture age-synchronized the hatching of offspring has to be prevented. This can be achieved by moving the animals every second day on new plates, by using temperature-sensitive sterile mutations like *spe-9 (hc88)* affecting sperm production, or by supplementing the plates with the DNA synthesis inhibitor 5-Fluoro-2'-deoxyuridine (FUDR). Since adult *C. elegans* are post mitotic, DNA synthesis is only disrupted in developing animals (Wang et al., 2019).

One of the major methods to study gene function in *C. elegans* is downregulation by RNA interference (RNAi). RNAi is an inexpensive and relatively simple method to knock down the expression level of a gene post-transcriptionally. In *C. elegans*, there are three ways to transfer double-stranded RNA (dsRNA) into the organism: through injection (Fire et al., 1998), soaking animals in a high concentration of dsRNA solution (Tabara et al., 1999), or feeding the worms with bacteria expressing the desired dsRNA (Timmons and Fire, 1998). For the latter two, huge RNAi feeding libraries are available. The libraries comprise approximately 80% of the genes in the genome, allowing for extensive forward and reverse genetic screens (Kamath et al., 2003; Rual et al., 2004).

1.3.2. The extracellular matrices of *C. elegans*

C. elegans has two major ECMs, one is the cuticle which is the exoskeleton of the animal, the other is the basement membrane, which is a specialized extracellular matrix surrounding most tissues in all metazoans (Kramer, 2005; Page and Johnstone, 2007)(Fig. 2). It also has some smaller tissue-specific, highly specialized matrices, like the mantle, that surrounds the four mechanosensory neurons, the rachis coat, covering the central rachis in both gonad arms, the

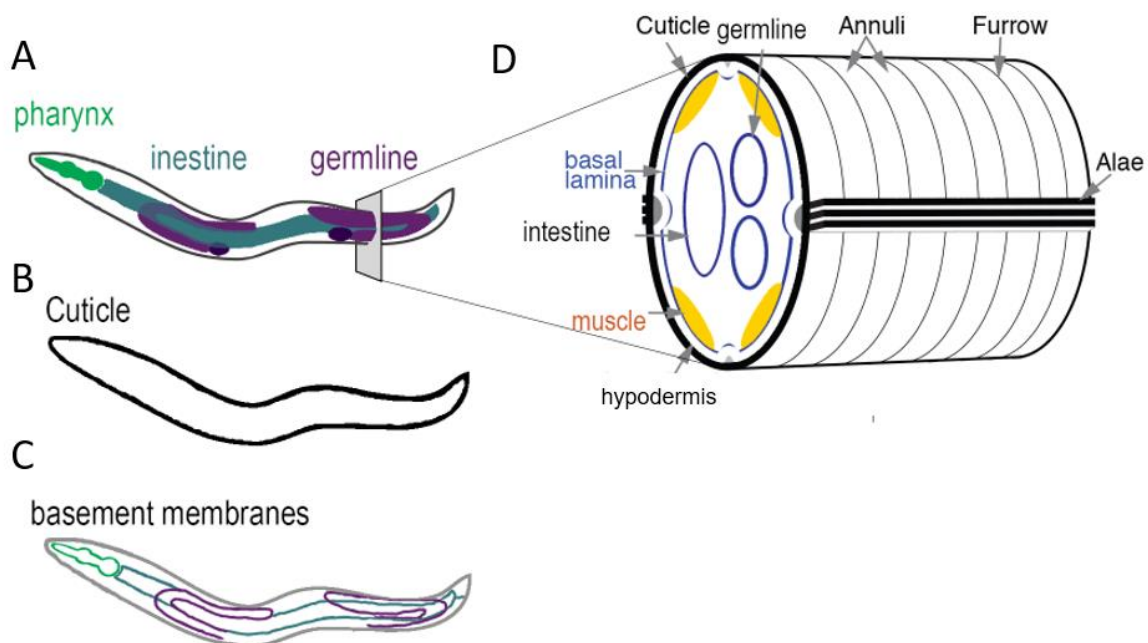


Figure 2: Schematic overview of major *C. elegans* ECMs

(A) Schematic side view. For clarity some tissues are highlighted: In green the pharynx, in blue the intestine and in purple the germline. (B) Side view of the first major ECM, the cuticle, in black. (C) Side view of the second major ECM: the basement membrane. In grey the layer below the cuticle, in green surrounding the pharynx, in blue the one around the intestine, and in purple the parts that covering the germline. (D) Schematic cut through *C. elegans*. On the outside the annuli, furrows, and alae of the cuticle (black) are displayed. Below the cuticle is the hypodermis. The basal lamina (basement membrane) is highlighted in blue, laying below the hypodermis and surrounding the intestine and germline. The muscles are shown in yellow.

four tendons holding the pharynx and the zona pellucina, which covers unfertilized primary oocytes, while they are in the somatic gonad (Altun and Hall, 2009; Bumbarger et al., 2006; Hekimi and Kershaw, 1993; Huang et al., 2003; Vogél and Hedgecock, 2001). In *C. elegans* no visible matrix was reported between cells within tissues, likely due to their close proximity to either the basement membrane or the cuticle (Kramer, 1994). In the following section I want to focus on the cuticle and the basement membrane of *C. elegans*.

Basement membrane

The basement membrane in higher organisms is subdivided into two different layers, the basal lamina and the reticula lamina. However, these layers cannot be distinguished in nematodes (Altun and Hall, 2009; Kramer, 2005). They play an important role in providing mechanical stability, in cellular polarity signaling, and in cell and axon guidance. Furthermore, they are thought to sense and response to external physical forces (Clay and Sherwood, 2015). In *C. elegans*, the basement membrane covers the apical part of body wall muscles, pharynx, intestine, gonad, and the part of the hypodermis which is facing the inside of the animal (Figure 2) (Kramer, 2005). Major vertebrate basement membrane proteins are conserved in *C. elegans*, but in general contain less genes within each family (Hutter et al., 2000; Teuscher et al., 2019). *C. elegans* has orthologs of laminin, type IV collagen, type XVIII collagen, nidogen, perlecan, agrin, fibulin-1, hemicentin, SPARC, F-spondin, and papilin (Clay and Sherwood, 2015; Hrus et al., 2007; Kramer, 2005; Woo et al., 2008).

One of the major basement membrane proteins are laminins, which are essential for the formation of the basement membrane (Aumailley and Smyth, 1998). While vertebrates have eleven laminin chain genes, *C. elegans* only has four genes, two α (α A LAM-3 and α B EPI-1), a single β (LAM-1) and one γ (LAM-2) chain, resulting in two laminin isoforms, depending on which of the two α -chains is used. These isoforms have overlapping, but different localization patterns. (Huang et al., 2003)

The family of type IV collagens is present and abundant in nearly all *C. elegans* basement membranes. While this family consists of six genes in humans, *C. elegans* contains two: the α A-like *emb-9* and the α B-like *let-2*. Together they form heterotrimeric proteins consisting of two α 1-like and one α 2-like chain. The crosslinking of these chains is thought to enable the matrix to withstand physical stress (Clay and Sherwood, 2015; Fidler et al., 2014; Hohenester and Yurchenco, 2013; Kramer, 2005; LeBleu et al., 2007; Vanacore et al., 2009).

In order to move, the movements of the body wall muscles must be mechanically transmitted to the hypodermis and cuticle of *C. elegans*. In the basement membrane, the *C. elegans* ortholog of the vertebrate heparan sulfate proteoglycan perlecan *unc-52* is required for this

force transmission (Clay and Sherwood, 2015; Francis and Waterston, 1991). It can only be found in basement membranes close to muscle cells. UNC-52 is also so far the only known protein necessary for integrin localization to the basal muscle cell membrane (Kramer, 2005; Moerman and Williams, 2006; Mullen et al., 1999; Rogalski et al., 1995). Integrins use the perlecan-dependent anchoring to the basement membrane to transmit muscle contractions resulting in animal movement (Battaglia et al., 1993; Bix and Iozzo, 2008; Hayashi et al., 1992).

Integrins are transmembrane $\alpha\beta$ heterodimer proteins that mediate cell adhesion and signal transduction. They are important for cell migration, proliferation, differentiation, apoptosis, as well as matrix assembly and remodeling (Bökel and Brown, 2002; Cox et al., 2004; Zamir and Geiger, 2001). Instead of 24 integrin genes in vertebrates, *C. elegans* has only three different ones. The two α -integrins *ina-1* and *pat-2* can form a heterodimer with the sole β -integrin *pat-3* (Kramer, 2005). While *pat-3*, as the only β -integrin subunit, is broadly expressed, *ina-1* is expressed in early embryos and is in adult restricted to the neurons, to migrating cells, and to cells involved in morphogenesis (Cox et al., 2004). The α INA-1/ β PAT-3 heterodimers were shown to play an important role in commissural axon navigation (Baum and Garriga, 1997). *pat-2* on the other hand is strongly expressed in muscle cells (Hsieh et al., 2012). The α PAT-2/ β PAT-3 heterodimers were found to be essential for sarcomere assembly, as *pat-2* and *pat-3* mutants both show a Pat (paralyzed at two-fold) phenotype and fail to form dense bodies, an analog to the mammalian Z-disc or organize sarcomeres (Cox and Hardin, 2004; Cox et al., 2004; Kramer, 2005).

Cuticle

C. elegans has an exoskeleton, also called cuticle, that serves as physical barrier against pathogens and protects from other environmental stressors, such as dehydration (Cassada and Russell, 1975; Gravato-Nobre et al., 2016; Lints and Hall, 2003; Mei Xiong et al., 2017). The cuticle is essential for maintenance of the body morphology and it permits the animal's movement through its attachment to the body wall (Mesbahi et al., 2020; Page and Johnstone, 2007). During development *C. elegans* undergoes several moltings. At each larval stage, an entirely new cuticle has to be made, while the old one is shed and often eaten (Lintz and Hall, 2003). The cuticle is highly structured and multilayered and synthesized by the underlying hypodermal cells. It consists mainly of the large cross-linked cuticular collagen family, which is nematode specific. (Lintz and Hall, 2003; Page and Johnstone, 2007). A total of 173 genes encoding for this family can be found in *C. elegans* (Teuscher et al., 2019). All of them undergo several co- and post-translational modifications during biosynthesis, before they are secreted and integrated into the ECM. Additionally, non-collagenous cuticulins, glycoproteins, and lipids contribute to the cuticle (Page and Johnstone, 2007). The whole cuticle is covered by a surface

coat or glycocalyx, consisting of a lipid-rich layer and a negatively charged layer consisting of proteoglycans on top (Blaxter et al., 1992; Page and Johnstone, 2007).

1.3.3. Mechanical linkage of muscles to the cuticle

Below the cuticle is the hypodermis, which lays on top of the basement membrane covering the body wall muscles. In order to allow the animal's locomotion, the muscle movement has to be transmitted through all layers up to the cuticle (Lints and Hall, 2003). The dense-bodies and the M-line in the muscle are connected to the basement membrane through α PAT-2/ β PAT-3 heterodimers, which likely are linked to the basement membrane network via *unc-52* (see basement membrane). Hemidesmosome-like junctions in the hypodermis, also called fibrous organelles, act like trans-epithelial tendons and connect the cuticle across the hypodermis to the basement membrane (Hetherington et al., 2011). They consist of MUA-3 (homolog of the mammalian fibrillin1), MUP-4 (homolog of the mammalian matrilin2), the intermediate filaments, VAB-10A (homologous to both plectin and BP230), and the myotactin LET-805 that reaches through the membrane into the basement membrane (Bosher et al., 2003; Francis and Waterston, 1991; Labouesse, 2006; Woo et al., 2004; Zhang and Labouesse, 2010)(see Figure 3).

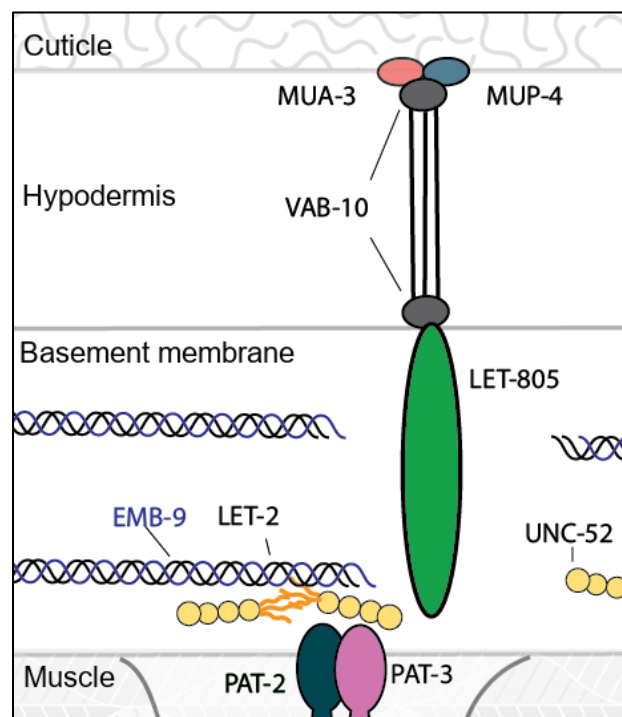


Figure 3: mechanical linkage of the cuticle to the muscle in *C. elegans*

In cuticle in the upper part is linked via hemidesmosome-like fibrous organelles in the hypodermis that consists of MUA-3, MUP-4, VAB-10, Intermediate filaments and LET-805, which reaches into the basement membrane. In the basement membrane the perlecan UNC-52 binds to the collagen type IV collagen heterotrimers of EMB-9 and LET-2 and likely also to the Integrin PAT-2/PAT-3, which anchors the basement membrane to the dense bodies and M-lines in the muscle.

1.3.4. *daf-2* and *glp-1* longevity in *C. elegans*

In previous studies the ECM was already connected to different longevity treatments and pathways. One was a reduced insulin/IGF-1 signaling pathway in from of *daf-2* mutants (Ewald, 2020; Ewald et al., 2015). DAF-2 was one of the first proteins identified to modulate the lifespan of an organism (Kenyon et al., 1993). *daf-2* mutants became a popular model for lifespan extension in *C. elegans*. The protein is part of the insulin/insulin-like growth factor signaling (IIS) pathway and encodes for the homolog of the Insulin/ insulin-like growth factor-1 receptor (Kimura et al., 1997). When DAF-2 activity is down-regulated, the forkhead box FoxO transcription factor homolog DAF-16 translocates to the nucleus. The active transcription factor regulates genes involved in the cellular stress response, metabolism, and autophagy, leading to an extension of lifespan (Lee et al., 2003; Meléndez et al., 2003; Murphy et al., 2003; Uno and Nishida, 2016). In *C. elegans* the IIS is also involved into the entry of a developmental diapause called the dauer stage. The IIS can sense absence of food and enables a developmental program that forces L1 larvae into the dauer stage. In this stage, animals can survive harsh conditions for months (see Figure 1) (Altun and Hall, 2006; Kimura et al., 1997). A reanalysis of expression profiles of *daf-2* mutants revealed that almost 20% of 426 upregulated genes in these long-lived animals were matrisome genes with 48 out of the up-regulated 79 being collagens.

Apart from *daf-2*, the gene *glp-1* was also found to promote lifespan extensions in *C. elegans*. It encodes for the Notch-receptor, which receives germline specific proliferation signals from the distal tip cells of the somatic gonad. Loss-of-function mutants of these gene only have the somatic part of the gonad and lack the germline. This leads to a *daf-12* and *daf-9* dependent (but *daf-2* independent) re-localization of DAF-16 from the cytosol to the nucleus in the adult nematode and to the up-regulation of lifespan-extending target genes (Arantes-Oliveira et al., 2002; Austin and Kimble, 1987; Berman and Kenyon, 2006; Lee et al., 2016). When proteomic data was reanalyzed comparing *glp-1* mutants to wild-type *C. elegans*, 177 proteins were found to be up-regulated with 25 being matrisome proteins. *glp-1* mutants are also attractive longevity models within a *C. elegans* aging screen setting (Ewald, 2020). Their sterility prevents the mix-up of adults with their offspring, without the need to use sterilizing chemicals, additional mutations or manual separation.

1.4. Matrisome during aging

During aging, the overall integrity of the ECM is deteriorating due to the continuous decline in ECM protein biosynthesis and an increase in ECM degradation (Ewald, 2020). Metadata analysis of gene expression profiles of mice, rats, and humans suggest that this decline of

ECM components is a common signature of aging (de Magalhães et al., 2009). The composition of the ECM is dominated by fibrillar proteins like elastin and especially collagens. Both are long-lived proteins and therefore prone to enzymatic post-translational modifications and fragmentation (Birch, 2018). During human aging, this major component of the ECM, therefore not only gets fragmented, but also oxidated and glycated, while at the same time the total collagens mass is declining by 1% per year in the human skin (Fisher et al., 2009; Myllyharju and Kivirikko, 2004; Ricard-Blum, 2011; Shoulders and Raines, 2009; Snedeker and Gautieri, 2014). The build-up of damage in the ECM seems to be a driver of cellular aging and disease progression (Bonnans et al., 2014). In the model organism *C. elegans*, 1254 age-related genes were found to be either up-regulated (around 300) or down-regulated (around 900) during aging (Budovskaya et al., 2008; Ewald, 2020). 150 out of these 1254 genes are matrisome genes, including 92 collagens, the major component of the ECM (Budovskaya et al., 2008; Ewald, 2020).

1.4.1. Collagen glycation

Over time, the extracellular matrix becomes glycated and crosslinked (Chaudhuri et al., 2018), which stiffens the matrix and causes wound healing impairment and problems in diabetic patients. Hyperglycemia increases glycation leading to dysfunctions in collagenous tissues like renal, cardiovascular and retinal tissues (Paul and Bailey, 1996). The product of collagen glycation is advanced glycation end products (AGEs). AGEs are a heterogeneous group. They are produced in a non-enzymatic fashion involving the Maillard reaction (Chaudhuri et al., 2018). Neighboring cells respond to the increase in stiffness with an elevated production of proteases to reduce it. However, AGEs potentially impede proteolytic cleavage and, instead, the proteases potentially damage non-glycosylated structures (Humphrey et al., 2014).

1.5. ECM and longevity

In mice, mutations promoting longevity led to a longer preservation of connective tissue elasticity and integrity during aging (Flurkey et al., 2002; Wilkinson et al., 2012). In human cell culture, it was further shown that a "young" ECM was able to rejuvenate senescent cells (Choi et al., 2011). In *C. elegans*, ECM genes are a major group of up-regulated genes in long-lived strains compared to wild type animals (Ewald et al., 2015). Collagens are relatively large proteins and synthesizing them is a large investment. So why does a long-lived organism invest that much energy into enhanced collagen expression?

Some collagens are necessary to achieve the full lifespan extension of long-lived *C. elegans* mutants (Ewald et al., 2015). Knock-down of single collagens in long-lived *daf-2* mutants

abolishes the lifespan extension, while over-expression of one of these collagens is already sufficient to increase the lifespan of wildtype *C. elegans* (Ewald et al., 2015). One of these collagens is COL-120, a collagen located in the cuticle of *C. elegans* (Ewald et al., 2015). Interestingly, knocking down *col-120* did also block the transcriptional upregulation of another cuticular collagen *col-144* expression (Ewald et al., 2015).

These findings do not only indicate a connection between the ECM and longevity, but also that longevity-assurance pathways potentially slow aging via ECM remodeling to slow its decline of integrity during aging (Ewald, 2020). However, how this is regulated or how this extends the lifespan in *C. elegans* remains unknown.

1.6. Matrisome, Adhesome and Mechano-transduction

One important function of the ECM is ECM-to-cell signaling via mechanotransduction. Mechanotransduction describes the conversion of extracellular physical forces into intracellular signals at the cell surface (Wang et al., 2009). Cells are able to monitor these physical forces or mechanosensations coming from the ECM and in turn adjust their surrounding environment by synthesizing and remodeling the ECM (Bonnans et al., 2014).

Integrin receptors serve as connectors between the ECM and the intracellular cytoskeleton by binding to collagens, elastins, laminins. Also, discoidin domain receptors (DDR) can attach to fibrillar collagen and specific collagen triple helix motifs. Together they translate physical signals into an intracellular response and the other way around, which is essential for cell survival, migration, differentiation, and metabolic state of a cell. In vertebrates, integrins and DDRs are the predominant collagen cell surface receptors, with each of them binding to a specific set of collagens and triggering different kind of responses (Birch, 2018; Itoh, 2018; Valiathan et al., 2012; Xu et al., 2012). Interestingly, the ability of cells to respond to mechanical signals decreases with age, hinting at a possible mechanism of how impaired ECM integrity might accelerates aging (Phillip et al., 2015).

1.7. References

- Altun, Z.F., and Hall, D.H. (2006). WormAtlas Hermaphrodite Handbook - Introduction. WormAtlas.
- Altun, Z.F., and Hall, D.H. (2009). WormAtlas Hermaphrodite Handbook - Pericellular Structures. WormAtlas.
- Andersen, S.L., Sebastiani, P., Dworkis, D.A., Feldman, L., and Perls, T.T. (2012). Health span approximates life span among many supercentenarians: Compression of morbidity at the approximate limit of life span. *Journals Gerontol. - Ser. A Biol. Sci. Med. Sci.* 67 A, 395–405.
- Arantes-Oliveira, N., Apfeld, J., Dillin, A., and Kenyon, C. (2002). Regulation of life-span by germ-line stem cells in *Caenorhabditis elegans*. *Science* (80-). 295.
- Aumailley, M., and Smyth, N. (1998). The role of laminins in basement membrane function. *J. Anat.* 193.
- Austin, J., and Kimble, J. (1987). *glp-1* is required in the germ line for regulation of the decision between mitosis and meiosis in *C. elegans*. *Cell* 51.
- Battaglia, C., Aumailley, M., Mann, K., Mayer, U., and Timpl, R. (1993). Structural basis of $\beta 1$ integrin-mediated cell adhesion to a large heparan sulfate proteoglycan from basement membranes. *Eur. J. Cell Biol.* 61.
- Baum, P.D., and Garriga, G. (1997). Neuronal migrations and axon fasciculation are disrupted in *ina-1* integrin mutants. *Neuron* 19.
- Berman, J.R., and Kenyon, C. (2006). Germ-cell loss extends *C. elegans* life span through regulation of DAF-16 by *kri-1* and lipophilic-hormone signaling. *Cell* 124.
- Birch, H.L. (2018). Extracellular matrix and ageing. In *Subcellular Biochemistry*, p.
- Bix, G., and Iozzo, R. V. (2008). Novel interactions of perlecan: Unraveling Perlecan's role in angiogenesis. *Microsc. Res. Tech.* 71.
- Blaxter, M.L., Page, A.P., Rudin, W., and Maizels, R.M. (1992). Nematode surface coats: Actively evading immunity. *Parasitol. Today* 8.
- Bökel, C., and Brown, N.H. (2002). Integrins in development: Moving on, responding to, and sticking to the extracellular matrix. *Dev. Cell* 3.
- Bonnans, C., Chou, J., and Werb, Z. (2014). Remodelling the extracellular matrix in development and disease. *Nat. Rev. Mol. Cell Biol.* 15.
- Bosher, J.M., Hahn, B.S., Legouis, R., Sookhareea, S., Weimer, R.M., Gansmuller, A., Chisholm, A.D., Rose, A.M., Bessereau, J.L., and Labouesse, M. (2003). The *Caenorhabditis elegans* *vab-10* spectraplakins isoforms protect the epidermis against internal and external

forces. *J. Cell Biol.* 161.

Brenner, S. (1973). The genetics of *Caenorhabditis elegans*.

Budovskaya, Y. V., Wu, K., Southworth, L.K., Jiang, M., Tedesco, P., Johnson, T.E., and Kim, S.K. (2008). An elt-3/elt-5/elt-6 GATA Transcription Circuit Guides Aging in *C. elegans*. *Cell* 134, 291–303.

Budovsky, A., Craig, T., Wang, J., Tacutu, R., Csordas, A., Lourenço, J., Fraifeld, V.E., and De Magalhães, J.P. (2013). LongevityMap: A database of human genetic variants associated with longevity. *Trends Genet.* 29.

Bumbarger, D.J., Crum, J., Ellisman, M.H., and Baldwin, J.G. (2006). Three-dimensional reconstruction of the nose epidermal cells in the microbial feeding nematode, *Acrobelus complexus* (Nematoda: Rhabditida). *J. Morphol.* 267.

Cassada, R.C., and Russell, R.L. (1975). The dauerlarva, a post-embryonic developmental variant of the nematode *Caenorhabditis elegans*. *Dev. Biol.* 46.

Chaudhuri, J., Bains, Y., Guha, S., Kahn, A., Hall, D., Bose, N., Gugliucci, A., and Kapahi, P. (2018). The Role of Advanced Glycation End Products in Aging and Metabolic Diseases: Bridging Association and Causality. *Cell Metab.* 28.

Choi, H.R., Cho, K.A., Kang, H.T., Lee, J. Bin, Kaeberlein, M., Suh, Y., Chung, I.K., and Park, S.C. (2011). Restoration of senescent human diploid fibroblasts by modulation of the extracellular matrix. *Aging Cell* 10, 148–157.

Christensen, K., Johnson, T.E., and Vaupel, J.W. (2006). The quest for genetic determinants of human longevity: Challenges and insights. *Nat. Rev. Genet.* 7.

Chung, W.H., Dao, R.L., Chen, L.K., and Hung, S.I. (2010). The role of genetic variants in human longevity. *Ageing Res. Rev.* 9.

Clay, M.R., and Sherwood, D.R. (2015). Basement Membranes in the Worm: A Dynamic Scaffolding that Instructs Cellular Behaviors and Shapes Tissues. *Curr. Top. Membr.* 76.

Cox, E.A., and Hardin, J. (2004). Sticky worms: Adhesion complexes in *C. elegans*. *J. Cell Sci.* 117.

Cox, E.A., Tuskey, C., and Hardin, J. (2004). Cell adhesion receptors in *C. elegans*. *J. Cell Sci.* 117.

Driscoll, M., and Gerstbrein, B. (2003). Dying for a cause: Invertebrate genetics takes on human neurodegeneration. *Nat. Rev. Genet.* 4, 181–194.

Edgar, R.S., and Wood, W.B. (1977). The nematode *caenorhabditis elegans*: A new organism for intensive biological study. *Science* (80-). 198.

Ewald, C.Y. (2020). The Matrisome during Aging and Longevity: A Systems-Level Approach

toward Defining Matreotypes Promoting Healthy Aging. *Gerontology* 66.

Ewald, C.Y., Landis, J.N., Abate, J.P., Murphy, C.T., and Blackwell, T.K. (2015). Dauer-independent insulin/IGF-1-signalling implicates collagen remodelling in longevity. *Nature* 519, 97–101.

Fidler, A.L., Vanacore, R.M., Chetyrkin, S. V., Pedchenko, V.K., Bhave, G., Yin, V.P., Stothers, C.L., Rose, K.L., McDonald, W.H., Clark, T.A., et al. (2014). A unique covalent bond in basement membrane is a primordial innovation for tissue evolution. *Proc. Natl. Acad. Sci. U. S. A.* 111.

Fire, A., Xu, S., Montgomery, M.K., Kostas, S.A., Driver, S.E., and Mello, C.C. (1998). Potent and specific genetic interference by double-stranded RNA in *Caenorhabditis elegans*. *Nature* 391.

Fisher, G.J., Quan, T., Purohit, T., Shao, Y., Moon, K.C., He, T., Varani, J., Kang, S., and Voorhees, J.J. (2009). Collagen fragmentation promotes oxidative stress and elevates matrix metalloproteinase-1 in fibroblasts in aged human skin. *Am. J. Pathol.* 174, 101–114.

Flurkey, K., Papaconstantinou, J., Miller, R.A., and Harrison, D.E. (2002). Lifespan extension and delayed immune and collagen aging in mutant mice with defects in growth hormone production. *Proc. Natl. Acad. Sci.* 98, 6736–6741.

Francis, R., and Waterston, R.H. (1991). Muscle cell attachment in *Caenorhabditis elegans*. *J. Cell Biol.* 114.

Gravato-Nobre, M.J., Vaz, F., Filipe, S., Chalmers, R., and Hodgkin, J. (2016). The Invertebrate Lysozyme Effector ILYS-3 Is Systemically Activated in Response to Danger Signals and Confers Antimicrobial Protection in *C. elegans*. *PLoS Pathog.* 12.

Harrison, D.E., Strong, R., Sharp, Z.D., Nelson, J.F., Astle, C.M., Flurkey, K., Nadon, N.L., Wilkinson, J.E., Frenkel, K., Carter, C.S., et al. (2009). Rapamycin fed late in life extends lifespan in genetically heterogeneous mice. *Nature* 460, 392–395.

Hayashi, K., Madri, J.A., and Yurchenco, P.D. (1992). Endothelial cells interact with the core protein of basement membrane perlecan through $\beta 1$ and $\beta 3$ integrins: An adhesion modulated by glycosaminoglycan. *J. Cell Biol.* 119.

Hekimi, S., and Kershaw, D. (1993). Axonal guidance defects in a *Caenorhabditis elegans* mutant reveal cell- extrinsic determinants of neuronal morphology. *J. Neurosci.* 13.

Herrera, J., Henke, C.A., and Bitterman, P.B. (2018). Extracellular matrix as a driver of progressive fibrosis. *J. Clin. Invest.* 128.

Hetherington, S., Gally, C., Fritz, J.A., Polanowska, J., Reboul, J., Schwab, Y., Zahreddine, H., Behm, C., and Labouesse, M. (2011). PAT-12, a potential anti-nematode target, is a new

spectraplakins partner essential for *Caenorhabditis elegans* hemidesmosome integrity and embryonic morphogenesis. *Dev. Biol.* 350.

Hohenester, E., and Yurchenco, P.D. (2013). Laminins in basement membrane assembly. *Cell Adhes. Migr.* 7.

Houtkooper, R.H., Pirinen, E., and Auwerx, J. (2012). Sirtuins as regulators of metabolism and healthspan. *Nat. Rev. Mol. Cell Biol.* 13, 225–238.

Hsieh, H.H., Hsu, T.Y., Jiang, H.S., and Wu, Y.C. (2012). Integrin α PAT-2/CDC-42 signaling is required for muscle-mediated clearance of apoptotic cells in *Caenorhabditis elegans*. *PLoS Genet.* 8.

Huang, C.C., Hall, D.H., Hedgecock, E.M., Kao, G., Karantza, V., Vogel, B.E., Hutter, H., Chisholm, A.D., Yurchenco, P.D., and Wadsworth, W.G. (2003). Laminin α subunits and their role in *C. elegans* development. *Development* 130.

Humphrey, J.D., Dufresne, E.R., and Schwartz, M.A. (2014). Mechanotransduction and extracellular matrix homeostasis. *Nat. Rev. Mol. Cell Biol.* 15.

Hutter, H., Vogel, B.E., Plenefisch, J.D., Norris, C.R., Proenca, R.B., Spieth, J., Guo, C., Mastwal, S., Zhu, X., Scheel, J., et al. (2000). Conservation and novelty in the evolution of cell adhesion and extracellular matrix genes. *Science* (80-). 287.

Hynes, R.O. (2009). The extracellular matrix: Not just pretty fibrils. *Science* (80-). 326, 1216–1219.

Hynes, R.O., and Naba, A. (2012). Overview of the matrisome—An inventory of extracellular matrix constituents and functions. *Cold Spring Harb. Perspect. Biol.* 4.

Itoh, Y. (2018). Discoidin domain receptors: Microenvironment sensors that promote cellular migration and invasion. *Cell Adhes. Migr.* 12.

Kamath, R.S., Fraser, A.G., Dong, Y., Poulin, G., Durbin, R., Gotta, M., Kanapink, A., Le Bot, N., Moreno, S., Sohrmann, M., et al. (2003). Systematic functional analysis of the *Caenorhabditis elegans* genome using RNAi.

Kenyon, C., Chang, J., Gensch, E., Rudner, A., and Tabtiang, R. (1993). A *C. elegans* mutant that lives twice as long as wild type. *Nature* 366.

Kimura, K.D., Tissenbaum, H.A., Liu, Y., and Ruvkun, G. (1997). *Daf-2*, an insulin receptor-like gene that regulates longevity and diapause in *Caenorhabditis elegans*. *Science* (80-). 277.

Kramer, J.M. (1994). genetic analysis of extracellular matrix in *c. elegans*.

Kramer, J.M. (2005). Basement membranes. *WormBook*.

Labouesse, M. (2006). Epithelial junctions and attachments. *WormBook*.

-
- LeBleu, V.S., MacDonald, B., and Kalluri, R. (2007). Structure and function of basement membranes. *Exp. Biol. Med.* 232.
- Lee, C.H., Sorensen, E.B., Lynch, T.R., and Kimble, J. (2016). *C. elegans* GLP-1/Notch activates transcription in a probability gradient across the germline stem cell pool. *Elife* 5.
- Lee, S.S., Kennedy, S., Tolonen, A.C., and Ruvkun, G. (2003). DAF-16 target genes that control *C. elegans* Life-span and metabolism. *Science* (80-.). 300.
- Lints, R., and Hall, D.H. (2003). *WormAtlas Hermaphrodite Handbook - The Cuticle*. WormAtlas.
- López-Otín, C., Blasco, M.A., Partridge, L., Serrano, M., and Kroemer, G. (2013). The hallmarks of aging. *Cell* 153, 1194–1217.
- Lu, P., Takai, K., Weaver, V.M., and Werb, Z. (2011). Extracellular Matrix degradation and remodeling in development and disease. *Cold Spring Harb. Perspect. Biol.* 3.
- de Magalhães, J.P., Curado, J., and Church, G.M. (2009). Meta-analysis of age-related gene expression profiles identifies common signatures of aging. *Bioinformatics* 25, 875–881.
- Mannick, J.B., Del Giudice, G., Lattanzi, M., Valiante, N.M., Praestgaard, J., Huang, B., Lonetto, M.A., Maecker, H.T., Kovarik, J., Carson, S., et al. (2014). mTOR inhibition improves immune function in the elderly. *Sci. Transl. Med.* 6, 268ra179.
- Mei Xiong, Z., O'Donovan, M., Sun, L., Young Choi, J., Ren, M., and Cao, K. (2017). Anti-Aging Potentials of Methylene Blue for Human Skin Longevity. *Sci. Rep.* 7.
- Meléndez, A., Tallóczy, Z., Seaman, M., Eskelinen, E.L., Hall, D.H., and Levine, B. (2003). Autophagy genes are essential for dauer development and life-span extension in *C. elegans*. *Science* (80-.). 301.
- Mesbahi, H., Pho, K.B., Tench, A.J., Guerrero, V.L.L., and MacNeil, L.T. (2020). Cuticle collagen expression is regulated in response to environmental stimuli by the GATA transcription factor ELT-3 in *Caenorhabditis elegans*. *Genetics* 215.
- Moerman, D.G., and Williams, B.D. (2006). Sarcomere assembly in *C. elegans* muscle. *WormBook*.
- Mullen, G.P., Rogalski, T.M., Bush, J.A., Gorji, P.R., and Moerman, D.G. (1999). Complex patterns of alternative splicing mediate the spatial and temporal distribution of perlecan/UNC-52 in *Caenorhabditis elegans*. *Mol. Biol. Cell* 10.
- Murphy, C.T., McCarroll, S.A., Bargmann, C.I., Fraser, A., Kamath, R.S., Ahringer, J., Li, H., and Kenyon, C. (2003). Genes that act downstream of DAF-16 to influence the lifespan of *Caenorhabditis elegans*. *Nature* 424.
- Myllyharju, J., and Kivirikko, K.I. (2004). Collagens, modifying enzymes and their mutations in

humans, flies and worms. *Trends Genet.* 20, 33–43.

Olshansky, S.J., Carnes, B.A., and Cassel, C. (1990). In search of methuselah: Estimating the upper limits to human longevity. *Science* (80-.). 250.

Onken, B., and Driscoll, M. (2010). Metformin induces a dietary restriction-like state and the oxidative stress response to extend *C. elegans* healthspan via AMPK, LKB1, and SKN-1. *PLoS One* 5.

Page, A.P., and Johnstone, I.L. (2007). The cuticle. *WormBook*.

Passarino, G., De Rango, F., and Montesanto, A. (2016). Human longevity: Genetics or Lifestyle? It takes two to tango. *Immun. Ageing* 13.

Paul, R.G., and Bailey, A.J. (1996). Glycation of collagen: The basis of its central role in the late complications of ageing and diabetes. *Int. J. Biochem. Cell Biol.* 28.

Phillip, J.M., Aifuwa, I., Walston, J., and Wirtz, D. (2015). The Mechanobiology of Aging. *Annu. Rev. Biomed. Eng.* 17.

Ricard-Blum, S. (2011). The collagen family. *Cold Spring Harb. Perspect. Biol.* 3, 1–19.

Rogalski, T.M., Gilchrist, E.J., Mullen, G.P., and Moerman, D.G. (1995). Mutations in the *unc-52* gene responsible for body wall muscle defects in adult *Caenorhabditis elegans* are located in alternatively spliced exons. *Genetics* 139.

Rual, J.F., Ceron, J., Koreth, J., Hao, T., Nicot, A.S., Hirozane-Kishikawa, T., Vandenhoute, J., Orkin, S.H., Hill, D.E., van den Heuvel, S., et al. (2004). Toward improving *Caenorhabditis elegans* phenome mapping with an ORFeome-based RNAi library. *Genome Res.* 14, 2162–2168.

Sánchez-Blanco, A., and Kim, S.K. (2011). Variable pathogenicity determines individual lifespan in *caenorhabditis elegans*. *PLoS Genet.* 7.

Shaye, D.D., and Greenwald, I. (2011). Ortholist: A compendium of *C. elegans* genes with human orthologs. *PLoS One* 6.

Shi, Y., Hu, X., Cheng, J., Zhang, X., Zhao, F., Shi, W., Ren, B., Yu, H., Yang, P., Li, Z., et al. (2019). A small molecule promotes cartilage extracellular matrix generation and inhibits osteoarthritis development. *Nat. Commun.* 10.

Shoulders, M.D., and Raines, R.T. (2009). Collagen Structure and Stability. *Annu. Rev. Biochem.* 78, 929–958.

Snedeker, J.G., and Gautieri, A. (2014). The role of collagen crosslinks in ageing and diabetes - the good, the bad, and the ugly. *Muscles. Ligaments Tendons J.* 4, 303–308.

Sroga, G.E., and Vashishth, D. (2012). Effects of bone matrix proteins on fracture and fragility in osteoporosis. *Curr. Osteoporos. Rep.* 10.

-
- Sulston, J.E., Schierenberg, E., White, J.G., and Thomson, J.N. (1983). The embryonic cell lineage of the nematode *Caenorhabditis elegans*. *Dev. Biol.* 100.
- Tabara, H., Sarkissian, M., Kelly, W.G., Fleenor, J., Grishok, A., Timmons, L., Fire, A., and Mello, C.C. (1999). The *rde-1* gene, RNA interference, and transposon silencing in *C. elegans*. *Cell* 99.
- Teuscher, A.C., Jongsma, E., Davis, M.N., Statzer, C., Gebauer, J.M., Naba, A., and Ewald, C.Y. (2019). The in-silico characterization of the *Caenorhabditis elegans* matrisome and proposal of a novel collagen classification. *Matrix Biol. Plus* 1–13.
- Thomas B. L. Kirkwood (2008). A new look at an old problem. *Nature* 451, 1–5.
- Timmons, L., and Fire, A. (1998). Specific interference by ingested dsRNA [10]. *Nature* 395.
- Tissenbaum, H.A. (2015). Using *C. elegans* for aging research. *Invertebr. Reprod. Dev.* 59, 59–63.
- Toyama, B.H., and Hetzer, M.W. (2013). Protein homeostasis: Live long, won't prosper. *Nat. Rev. Mol. Cell Biol.* 14.
- Uno, M., and Nishida, E. (2016). Lifespan-regulating genes in *c. Elegans*. *Npj Aging Mech. Dis.* 2.
- Valiathan, R.R., Marco, M., Leitinger, B., Kleer, C.G., and Fridman, R. (2012). Discoidin domain receptor tyrosine kinases: New players in cancer progression. *Cancer Metastasis Rev.* 31.
- Vanacore, R., Ham, A.J.L., Voehler, M., Sanders, C.R., Conrads, T.P., Veenstra, T.D., Sharpless, B., Dawson, P.E., and Hudson, B.G. (2009). A Sulfilimine Bond Identified in Collagen IV. *Science* (80-.). 325.
- Vellai, T., Takacs-Vellai, K., Zhang, Y., Kovacs, A.L., Orosz, L., and Müller, F. (2003). Influence of TOR kinase on lifespan in *C. elegans*. *Nature* 426, 620–620.
- Vogél, B.E., and Hedgecock, E.M. (2001). Hemicentin, a conserved extracellular member of the immunoglobulin superfamily, organizes epithelial and other cell attachments into oriented line-shaped junctions. *Development* 128.
- Wang, H., Zhao, Y., and Zhang, Z. (2019). Age-dependent effects of floxuridine (FUdR) on senescent pathology and mortality in the nematode *Caenorhabditis elegans*. *Biochem. Biophys. Res. Commun.* 509.
- Wang, N., Tytell, J.D., and Ingber, D.E. (2009). Mechanotransduction at a distance: Mechanically coupling the extracellular matrix with the nucleus. *Nat. Rev. Mol. Cell Biol.* 10.
- Wilkinson, J.E., Burmeister, L., Brooks, S. V., Chan, C.C., Friedline, S., Harrison, D.E., Hejtmancik, J.F., Nadon, N., Strong, R., Wood, L.K., et al. (2012). Rapamycin slows aging in

mice. *Aging Cell* 11, 675–682.

Woo, W.M., Goncharov, A., Jin, Y., and Chisholm, A.D. (2004). Intermediate filaments are required for *C. elegans* epidermal elongation. *Dev. Biol.* 267.

World Health Organization (2018). WHO | Ageing and health. Website WHO; Media Cent.

Xu, H., Bihan, D., Chang, F., Huang, P.H., Farndale, R.W., and Leitinger, B. (2012). Discoidin Domain Receptors Promote $\alpha1\beta1$ - and $\alpha2\beta1$ -Integrin Mediated Cell Adhesion to Collagen by Enhancing Integrin Activation. *PLoS One* 7.

Yue, B. (2014). Biology of the extracellular matrix: An overview. *J. Glaucoma* 23.

Zamir, E., and Geiger, B. (2001). Molecular complexity and dynamics of cell-matrix adhesions. *J. Cell Sci.* 114.

Zhang, H., and Labouesse, M. (2010). The making of hemidesmosome structures in vivo. *Dev. Dyn.* 239.

2. Scope of the thesis

In this thesis we aimed to gain a deeper understanding of the role of the ECM during aging. As mentioned above, previous studies have shown a connection between the ECM and longevity as well as the importance of ECM integrity for healthy aging. But the mechanisms by which the ECM can elongate the lifespan of *C. elegans* is still unknown nor do we know how the ECM itself is regulated/maintained during aging.

Therefore, I used the model organism *C. elegans* to investigate the following problems and questions:

1. Assembling a list of all important ECM proteins in *C. elegans* proved to be a challenge as some were poorly defined in *C. elegans* and/ or were difficult to find using GO terms alone. Additionally, we were not only interested in genes located in the extracellular region, but also in genes that regulate the ECM. Therefore, we joined forces with Alexandra Naba's lab and Jan Gebauer in order to define the *in-silico* *C. elegans* matrisome.
2. Using common GFP filter sets to image the Collagen::GFP strains was impossible as the continuous increase of autofluorescent age-pigments from the *C. elegans* intestine masked the fluorescence from GFP signal. We therefore developed a novel combination of a triple-band filter set, that separates GFP from autofluorescence.
3. To gain insights into the collagen deposition during aging, we aimed to increase our toolbox. Therefore, we introduced and established the trichrome Herovici collagen staining for *C. elegans*.
4. We used the knowledge and tools from 1.-3. to work on the main question of this thesis: Identification of regulators and mechanisms involved in the enhancement of ECM and the promotion of longevity and healthy aging.

3. The *in-silico* characterization of the *Caenorhabditis elegans* matrisome and proposal of a novel collagen classification

Alina C. Teuscher¹, Elisabeth Jongsma¹, Martin N. Davis², Cyril Statzer¹, Jan M. Gebauer^{3*}, Alexandra Naba^{2,4*}, and Collin Y. Ewald^{1*}

Matrix Biology Plus. 2019 <https://doi.org/10.1016/j.mbplus.2018.11.001>

In this chapter we define the *in-silico* matrisome of *C. elegans*. The matrisome list is a compendium of all proteins that are part of the extracellular matrix or contribute to it. In collaboration with Alexandra Naba's lab, which was already involved in the characterization of the human, mice and zebrafish matrisome (Hynes and Naba, 2012; Naba et al., 2011; Nauroy et al., 2018) Jan Gebauer, a structural biologist, we combined gene-, protein-sequence analysis and excessive literature research to predict the *C. elegans* matrisome. This definition of the matrisome serves as the foundation for the experimental analysis of the extracellular matrix (ECM) and as a tool to analyze -omics data.

Websites and tools for the matrisome:

Matrisome list:

<http://matrisome.org/>

database for cuticular collagens (by Jan Gebauer):

<http://CeColDB.permalink.cc/>

Matrisome Annotator (by Cyril Statzer):

ec2-3-120-159-30.eu-central-1.compute.amazonaws.com:3838/ubuntu/ecm_analyzer/

I contributed to the *in-silico*-analysis of the Matrisome, especially for the *C. elegans* orthologues of human matrisome genes and GO terms. Furthermore, I participated in data mining (wormbase), literature research and writing of the manuscript.



The *in-silico* characterization of the *Caenorhabditis elegans* matrisome and proposal of a novel collagen classification



Alina C. Teuscher^a, Elisabeth Jongsma^a, Martin N. Davis^b, Cyril Statzer^a, Jan M. Gebauer^c, Alexandra Naba^{b,d} and Collin Y. Ewald^a

a - Eidgenössische Technische Hochschule (ETH) Zürich, Department of Health Sciences and Technology, Institute of Translational Medicine, Schwerzenbach, Zürich, Switzerland

b - Department of Physiology and Biophysics, University of Illinois at Chicago, Chicago, IL 60612, USA

c - Institute of Biochemistry, University of Cologne, Cologne, Germany

d - University of Illinois Cancer Center, Chicago, IL 60612, USA

Correspondence to Jan M. Gebauer, Alexandra Naba and Collin Y. Ewald: Co-corresponding authors. jan.gebauer@uni-koeln.de, anaba@uic.edu, collin-ewald@ethz.ch.

jan.gebauer@uni-koeln.de, anaba@uic.edu, collin-ewald@ethz.ch.

<https://doi.org/10.1016/j.mbplus.2018.11.001>

Abstract

Proteins are the building blocks of life. While proteins and their localization within cells and sub-cellular compartments are well defined, the proteins predicted to be secreted to form the extracellular matrix - or matrisome - remain elusive in the model organism *C. elegans*. Here, we used a bioinformatic approach combining gene orthology and protein structure analysis and an extensive curation of the literature to define the *C. elegans* matrisome. Similar to the human genome, we found that 719 out of ~20,000 genes (~4%) of the *C. elegans* genome encodes matrisome proteins, including 181 collagens, 35 glycoproteins, 10 proteoglycans, and 493 matrisome-associated proteins. We report that 173 out of the 181 collagen genes are unique to nematodes and are predicted to encode cuticular collagens, which we are proposing to group into five clusters. To facilitate the use of our lists and classification by the scientific community, we developed an automated annotation tool to identify ECM components in large datasets. We also established a novel database of all *C. elegans* collagens (CeCoIDB). Last, we provide examples of how the newly defined *C. elegans* matrisome can be used for annotations and gene ontology analyses of transcriptomic, proteomic, and RNAi screening data. Because *C. elegans* is a widely used model organism for high throughput genetic and drug screens, and to study biological and pathological processes, the conserved matrisome genes may aid in identifying potential drug targets. In addition, the nematode-specific matrisome may be exploited for targeting parasitic infection of man and crops.

© 2018 The Author(s). Published by Elsevier B.V. This is an open access article under the CC BY-NC-ND license (<http://creativecommons.org/licenses/by-nc-nd/4.0/>).

Introduction

Around one third of the human world population, including a majority of children, is infected by parasitic nematodes [1,2]. In addition, plant-parasitic nematodes are one of the most infectious species in agriculture with an impact on economic loss of about 100 billion dollars per year [3]. The major barriers for drugs to penetrate parasitic nematodes are its collagenous cuticle, an exoskeleton, and an extracellular matrix (ECM). The free-living nematode *C.*

elegans has been widely used as a surrogate model organism for parasitic nematodes [4], as well as for host-pathogen interactions [5], and other fundamental biological processes [6]. *C. elegans* is also used as a pioneering in-vivo model for biomedical research because about 40% of *C. elegans* genes are conserved in the human genome [7], and vice versa between 60 and 80% of human genes have a corresponding orthologue in the *C. elegans* genome [8]. In addition, 40% of human genes associated with diseases are well conserved in *C. elegans* [9]. *C.*

C. elegans is genetically tractable for high throughput screens and is one of the best curated organisms for genetic, genomic, and phenotypic data. The vast array of openly shared molecular tools paved the way to gain molecular, functional, and mechanistic insights into gene and protein functions [8]. In particular, the two major extracellular matrices of *C. elegans*, the cuticle [10] and basement membrane [11–13], have recently become models to study cancer cell invasion [14] and aging [15]. However, a precise Gene Ontology term or a comprehensive compendium of genes predicted to form the *C. elegans* matrisome remains to be defined.

Using characteristic features of ECM proteins and a computational pipeline combining interrogation of protein and gene databases, we previously defined the matrisome as the ensemble of ECM and ECM-associated proteins [16–18]. In mammals, the matrisome represents 4% of the genome, or approximately 1000 genes. We further classified these genes into core matrisome components, consisting of collagens, proteoglycans, and glycoproteins (including laminins, fibronectins, etc.), and matrisome-associated components, including proteins that could incorporate into ECMs or are co-purified with ECM proteins. These components are further subdivided into ECM-affiliated proteins (e.g., C-type lectins, galectins, annexins, semaphorins, syndecans, and glypicans), ECM regulators (e.g., MMPs, ADAMs, and crosslinking enzymes), and secreted factors (e.g., TGF- β , BMPs, FGFs, Wnt proteins, and chemokines) [16–18]. More recently, we employed a computational approach to predict the *in-silico* matrisome of the zebrafish [19]. Defining the matrisome of organisms has been instrumental

to annotate transcriptomic and proteomic data and has permitted the identification of ECM signatures of biological processes [20] and of human diseases including cancers and fibrosis [21–25].

Here, we devised a novel bioinformatic pipeline combining gene orthology and *de-novo* identification to define the *C. elegans* matrisome. We report the identification of 719 genes potentially encoding ECM and ECM-associated proteins, including 181 collagens of which 173 are predicted to be components of the cuticle. Based on their collagen-domain organization, we propose to group these cuticular collagens into five novel clusters and further divide them in sub-clusters. In addition, we demonstrate that the newly defined *C. elegans* matrisome can be used to annotate data from high throughput RNAi screens, transcriptomic, and proteomic data, and can assist with the identification of ECM genes or signatures relevant in the context of various physiological and pathological processes.

Computational approach to define the *C. elegans* matrisome

The workflow and steps for defining the *C. elegans* matrisome are outlined in Fig. 1.

Identification of *C. elegans* orthologues of human matrisome genes

The orthologue list was created by comparing the human matrisome gene list downloaded from the Matrisome Project website (<http://matrisome.org/>) [26] with the *C. elegans* genome using the Greenwald Lab

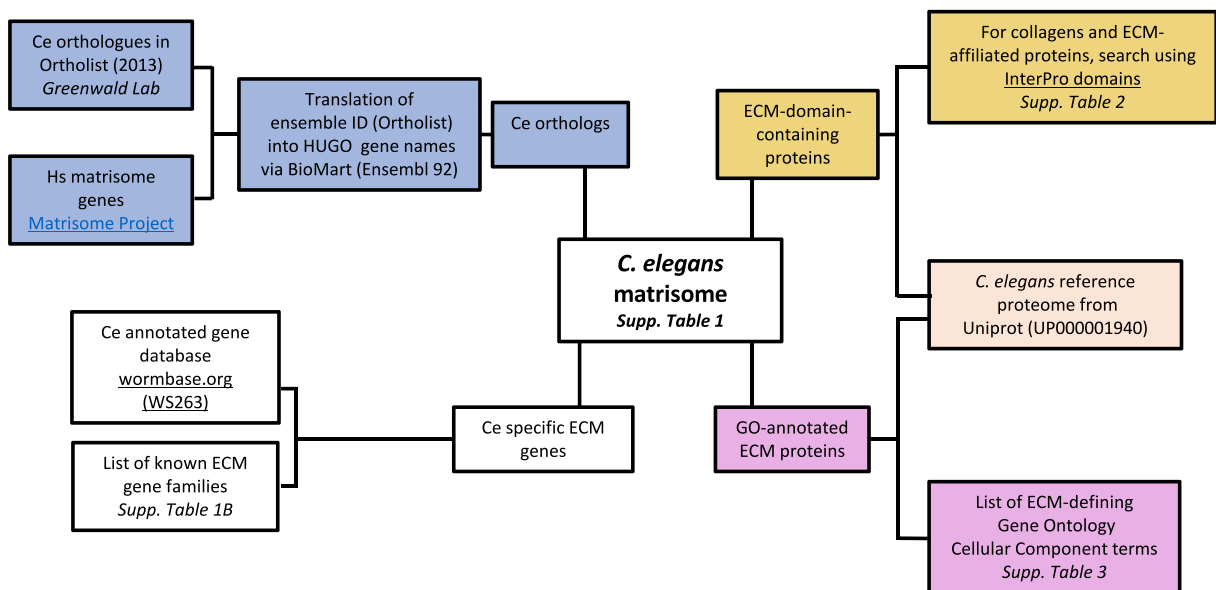


Fig. 1. Workflow of the pipeline devised to define the *in-silico* *C. elegans* matrisome.

Table 1.

Comparison of the number of human to *C. elegans* matrisome genes. Corresponding genes for each category are found in Supplementary Table 1.

		Human	<i>C. elegans</i>
Complete matrisome		1027	719
Core matrisome	ECM glycoproteins	195	35
	Collagens	44	181
	Proteoglycans	35	10
	Cuticlins	0	12
	Total	274	238
Matrisome-associated	ECM-affiliated proteins	171	301
	ECM regulators	238	128
	Secreted factors	344	52
	Total	753	481

OrthoList website (<http://greenwalddlab.org/ortholist/>; accessed 07.04.2017, [7]). The OrthoList uses four different orthology-prediction programs (Ensembl Compara, In Paranoïd, Homologene, and OrthoMCL) to obtain the *C. elegans* orthologues from human Ensembl ID numbers. We included all genes that were found by at least one prediction program from the OrthoList. The human Ensembl IDs were then translated back into HUGO gene names using Ensembl BioMart [27]. This approach allows the identification of 348 *C. elegans* genes orthologous to human matrisome genes (Supplementary Table 1).

Domain-based definition and Gene Ontology annotations of matrisome proteins

We initially defined the mammalian matrisome by using the presence of characteristic protein domains commonly found in ECM proteins [17,18]. To verify that the orthology approach identified key components of the *C. elegans* matrisome, we focused on a specific category of matrisome proteins: the ECM-affiliated proteins, which are proteins that share structural and functional homologies with ECM components [17,18]. To do so, we retrieved the *C. elegans* reference

proteome (UP000001940 downloaded August 14, 2017; Supplementary Table 2A) from the UniProt database [28] and identified proteins containing domains previously defined as characteristic of the 6 families of ECM-affiliated components (Fig. 1 and Supplementary Table 2B): the transmembrane proteoglycans syndecans and glypicans, the galectins, the plexins and semaphorins, and the annexins. Comparison of the list of proteins obtained using this approach (Supplementary Table 2C–H) and the list of genes identified by orthology revealed that all but 2 ECM-affiliated proteins were found by both approaches (Supplementary Table 1), suggesting that both approaches may be used to define the complete matrisome. However, the orthology-based approach does not permit to identify nematode-specific ECM proteins. One ECM structure specific to *C. elegans* is the cuticle. It is made of cuticular collagens and cuticlins [10,29,30]. To define the ensemble of proteins potentially contributing to cuticle ECM, we identified an InterPro domain termed “Nematode cuticle collagen, N-terminal” (InterPro domain IPR002486; [31]), this domain retrieved 171 UniProt entries in the *C. elegans* proteome, out of which 128 also contain the canonical collagen triple helix repeat (IPR008160) (Supplementary Table S2I and J). Close examination of the list of collagen genes obtained revealed that some might not have been found using the InterPro domain. We thus further sought to define *C. elegans* collagens using a more rigorous structure-based approach.

De-novo identification of *C. elegans* collagens

To identify in an unbiased manner and *de-novo* all the collagen proteins in *C. elegans*, we downloaded all reviewed and unreviewed protein entries from the UniProt database (release 2018_01; [28]). Using HMMER3 [32] and the standard HMM profile (PF01391) for collagens from the Pfam website [33] identified 219 sequences, which included several duplicated entries. However, this approach missed

Table 2.

Comparison of conserved versus nematode-specific matrisome genes. Corresponding genes for each category are found in Supplementary Table 1.

		Conserved matrisome	Nematode-specific matrisome
		Human to <i>C. elegans</i> orthologues [# found/total (percentage)]	Not found in mammals [# found/total (percentage)]
Complete matrisome		467/1027 (45%)	252/719 (35%)
Core matrisome	ECM glycoproteins	35/195 (18%)	0/35 (0%)
	Collagens	4/44 (9%)	177/181 (98%)
	Proteoglycans	3/35 (9%)	7/10 (70%)
	Cuticlins	–	12/12 (100%)
	Total	42/274 (15%)	196/238 (82%)
Matrisome-associated	ECM-affiliated proteins	290/171 (170%)	11/301 (4%)
	ECM regulators	97/238 (41%)	31/128 (24%)
	Secreted factors	38/344 (11%)	14/52 (27%)
	Total	425/753 (56%)	56/481 (12%)

various bona fide collagens in *C. elegans*, such as *col-51* and *col-142*, probably due to their small collagenous domains interrupted by non-collagenous stretches. Collagen domains are characterized by their glycine-X-Y amino acid triplet repeats, whereby X and Y are frequently proline and 4-hydroxyproline residues, respectively. *In vitro*, 10 Gly-X-Y repeats are typically sufficient to form stable triple helices with melting temperatures, depending on the content of proline and hydroxyproline residues on the X and Y positions. Therefore, for a more sensitive approach, we generated a simple regular expression in Python matching at least 10 Gly-X-Y repeats (regex = r(G.){10,}) and used it against the above-mentioned dataset. In total, we found 243 entries in the UniProt database matching this pattern. After deleting duplicated entries and cross-referencing against WormBase (WS262) [34], we obtained a list of 201 unique entries. However, besides a repeating Gly-X-Y pattern, collagens also need frequent proline residues at the X and Y positions as this amino acid is important for the formation of single poly-proline II helices, which are the backbone of the collagen triple helix. In vertebrates, the percentage of proline residues at the X and Y position is approximately 30%. To avoid missing any potential sequences, we decided to use a cut-off of 10% proline at both positions, which still represents the double of the normal frequency of proline residues in the *C. elegans* proteome [35]. With this criterion, the list was narrowed to 190 potential collagen sequences, which were all curated manually for the likelihood of being a collagen. Five sequences (UniProt Q4W4Y5, G5EDS0, B3GWA1, O61209, Q9N3I0) were excluded, since they contain short glycine rich repeats, with only very few proline residues and no apparent collagen structures. These five proteins were also not recognized by the Pfam collagen profile. On the other hand, various sequences were not predicted to be collagen by the Pfam profile, but upon manual inspection have proper collagen domains (COL-51, COL-103, COL-161, COLI-142 and COL-183). Finally, after manual curation, we identified 185 genes in total that encode collagen-domain containing proteins in *C. elegans* (Supplementary Table 4). Of these, 4 genes could be classified as gliomedins or collectins based on their small collagenous domain and the presence of further signature domains (*see below*). The remaining 181 proteins define the existent collagens in *C. elegans*.

The *C. elegans* matrisome consists of 719 genes

After combining the lists of genes and proteins identified above, we manually curated each entry and assigned them to matrisome divisions and categories. Last, in order to identify putative matrisome genes and proteins that have not been captured by the gene orthology approach or the structural domain-based approach, we searched both WormBase (<http://www.wormbase.org/>, release WS263; [34]) and the *C.*

elegans reference proteome from UniProt to identify genes and proteins annotated as ECM genes by a selection of Gene Ontology – Cellular Component terms (Supplementary Table 3). This last step allowed us to identify an additional 11 genes that had not been identified otherwise and may be considered as matrisome components (Supplementary Table 1; see Column A, with the exception of *col-78*, which was identified earlier by the structural domain-based approach).

Altogether, we identified 719 *C. elegans* matrisome genes out of the total ~20,000 *C. elegans* protein-encoding genes, suggesting that 4% of the *C. elegans* genome is dedicated to ECM genes (Table 1; Supplementary Table 1). This is comparable to the 1027 human matrisome genes, which also represents about 4% the human genome [17,26]. We further classified these 719 genes into divisions and categories proposed to classify the mammalian matrisomes. We found 226 genes for the *C. elegans* core-matrisome (ECM glycoproteins, collagens, proteoglycans). 181 out of the 226 core-matrisome genes are collagen genes (Table 1), of which 173 are predicted to be nematode-specific cuticular collagens (*see below*). We found that the *C. elegans* genome encodes 35 ECM glycoproteins compared to 195 found in humans (Table 1). All 35 *C. elegans* ECM glycoproteins have mammalian orthologues and thus far no *C. elegans*-specific ECM glycoprotein was identified (Table 2). By contrast, 7 out of the 10 *C. elegans* proteoglycans are nematode-specific and several are sulfate-less-chondroitin-binding proteoglycans (*cpg-1-4*, *cpg-7-9*) [36]. The remaining three proteoglycans are similar to the heparan sulfate proteoglycan perlecan (*unc-52*; *Hspg2 in mammals*) [13], a SPOCK/Testican (*test-1*), and a leucine-rich proteoglycan nycalopin (*Iron-8*) (Supplementary Table 1).

The *C. elegans* genome comprises 493 matrisome-associated genes (ECM-affiliated proteins, ECM regulators, and secreted factors) compared to the 753 human matrisome-associated genes. The majority of these 493 *C. elegans* matrisome-associated genes are C-type lectins (240 genes; Table 1 and Supplementary Table 1) [37].

Orthology relationship between human and *C. elegans* matrisome genes

Next, we determined the conserved versus nematode-specific matrisome genes for each matrisome category (Table 2). We compared the human matrisome genes to the *C. elegans* matrisome genes and vice-versa using OrthoList [7], or directly aligned them and examined the conservation of domains. In agreement with previous reports [10,38], most of the *C. elegans* collagens are predicted to be cuticular collagens that share no or little orthology to mammalian collagens (Table 2). However, other collagens and

ECM proteins that originated in basal metazoans are found to be well conserved in *C. elegans* (Fig. 2). These include basement membrane proteins (laminins, collagen type IV, nidogen, perlecan), transmembrane proteoglycans classified as ECM-affiliated proteins, syndecan and glypican, other collagens (type IX, XVIII, and XXV collagens), and axon guidance proteins (netrins, slits, agrin, fibrillin) (Fig. 2). Although thrombospondins are found in metazoans and we found many *C. elegans* proteins containing thrombospondin domains, we did not find a thrombospondin orthologue in agreement with previous reports [39]. Furthermore, ECM proteins that evolved during the vertebrate expansions, such as fibronectin, complex collagens, LINK proteins, and hyalectans (Fig. 2), were not identified in the *in-silico* searches in *C. elegans*, consistent with previous reports [16]. Last, some ECM proteins identified are shared between nematodes and humans, but not with other organisms like yeasts or *Drosophila*. These proteins include hemicentin (*him-4*) [40], SPARC/osteonectin (*ost-1*) [41,42], fibulin (*fbf-1*) [43], spondin (*spon-1*) [44], and olfactomedin (*unc-122*) [45].

Taken together, our survey of the *C. elegans* genome and proteome provides the first comprehensive compendium of the *C. elegans* matrisome. To facilitate the use of our lists of predicted genes encoding ECM and ECM-associated proteins in the *C. elegans* genome, we have deposited them on a dedicated page of the Matrisome Project website

(<http://matrisome.org>) [26]. In addition, we have built an online tool, the *C. elegans* Matrisome Annotator, which, provided a list of genes, returns it annotated for matrisome components (<http://ce-matrisome-annotator.permalink.cc/>; tutorial provided as Supplementary Data).

Proposal of a novel classification of *C. elegans* collagens

In order to better classify and study the 185 collagen-domain-containing proteins in *C. elegans*, we propose to define a novel nomenclature based on their collagen-domain organization and the addition of other characteristic protein domains (e.g. C-type lectin; C4, the collagen IV NC1 domain; TSP; FNIII), similar to the mammalian collagen classification [46]. To do so, we clustered the 181 collagens and the 4 collagen-domain containing proteins into four major groups: (1) the vertebrate-like collagens (similar to mammalian type IV, XVIII, XXV), (2) the collagen-domain-containing proteins with mammalian orthologues (collectins and gliomedin), (3) the non-cuticular collagens with no clear orthology to mammalian collagens, and (4) the cuticular collagens. This last group contains the largest number of 173 collagens and which we further propose to subdivide into five main clusters (A to E). For detailed comparison and to facilitate the

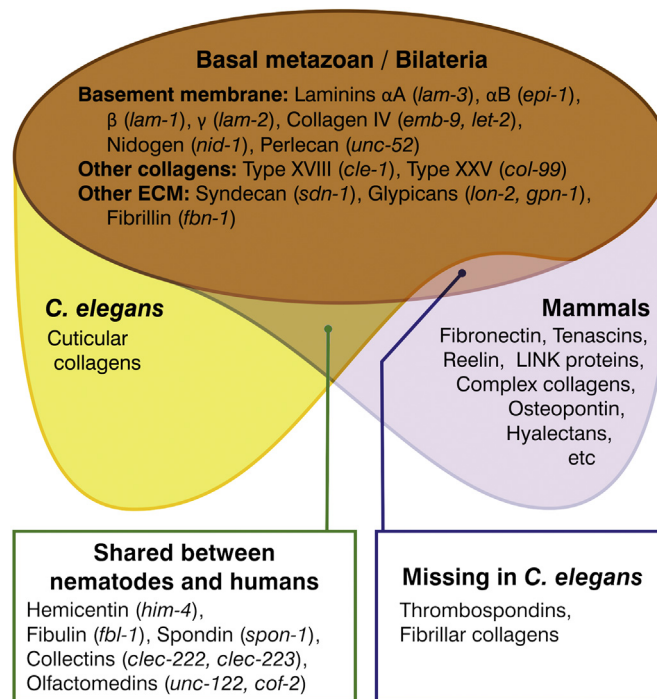


Fig. 2. Conserved *C. elegans* matrisome in the context of the evolution of ECM proteins. Figure is adapted from [16]. Corresponding *C. elegans* orthologues are italicized and indicate in parenthesis e.g. (*lam-1*). Individual genes and corresponding orthologues are found in Supplementary Table 1.

diffusion of this proposed classification, we constructed the *C. elegans* collagen database, CeColDB, available at: <http://CeColDB.permalink.cc/>.

Group 1: the conserved vertebrate-like collagens in *C. elegans*

Although fibrillar collagens are found in metazoans [47,48], our computational approach did not find any genes encoding fibrillar collagens in the *C. elegans* genome, which is in agreement with previous reports [49]. It has been hypothesized that *C. elegans* might have lost fibrillar collagens, since no evidence for an interstitial matrix is found in *C. elegans* [14,49,50]. However, the basement membrane type IV collagens are well conserved in *C. elegans* [13]. The *C. elegans* collagen-IV-like proteins are encoded by two genes *emb-9* and *let-2*, which both have collagenous domains of 1488 and 1487 amino acids, respectively, similar to their vertebrate (1398 amino acids) counterparts (Fig. 3A). The C-terminal domain (C4) is well conserved and the sequence identity of 52% and 69% among the nematode and human domains are similar to the variance in the 6 existing human genes. In phylogenetic analyses, the C-terminal domain of LET-2 consistently clusters with the even-numbered collagen alpha chains ($\alpha 2$ (IV), $\alpha 4$ (IV) and $\alpha 6$ (IV)), while EMB-9 groups with the odd-numbered collagen IV chains ($\alpha 1$ (IV), $\alpha 3$ (IV) and $\alpha 5$ (IV)) (Fig. 3B). In humans, heterotrimers of collagen IV are formed by one even-numbered and two odd-numbered chains ($[\alpha 1]_2[\alpha 2]$, $[\alpha 3][\alpha 4][\alpha 5]$, $[\alpha 5]_2[\alpha 6]$). Thus, we speculate that the collagen IV in *C. elegans* is an [EMB-9]₂[LET-2] heterotrimer. In addition, *let-2* is alternatively spliced whereby one version is predominantly found in embryos and the other version in larval stages [51]. Both *emb-9* and *let-2* are essential genes and glycine mutations in the Gly-X-Y repeats result in retainment of this mutant collagen in the endoplasmic reticulum and arrest in embryonic development [52,53].

The *C. elegans* CLE-1 protein has similarities to collagen type XV [54] and XVIII [55]. CLE-1 is also found in basement membranes, but predominantly localized around neurons. Similar to the phenotype of the *Col18a1*-null mice [55], reduction of *C. elegans cle-1* function results in defects in the organization of the nervous system, but, in contrast, also results in a partially-penetrant embryonic lethality which may be due to failure of epidermal cell migration [56]. CLE-1 has one or two fibronectin-type-III-like domains, a laminin G-like domain, a very short interrupted collagenous domain, and an endostatin domain (Fig. 3C). Based on the last domains, CLE-1 is classified as an orthologue of collagen type XV [54] or XVIII [55], however, it is worth noting that the overall sequence identity is only 14% and 18% for collagen XV and XVIII, respectively, and the collagenous domain of CLE-1 is short in contrast to collagen XV or XVIII. The *C. elegans*

collagen COL-99 is also not an essential protein, but is important for the organization of the nervous system [57]. COL-99 is a type II transmembrane-domain-containing protein with a smaller cytoplasmic region and a larger extracellular region containing 10 smaller collagenous domains. It therefore formally groups with the vertebrate Membrane-Associated Collagens with Interrupted Triple-helices (MACITs: collagen types XIII, XXIII, and XXV; Fig. 3D) [58].

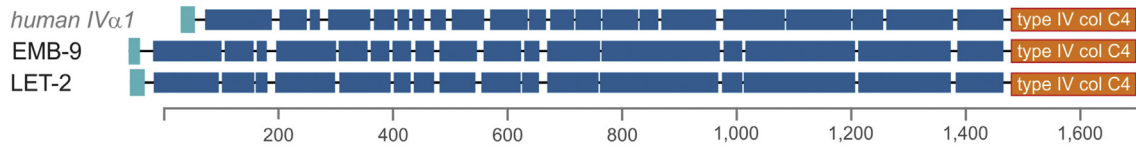
Group 2: collagen-domain-containing proteins with mammalian orthologues

We identified four collagens with additional non-collagenous domains, which, based on their domain organization, resemble mammalian gliomedins and collectins. The group of gliomedin-like proteins consists of *cof-2* and *unc-122*. Both have a predicted N-terminal transmembrane domain, followed by a collagenous domain of 15 triplets and a C-terminal olfactomedin-like domain (Fig. 4A). However, despite their similar domain organization both proteins only share approximately 26% sequence identity with each other. Mutations in *unc-122* cause an uncoordinated locomotory behavior, the so-called Unc phenotype [59]. The group of collectins harbours two genes (*clcc-222* and *clcc-223*) which are oriented in a head-to-tail fashion on chromosome V. Both have very short collagenous domains (10 triplets), which might still permit trimerization and 1 or 3 C-type lectin domains (Fig. 4B).

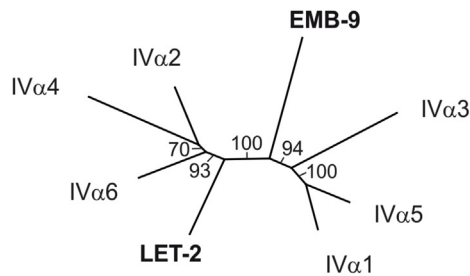
Group 3: the *C. elegans* non-cuticular collagens with no clear orthology to mammalian collagens

This group consists of four collagens that cluster neither with basement membrane or vertebrate-like collagens nor with cuticular collagens. We can speculate that they might have specialized functions or localize to other ECMs than the basement membrane or the cuticle. MEC-5 is a collagen of medium size with a short collagen domain, similar to the N-terminal pro-helices found in fibrillar collagens, followed by a major uninterrupted collagenous domain. There is no further domain predicted and no obvious similarities to vertebrate collagens (Fig. 4C). The MEC-5 collagen is produced and secreted from hypodermal cells to anchor the ion channel/degenerin complex (MEC-4/10) that is expressed from touch receptor neurons to the ECM and thus MEC-5 is essential for the mechanosensory response to gentle touch [60,61]. COL-55 and ROL-8 are similar to the cuticular collagens discussed below, but are missing certain features, like the N-Pro-helix or the characteristic cysteine knots. COL-55 and ROL-8 are predicted to have a transmembrane domain, which overlaps with the predicted N-cuticular domain (Fig. 4C). Mutations in *rol-8* cause a left-handed rolling phenotype (a helically twisted

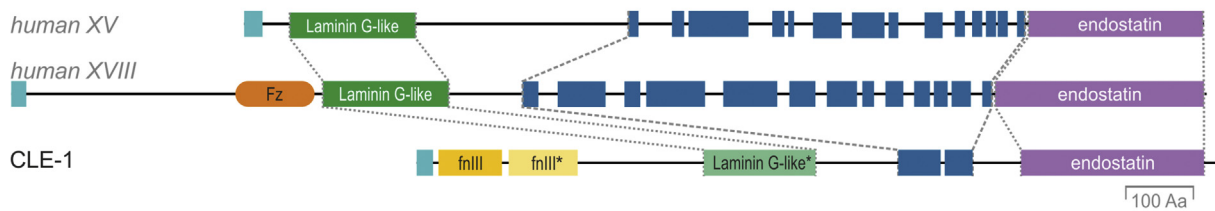
A Collagen type IV



B



C Endostatins



D Transmembrane collagens

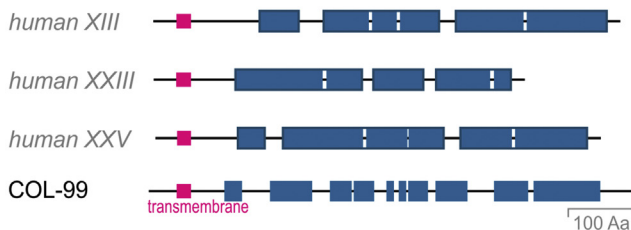


Fig. 3. Group 1: *C. elegans* collagens with orthologues in vertebrates. (A) Collagen type IV. Alignment of collagen type IV $\alpha 1$ from *Homo sapiens* with EMB-9 and LET-2 from *Caenorhabditis elegans*. (B) Phylogenetic analysis of collagen type IV. The C-terminal collagen type IV domains (C4) of humans and *C. elegans* were analyzed using ClustalO [70] followed by Neighbor Joining. The numbers indicate the bootstrap values of 100 replicates. The nematode-specific sequences are indicated in bold (EMB-9 and LET-2). (C) Endostatins. Comparison of CLE-1 from *C. elegans* with endostatin-containing collagens type XV and XVIII from *H. sapiens*. Asterisk (*) indicate domain predictions with weak significance. (D) Transmembrane collagens. Comparison of *C. elegans* COL-99, the only non-cuticular transmembrane collagen, with its human orthologues (collagens type XIII, XXIII, XXV). For human proteins, dark outlines group collagenous stretches recognized as collagen domains in earlier publications. All panels are drawn to scale. Colour codes are as follow: light blue: signal peptides; pink: transmembrane region; orange: frizzled domain or collagen C4 domain; yellow: Laminin G-like domain; purple: endostatin domain; blue: collagenous Gly-X-Y repeats.

body), suggesting its importance in cuticle assembly and/or chirality [62]. COL-135 has been predicted to be a collagen but has a very particular composition. Its sequence contains a signal peptide, three short collagen domains, and a rather large domain of Gly-

X-Y repeats. Proline residues are under-represented compared to other *C. elegans* collagens especially at the Y position (17.0% and 3.6% for X and Y in COL-135, 43.3% and 23.9% in all collagens), but lysine and aspartate residues are over-represented

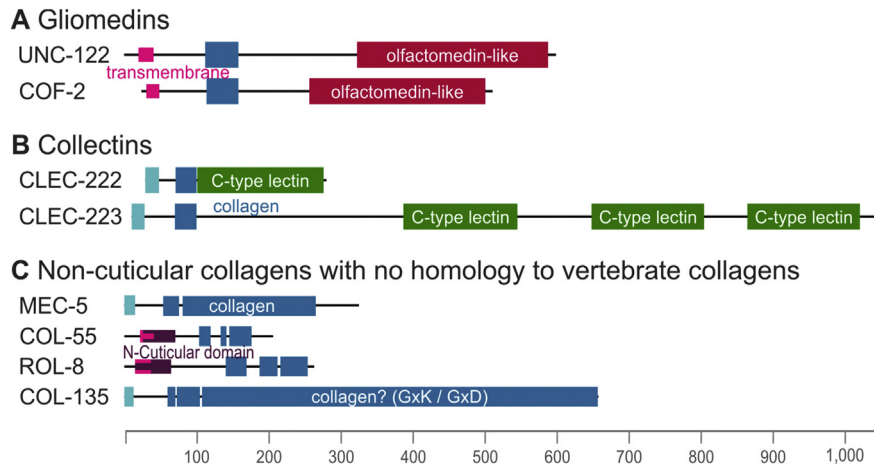


Fig. 4. Domain organization of *C. elegans* collagens from Group 2 and 3. (A-B) Group 2: Collagen-domain containing proteins with mammalian orthologues. (A) Gliomedin-like collagens are characterized by an olfactomedin-like domain. (B) Collectins carry C-type lectin domains and only small collagenous domains. (C) Group 3: The *C. elegans* non-cuticular collagens with no clear orthology to mammalian collagens. MEC-5 is a neuron-specific collagen. For COL-55 and ROL-8 the hypothetical Nematode cuticle collagen N-terminal domain (PF01484) overlaps with the predicted transmembrane domain. COL-135 is high in GxK and GxD repeats (Supplementary Fig. 1). All panels are drawn to a common scale. Colour codes are as follow: light blue: signal peptides; pink: transmembrane region; dark violet: N-cuticular domain (PF01484); green: C-type lectin; red: olfactomedin-like domain; blue: collagenous Gly-X-Y repeats.

(28.6% and 22.2%, respectively in COL-135, compared to 4.3% and 8.1% in all collagens) (Supplementary Fig. 1A). Furthermore, 109 out of the 198 triplets are Gly-X-Lys repeats (Supplementary Fig. 1B). Although COL-135 meets the criteria stated above for being recognized as a collagen, it is uncertain whether it is able to form a bona fide collagen triple helix.

Group 4: the cuticular collagens

Approximately 80% of the cuticle is made of collagenous proteins [29]. Previously, cuticular collagens were grouped according to their cysteine knots into 6 groups based on 20 collagen se-

quences known at that time [63]. Furthermore, these 20 known collagen sequences showed four shared amino-acid-sequence motifs (termed “homology blocks”) in the N-terminal region before the Gly-X-Y domains [63]. Expanding the analysis from 20 to the 173 cuticular collagen genes identified in our study, we did not identify these shared homology blocks. We found three conserved features which occur in various combinations in many but not all cuticular collagens: a serine (in position 21 in BLI-6 and position 78 in the alignment; conserved in 75% of all cuticular collagens), a potential furin cleavage site with an RxxR consensus (in position 71–74 and 195–198, respectively; 93% conservation), and a tyrosine (in

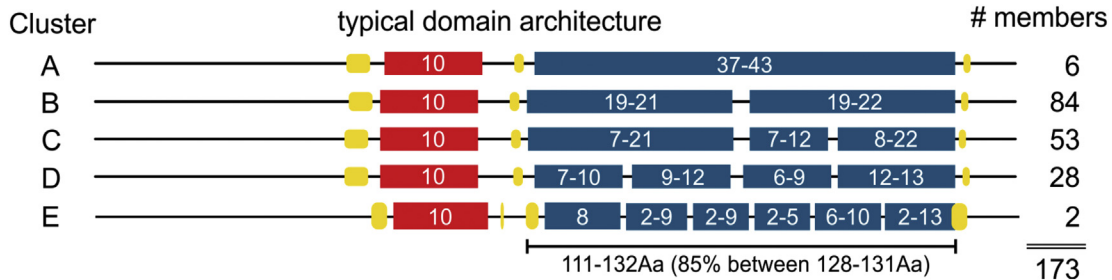


Fig. 5. Organization of the cuticular collagen clusters. The 173 cuticular collagens were grouped into 5 clusters based on the interruptions in their main collagenous domain (blue boxes). All cuticular collagens contain a shorter N-terminal helical domain (red box) and typically three cysteine-rich regions (yellow) flanking the collagenous domains. Numbers in the boxes correspond to the number of Gly-X-Y repeats.

position 78 and 273, respectively; approx. 50% conservation) that may be important for tyrosine-tyrosine crosslinking (Supplementary Fig. 2).

Here, we defined the cuticular collagens based on their characteristic collagenous domains consisting of 37 to 43 Gly-X-Y triplets, which are flanked by N- and C-terminal cysteine knots (Fig. 5; Supplementary Table 4). As in fibrillar collagens found in vertebrates, there is an additional N-Pro-helix of usually 10 G-X-Y repeats long located between 12 and 31 residues (in 97% of the cases between 13 and 23) N-terminally of the collagenous domain. This N-Pro-helix is often stabilized by an additional cysteine knot (Fig. 5; Supplementary Table 4). Based on the interruptions in their main collagenous domain, we grouped the cuticular collagens into five main clusters (A to E), having either 0, 1, 2, 3, or >3 interruptions (Fig. 5; Supplementary Table 4). We further classified these five main clusters based on the length of their collagenous domains, the positions of interruptions, and their prediction of being transmembrane or secreted (Supplementary Figs. 3–7; Supplementary Table 4). These sub-clusters are numbered based on the length of their uninterrupted collagenous stretches, counting from the C-terminus in an ascending manner (Supplementary Table 4). Members of a sub-cluster often have the same cysteine knot (Supplementary Table 4) although the same cysteine knot might also occur in different clusters (Supplementary Table 4). One type of cysteine knot, reported to be important for tyrosine-crosslinking [63], can be found in 35 collagens (Supplementary Table 4/CysKnot C-Col domain, red-marked Y). Many, but not all, of the predicted transmembrane collagens have predicted furin cleavage sites potentially enabling the shedding of these collagens (Supplementary Table 4).

Cluster A

Cluster A comprises six members and is subdivided into four sub-clusters (A1–4; Supplementary Fig. 3; Supplementary Table 4). Members of sub-clusters A2 and A4 are predicted to be transmembrane proteins. Interestingly, sub-clusters A3 and A4 have the same length of their collagenous domain (Supplementary Fig. 3; Supplementary Table 4).

Cluster B

Cluster B comprises 84 members divided into 18 sub-clusters (Supplementary Fig. 4; Supplementary Table 4). The two collagenous domains are typically 20 or 21 triplets long and the non-collagenous interruption only differs by a few amino acids.

Cluster C

Cluster C comprises 53 members divided into 27 sub-clusters. 19 out of the 27 C sub-clusters consist only of one cuticular collagen gene (Supplementary Fig. 5; Supplementary Table 4).

Cluster D

Cluster D comprises 28 members forming 17 sub-clusters (Supplementary Fig. 6; Supplementary Table 4). Of note, COL-51 is predicted to be a multispan-membrane protein with a total of four transmembrane (TM) regions, with the collagenous domain between the second and the third TM. If this prediction is correct, it would be interesting to know how the collagenous domain of COL-51 forms.

Cluster E

Cluster E comprises two members, with five interruptions in their collagenous domain (Supplementary Fig. 7; Supplementary Table 4).

Taken together, the newly proposed classification of cuticular collagens is based on the structural similarity of the collagenous domain. This will help identify similar collagens with similar, redundant or compensatory functions. Furthermore, it is likely that heterotrimers exist within the cuticular collagen family. We hope that our system will help to identify potential candidates for heterotrimerization.

Low amino acid sequence similarity among cuticular collagens

Among the 173 cuticular collagens, approximately 30 genes form 9 similarity groups that share high sequence similarity to each other (>90%, Supplementary Fig. 8, pink/white).

Sequences with a similarity of over 90% normally belong to the same sub-cluster, with the minor exception of COL-146 and COL-147, which belong to C21a and C21c, respectively. However, not all members of a sub-cluster group by sequence similarity. For example, although many members of the sub-cluster B9 group together based on the sequence alignment (Supplemental Fig. 8, green bars), some members, like COL-152 or COL-123, are separated and only show weak sequence similarity to the sub-cluster (approx. 35%, Supplementary Fig. 8 or visit <http://CeCoIDB.permalink.cc/> website and use “recursive on” with cluster B9). Additionally, some collagens show sequence similarity with members of B9, but group differently based on their collagen domain organization (e.g. COL-148 and COL-150). A similar pattern can be observed in the sub-cluster B14 (Supplemental Fig. 8, green bars). Overall, the cuticular collagens only show a relatively low sequence similarity (81% with

<40% identity; Supplementary Fig. 8), with the exception of COL-126 and COL-127. These two proteins are identical at the amino acid level, but also at the nucleotide level (in both exons and introns), which raises the question of whether this is one gene misannotated as two collagens. We confirmed by PCR that *col-126* and *col-127* are indeed two distinct genes located next to each other in inverse direction (Supplementary Fig. 9), suggesting a very recent gene duplication event.

As the structural similarity of cuticular collagens is striking, it is very likely that they originate from a common evolutionary ancestor. The low sequence identity further suggests that upon gene multiplication cuticular collagens diversified to fulfill various important functions in *C. elegans*. However, as the prerequisites for collagen helices are relatively low, there is also the possibility that evolutionary pressure was mostly directed towards domain organization and less to the primary sequence.

Functions of cuticular collagens

Twenty one out of the 173 cuticular collagens have been isolated in genetic mutagenesis screens [10] (*bli-1*, *bli-2*, *bli-6*, *dpy-2*, *dpy-3*, *dpy-4*, *dpy-5*, *dpy-7*, *dpy-8*, *dpy-9*, *dpy-10*, *dpy-13*, *dpy-14*, *dpy-17*, *lon-3*, *ram-2*, *rol-1*, *rol-6*, *sqt-1*, *sqt-2*, *sqt-3*; Supplementary Table 4). Mutations in these cuticular collagens affect the synthesis or assembly of the cuticle and thereby alter body morphology. These cuticular collagens are named based on their phenotype: long (*lon-#*) are about 1.5 times the length of wild type, dumpy (*dpy-#*) are short and fat-looking, roller (*rol-#*) roll around their helical axis instead of the sinusoid-curve crawling of wild type, blister (*bli-#*) show detachment of cuticular layer forming blisters along the body, Ray abnormal (*ram-#*) affects the morphology of the male tail, and squat (*sqt-#*) can lengthen, shorten, or helically twist *C. elegans* [10] (Supplementary Table 4). For instance, *sqt-1*(*e1350*) mutation leads to a R69C substitution altering the predicted furin **RVRR** cleavage site to **RVRC** before the collagen domains. These *sqt-1*(*e1350*) mutant *C. elegans* show stage-specific phenotypes: larval stage L1–2 are wild-type, L3 or dauer are rolling, and L4 are dumpy [64]. By contrast, *sqt-1* null mutants are wild type [64], suggesting that the absence of SQT-1 collagen has no effect on the cuticular structure and there is redundancy among the cuticular collagens to compensate for the absence of SQT-1. However, the genotype to phenotype interpretation of how these collagens interact to form and integrate into their ECM is complex [65]. For instance, *sqt-1* null mutations suppress the rolling phenotype of *rol-6* mutants, suggesting that collagen ROL-6 gene product depends on the presence of collagen SQT-1 [66], whereas both null mutations of *sqt-1* or *rol-6* suppress *lon-3* mutant phenotype [67]. Taken together, with the complete matrisome list, it becomes now

possible to start dissecting out the complex genetics underlying the formation of ECM structures *in vivo*.

Utilizing the *in-silico C. elegans* matrisome to annotate large datasets

RNA sequencing and proteomics are standard techniques used by many *C. elegans* research laboratories to elucidate physiological and pathological processes. In addition, genome-wide RNA interference (RNAi) screens are commonly used to identify the mechanism(s) underlying phenotypes of interest.

To demonstrate the applicability and power of our matrisome definition and classification, we used the Matrisome Annotator we developed here (<http://ce-matrisome-annotator.permalink.cc/>) to re-annotate existing datasets. We first re-analyzed our previously published study using transcriptomics to identify genes involved in longevity [15]. We found 79 matrisome genes out of the total 426 transcriptionally upregulated genes when comparing long-lived *C. elegans* under reduced Insulin/IGF-1 conditions with short-lived *C. elegans* that lack the oxidative stress transcription factor SKN-1/Nrf1,2,3 (Supplementary Table 5) [15]. Although, we previously recognized the upregulated collagens and potentially secreted proteases [15], the re-annotation of this data set paints a more complete picture to envision a remodeling of the ECM in long-lived *C. elegans*. Our list can also be used to annotate proteomic datasets. Here, we re-annotated a proteomic dataset from a recently published study aimed at studying longevity in *C. elegans* [68]. In contrast to the 11 collagens highlighted in their study, we found 25 matrisome proteins out of the 177 total upregulated proteins when comparing long-lived germ stem cell mutant *glp-1* with wild-type *C. elegans* (Supplementary Table 6). The additionally identified matrisome proteins includes laminin A and B (EPI-1 and LAM-1), prolyl 4-hydroxylase (DPY-18), and secreted proteases (Supplementary Table 6). Together with the 11 previously identified collagens [68], this suggests a potential remodeling of the ECM in long-lived *C. elegans*, consistent with the findings from the mRNA expression profile [15]. Last, we set out to re-annotate data from a whole-genome RNAi screen aimed at identifying antifungal innate immunity genes [69], since this would help to identify functional importance of matrisome genes. We found that 18 out of the 297 gene hits that regulate antimicrobial peptide gene expression are matrisome genes (Supplementary Table 7) [69]. These 18 matrisome genes include six cuticular collagens, three secreted proteases, and one collagen cross-linking enzyme (Supplementary Table 7), suggesting a potential role for strengthening or stiffening of the ECM to form a protective barrier against fungal infections.

By using the *C. elegans* Matrisome Annotator tool, we found substantial enrichment for matrisome genes in these data sets. Thus, re-analyzing -omic datasets with the *C. elegans* Matrisome Annotator tool may be useful to generate novel hypotheses about the role of the *C. elegans* matrisome for various biological processes.

Conclusions

Defining proteins in cellular compartments has helped understand their functions and implication in various processes. The ECM has been implicated in many biological processes. Components of the ECM have essential roles for *C. elegans* development, cell migration, and aging. In this study, we defined the *C. elegans* matrisome, an ensemble of ECM proteins and associated factors. We identified conserved and nematode-specific components, which informs biomedical research and provides potential targets to fight pathogenic nematodes. The categorization and clustering of *C. elegans* collagens lays the foundation to experimentally test, for example, whether cuticular collagens might form heterotrimers. Using the *C. elegans* Matrisome Annotator tool, we found enrichment of ECM genes at the mRNA, protein, and phenotypic level. This will assist researchers in delineating genotype-to-phenotype relationships for ECM genes. Modern science is hypothesis-driven. We hope that our contribution in defining the *C. elegans* matrisome and providing tools to analyze -omic data will aid generating novel hypotheses to propel science forward.

Supplementary data to this article can be found online at <https://doi.org/10.1016/j.mplus.2018.11.001>.

Acknowledgement

We thank Gary Williams from WormBase and Paolo Bazzicalupo for helpful discussions about *col-126/-127* and cuticlin-like genes, respectively, and members of the Naba and Ewald labs for discussion and comments on the manuscript.

Funding sources

This work was supported by Swiss National Science Foundation [163898] to ACT, CS, and CYE, the work of AN and MND was supported by a start-up fund from the Department of Physiology and Biophysics at the University of Illinois at Chicago. JMG was supported by the Deutsche Forschungsgemeinschaft SFB829/B11.

Author contributions

All authors participated in analyzing and interpreting the data.

AN, ACT, MND, EJ, and CYE defined the *in-vitro* matrisome and analyzed expression data. CS developed the online matrisome annotation script.

JMG identified and established the *C. elegans* collagen classification.

JMG, AN, and CYE wrote the manuscript in consultation with the other authors.

Author information

The authors have no competing interests to declare.

Received 19 October 2018;

Received in revised form 26 November 2018;

Accepted 26 November 2018

Available online 21 February 2019

Keywords:

Nematode;

Extracellular matrix;

Collagen;

Cuticle;

Basement membrane

References

- [1] G. Stepek, D.J. Buttle, I.R. Duce, J.M. Behnke, Human gastrointestinal nematode infections: are new control methods required? *Int. J. Exp. Pathol.* 87 (2006) 325–341, <https://doi.org/10.1111/j.1365-2613.2006.00495.x>.
- [2] Deworming for health and development: report of the third global meeting of the partners for parasite control, Partners for Parasite Control Meeting 3rd 2004 Geneva, World Health Organization 2005, pp. 1–64 <http://www.who.int/iris/handle/10665/69005>.
- [3] G.C. Bernard, M. Egnin, C. Bonsi, The impact of plant-parasitic nematodes on agriculture and methods of control, *Nematology-Concepts, Diagnosis and Control*, InTech 2017, pp. 1–33, <https://doi.org/10.5772/intechopen.68958>.
- [4] L. Holden-Dye, R.J. Walker, How relevant is *Caenorhabditis elegans* as a model for the analysis of parasitic nematode biology? *Parasitic Helminths*, Wiley-VCH Verlag GmbH & Co. KGaA, Weinheim, Germany 2012, pp. 23–41, <https://doi.org/10.1002/9783527652969.ch2>.
- [5] C.Y. Ewald, Redox signaling of NADPH oxidases regulates oxidative stress responses, immunity and aging, *Antioxidants* 7 (2018) 130–136, <https://doi.org/10.3390/antiox7100130>.
- [6] A.K. Corsi, B. Wightman, M. Chalfie, A transparent window into biology: a primer on *Caenorhabditis elegans*, *Genetics* 200 (2015) 387–407, <https://doi.org/10.1534/genetics.115.176099>.
- [7] D.D. Shaye, I. Greenwald, OrthoList: a compendium of *C. elegans* genes with human orthologues, *PLoS ONE* 6 (2011), e20085. <https://doi.org/10.1371/journal.pone.0020085>.

- [8] T. Kaletta, M.O. Hengartner, Finding function in novel targets: *C. elegans* as a model organism, *Nat. Rev. Drug Discov.* 5 (2006) 387–398, <https://doi.org/10.1038/nrd2031>.
- [9] E. Culetto, D.B. Sattelle, A role for *Caenorhabditis elegans* in understanding the function and interactions of human disease genes, *Hum. Mol. Genet.* 9 (2000) 869–877.
- [10] A.P. Page, I.L. Johnstone, The cuticle, *WormBook: the online review of C. elegans*, *Biology* (2007) 1–15, <https://doi.org/10.1895/wormbook.1.138.1>.
- [11] D.P. Keeley, D.R. Sherwood, Tissue linkage through adjoining basement membranes: the long and the short term of it, *Matrix Biol.* (2018)<https://doi.org/10.1016/j.matbio.2018.05.009>.
- [12] J.C. Adams, Matricellular proteins: functional insights from non-mammalian animal models, *Curr. Top. Dev. Biol.* 130 (2018) 39–105, <https://doi.org/10.1016/bs.ctdb.2018.02.003>.
- [13] J.M. Kramer, Basement membranes, *WormBook: the online review of C. elegans*, *Biology* (2005) 1–15, <https://doi.org/10.1895/wormbook.1.16.1>.
- [14] D.R. Sherwood, J. Plastino, Invading, leading and navigating cells in *Caenorhabditis elegans*: insights into cell movement in vivo, *Genetics* 208 (2018) 53–78, <https://doi.org/10.1534/genetics.117.300082>.
- [15] C.Y. Ewald, J.N. Landis, J. Porter Abate, C.T. Murphy, T.K. Blackwell, Dauer-independent insulin/IGF-1-signalling implicates collagen remodelling in longevity, *Nature* 519 (2015) 97–101, <https://doi.org/10.1038/nature14021>.
- [16] R.O. Hynes, A. Naba, Overview of the matrisome—an inventory of extracellular matrix constituents and functions, *Cold Spring Harb. Perspect. Biol.* 4 (2012) a004903, <https://doi.org/10.1101/cshperspect.a004903>.
- [17] A. Naba, K.R. Clauser, S. Hoersch, H. Liu, S.A. Carr, R.O. Hynes, The matrisome: in silico definition and in vivo characterization by proteomics of normal and tumor extracellular matrices, *Mol. Cell. Proteomics* 11 (2012), M111.014647. <https://doi.org/10.1074/mcp.M111.014647>.
- [18] A. Naba, S. Hoersch, R.O. Hynes, Towards definition of an ECM parts list: an advance on GO categories, *Matrix Biol.* 31 (2012) 371–372, <https://doi.org/10.1016/j.matbio.2012.11.008>.
- [19] P. Nauroy, S. Hughes, A. Naba, F. Ruggiero, The *in-silico* zebrafish matrisome: a new tool to study extracellular matrix gene and protein functions, *Matrix Biol.* 65 (2018) 5–13, <https://doi.org/10.1016/j.matbio.2017.07.001>.
- [20] P. Nauroy, A. Guiraud, J. Chlasta, M. Malbouyres, B. Gillet, S. Hughes, et al., Gene profile of zebrafish fin regeneration offers clues to kinetics, organization and biomechanics of basement membrane, *Matrix Biol.* (2018)<https://doi.org/10.1016/j.matbio.2018.07.005>.
- [21] A. Naba, K.R. Clauser, J.M. Lamar, S.A. Carr, R.O. Hynes, Extracellular matrix signatures of human mammary carcinoma identify novel metastasis promoters, *elife* 3 (2014), e01308. <https://doi.org/10.7554/eLife.01308>.
- [22] A.M. Socovich, A. Naba, The cancer matrisome: from comprehensive characterization to biomarker discovery, *Semin. Cell Dev. Biol.* (2018)<https://doi.org/10.1016/j.semcdb.2018.06.005>.
- [23] Y. Zhou, J.C. Horowitz, A. Naba, N. Ambalavanan, K. Atabai, J. Balestrini, et al., Extracellular matrix in lung development, homeostasis and disease, *Matrix Biol.* (2018)<https://doi.org/10.1016/j.matbio.2018.03.005>.
- [24] V.L. Massey, C.E. Dolin, L.G. Poole, S.V. Hudson, D.L. Siow, G.N. Brock, et al., The hepatic “matrisome” responds dynamically to injury: characterization of transitional changes to the extracellular matrix in mice, *Hepatology* 65 (2017) 969–982, <https://doi.org/10.1002/hep.28918>.
- [25] M.C. Staiculescu, J. Kim, R.P. Mecham, J.E. Wagenseil, Mechanical behavior and matrisome gene expression in the aneurysm-prone thoracic aorta of newborn lysyl oxidase knockout mice, *Am. J. Physiol. Heart Circ. Physiol.* 313 (2017) H446–H456, <https://doi.org/10.1152/ajpheart.00712.2016>.
- [26] A. Naba, K.R. Clauser, H. Ding, C.A. Whittaker, S.A. Carr, R. O. Hynes, The extracellular matrix: tools and insights for the “omics” era, *Matrix Biol.* 49 (2016) 10–24, <https://doi.org/10.1016/j.matbio.2015.06.003>.
- [27] R.J. Kinsella, A. Kähäri, S. Haider, J. Zamora, G. Proctor, G. Spudich, et al., Ensembl BioMarts: a hub for data retrieval across taxonomic space, *Database (Oxford)* (2011) <https://doi.org/10.1093/database/bar030>.
- [28] T. UniProt Consortium, UniProt: the universal protein knowledgebase, *Nucleic Acids Res.* 46 (2018) 2699, <https://doi.org/10.1093/nar/gky092>.
- [29] G.N. Cox, M. Kusch, R.S. Edgar, Cuticle of *Caenorhabditis elegans*: its isolation and partial characterization, *J. Cell Biol.* 90 (1981) 7–17.
- [30] M. Sebastiano, F. Lassandro, P. Bazzicalupo, cut-1 a *Caenorhabditis elegans* gene coding for a dauer-specific noncollagenous component of the cuticle, *Dev. Biol.* 146 (1991) 519–530.
- [31] R.D. Finn, T.K. Attwood, P.C. Babbitt, A. Bateman, P. Bork, A.J. Bridge, et al., InterPro in 2017—beyond protein family and domain annotations, *Nucleic Acids Res.* 45 (2017) D190–D199, <https://doi.org/10.1093/nar/gkw1107>.
- [32] S.R. Eddy, Accelerated profile HMM searches, *PLoS Comput. Biol.* 7 (2011), e1002195. <https://doi.org/10.1371/journal.pcbi.1002195>.
- [33] R.D. Finn, P. Coggill, R.Y. Eberhardt, S.R. Eddy, J. Mistry, A. L. Mitchell, et al., The Pfam protein families database: towards a more sustainable future, *Nucleic Acids Res.* 44 (2016) D279–D285, <https://doi.org/10.1093/nar/gkv1344>.
- [34] R.Y.N. Lee, K.L. Howe, T.W. Harris, V. Arnaboldi, S. Cain, J. Chan, et al., WormBase 2017: molting into a new stage, *Nucleic Acids Res.* 46 (2018) D869–D874, <https://doi.org/10.1093/nar/gkx998>.
- [35] Y. Zhuang, F. Ma, J. Li-Ling, X. Xu, Y. Li, Comparative analysis of amino acid usage and protein length distribution between alternatively and non-alternatively spliced genes across six eukaryotic genomes, *Mol. Biol. Evol.* 20 (2003) 1978–1985, <https://doi.org/10.1093/molbev/msg203>.
- [36] S.K. Olson, J.R. Bishop, J.R. Yates, K. Oegema, J.D. Esko, Identification of novel chondroitin proteoglycans in *Caenorhabditis elegans*: embryonic cell division depends on CPG-1 and CPG-2, *J. Cell Biol.* 173 (2006) 985–994, <https://doi.org/10.1083/jcb.200603003>.
- [37] K. Drickamer, R.B. Dodd, C-type lectin-like domains in *Caenorhabditis elegans*: predictions from the complete genome sequence, *Glycobiology* 9 (1999) 1357–1369.
- [38] I.L. Johnstone, Cuticle collagen genes. Expression in *Caenorhabditis elegans*, *Trends Genet.* 16 (2000) 21–27.
- [39] A.A. Bentley, J.C. Adams, The evolution of thrombospondins and their ligand-binding activities, *Mol. Biol. Evol.* 27 (2010) 2187–2197, <https://doi.org/10.1093/molbev/msq107>.
- [40] C.A. Whittaker, R.O. Hynes, Distribution and evolution of von Willebrand/integrin A domains: widely dispersed domains with roles in cell adhesion and elsewhere, *Mol. Biol. Cell* 13 (2002) 3369–3387, <https://doi.org/10.1091/mbc.e02-05-0259>.

- [41] J.E. Schwarzbauer, C.S. Spencer, The *Caenorhabditis elegans* homologue of the extracellular calcium binding protein SPARC/osteonectin affects nematode body morphology and mobility, *Mol. Biol. Cell* 4 (1993) 941–952.
- [42] M.A. Morrissey, R. Jayadev, G.R. Miley, C.A. Blebea, Q. Chi, S. Ihara, et al., SPARC promotes cell invasion in vivo by decreasing type IV collagen levels in the basement membrane, *PLoS Genet.* 12 (2016), e1005905. <https://doi.org/10.1371/journal.pgen.1005905>.
- [43] F. Segade, Molecular evolution of the fibulins: implications on the functionality of the elastic fibulins, *Gene* 464 (2010) 17–31, <https://doi.org/10.1016/j.gene.2010.05.003>.
- [44] W.-M. Woo, E. Berry, M.L. Hudson, R.E. Swale, A. Goncharov, A.D. Chisholm, The *C. elegans* F-spondin family protein SPON-1 maintains cell adhesion in neural and non-neural tissues, *Development* 135 (2008) 2747–2756, <https://doi.org/10.1242/dev.015289>.
- [45] C.A. Karavanich, R.R. Anholt, Molecular evolution of olfactomedin, *Mol. Biol. Evol.* 15 (1998) 718–726, <https://doi.org/10.1093/oxfordjournals.molbev.a025975>.
- [46] S. Ricard-Blum, The collagen family, *Cold Spring Harb. Perspect. Biol.* 3 (2011) a004978, <https://doi.org/10.1101/cshperspect.a004978>.
- [47] A.L. Fidler, C.E. Darris, S.V. Chetyrkin, V.K. Pedchenko, S.P. Boudko, K.L. Brown, et al., Collagen IV and basement membrane at the evolutionary dawn of metazoan tissues, *elife* 6 (2017), e15040. <https://doi.org/10.7554/eLife.24176>.
- [48] S. Ozbek, P.G. Balasubramanian, R. Chiquet-Ehrismann, R. P. Tucker, J.C. Adams, The evolution of extracellular matrix, *Mol. Biol. Cell* 21 (2010) 4300–4305, <https://doi.org/10.1091/mbc.E10-03-0251>.
- [49] H. Hutter, B.E. Vogel, J.D. Plenefisch, C.R. Norris, R.B. Proenca, J. Spieth, et al., Conservation and novelty in the evolution of cell adhesion and extracellular matrix genes, *Science* 287 (2000) 989–994.
- [50] R.P. Boot-Handford, D.S. Tuckwell, Fibrillar collagen: the key to vertebrate evolution? A tale of molecular incest, *Bioessays* 25 (2003) 142–151, <https://doi.org/10.1002/bies.10230>.
- [51] M.H. Sibley, J.J. Johnson, C.C. Mello, J.M. Kramer, Genetic identification, sequence, and alternative splicing of the *Caenorhabditis elegans* alpha 2(IV) collagen gene, *J. Cell Biol.* 123 (1993) 255–264.
- [52] X.D. Guo, J.J. Johnson, J.M. Kramer, Embryonic lethality caused by mutations in basement membrane collagen of *C. elegans*, *Nature* 349 (1991) 707–709, <https://doi.org/10.1038/349707a0>.
- [53] M.H. Sibley, P.L. Graham, N. von Mende, J.M. Kramer, Mutations in the alpha 2(IV) basement membrane collagen gene of *Caenorhabditis elegans* produce phenotypes of differing severities, *EMBO J.* 13 (1994) 3278–3285.
- [54] R. Ramchandran, M. Dhanabal, R. Volk, M.J. Waterman, M. Segal, H. Lu, et al., Antiangiogenic activity of restin, NC10 domain of human collagen XV: comparison to endostatin, *Biochem. Biophys. Res. Commun.* 255 (1999) 735–739, <https://doi.org/10.1006/bbrc.1999.0248>.
- [55] R. Heljasvaara, M. Aikio, H. Ruotsalainen, T. Pihlajaniemi, Collagen XVIII in tissue homeostasis and dysregulation - lessons learned from model organisms and human patients, *Matrix Biol.* 57–58 (2017) 55–75, <https://doi.org/10.1016/j.matbio.2016.10.002>.
- [56] B.D. Ackley, J.R. Crew, H. Elamaa, T. Pihlajaniemi, C.J. Kuo, J.M. Kramer, The NC1/endostatin domain of *Caenorhabditis elegans* type XVIII collagen affects cell migration and axon guidance, *J. Cell Biol.* 152 (2001) 1219–1232.
- [57] J. Taylor, T. Unsoeld, H. Hutter, The transmembrane collagen COL-99 guides longitudinally extending axons in *C. elegans*, *Mol. Cell. Neurosci.* 89 (2018) 9–19, <https://doi.org/10.1016/j.mcn.2018.03.003>.
- [58] H. Tu, P. Huhtala, H.-M. Lee, J.C. Adams, T. Pihlajaniemi, Membrane-associated collagens with interrupted triple-helices (MACITs): evolution from a bilaterian common ancestor and functional conservation in *C. elegans*, *BMC Evol. Biol.* 15 (2015) 281, <https://doi.org/10.1186/s12862-015-0554-3>.
- [59] P.M. Loria, J. Hodgkin, O. Hobert, A conserved postsynaptic transmembrane protein affecting neuromuscular signaling in *Caenorhabditis elegans*, *J. Neurosci.* 24 (2004) 2191–2201, <https://doi.org/10.1523/JNEUROSCI.5462-03.2004>.
- [60] L. Emtage, G. Gu, E. Hartwig, M. Chalfie, Extracellular proteins organize the mechanosensory channel complex in *C. elegans* touch receptor neurons, *Neuron* 44 (2004) 795–807, <https://doi.org/10.1016/j.neuron.2004.11.010>.
- [61] J.G. Cueva, A. Mulholland, M.B. Goodman, Nanoscale organization of the MEC-4 DEG/ENaC sensory mechanotransduction channel in *Caenorhabditis elegans* touch receptor neurons, *J. Neurosci.* 27 (2007) 14089–14098, <https://doi.org/10.1523/JNEUROSCI.4179-07.2007>.
- [62] D.C. Bergmann, J.R. Crew, J.M. Kramer, W.B. Wood, Cuticle chirality and body handedness in *Caenorhabditis elegans*, *Dev. Genet.* 23 (1998) 164–174, [https://doi.org/10.1002/\(SICI\)1520-6408\(1998\)23:3<164::AID-DVG2>3.0.CO;2-C](https://doi.org/10.1002/(SICI)1520-6408(1998)23:3<164::AID-DVG2>3.0.CO;2-C).
- [63] J.M. Kramer, Structures and functions of collagens in *Caenorhabditis elegans*, *FASEB J.* 8 (1994) 329–336.
- [64] J.M. Kramer, J.J. Johnson, R.S. Edgar, C. Basch, S. Roberts, The *sqt-1* gene of *C. elegans* encodes a collagen critical for organismal morphogenesis, *Cell* 55 (1988) 555–565.
- [65] A.P. Page, A.D. Winter, Enzymes involved in the biogenesis of the nematode cuticle, *Adv. Parasitol.* 53 (2003) 85–148.
- [66] J.M. Kramer, J.J. Johnson, Analysis of mutations in the *sqt-1* and *rol-6* collagen genes of *Caenorhabditis elegans*, *Genetics* 135 (1993) 1035–1045.
- [67] J. Nyström, Z.-Z. Shen, M. Aili, A.J. Flemming, A. Leroi, S. Tuck, Increased or decreased levels of *Caenorhabditis elegans* lon-3, a gene encoding a collagen, cause reciprocal changes in body length, *Genetics* 161 (2002) 83–97.
- [68] Y.-Z. Pu, Q.-L. Wan, A.-J. Ding, H.-R. Luo, G.-S. Wu, Quantitative proteomics analysis of *Caenorhabditis elegans* upon germ cell loss, *J. Proteomics*. 156 (2017) 85–93, <https://doi.org/10.1016/j.jprot.2017.01.011>.
- [69] O. Zugasti, N. Thakur, J. Belougne, B. Squiban, C.L. Kurz, J. Soulé, et al., A quantitative genome-wide RNAi screen in *C. elegans* for antifungal innate immunity genes, *BMC Biol.* 14 (2016) 35, <https://doi.org/10.1186/s12915-016-0256-3>.
- [70] F. Sievers, A. Wilm, D. Dineen, T.J. Gibson, K. Karplus, W. Li, et al., Fast, scalable generation of high-quality protein multiple sequence alignments using Clustal Omega, *Mol. Syst. Biol.* 7 (2011) 539, <https://doi.org/10.1038/msb.2011.75>.
- [71] G.E. Crooks, G. Hon, J.-M. Chandonia, S.E. Brenner, WebLogo: a sequence logo generator, *Genome Res.* 14 (2004) 1188–1190, <https://doi.org/10.1101/gr.849004>.
- [72] S.M. Reynolds, L. Käll, M.E. Riffle, J.A. Bिल्mes, W.S. Noble, Transmembrane topology and signal peptide prediction using dynamic bayesian networks, *PLoS Comput. Biol.* 4 (2008), e1000213. <https://doi.org/10.1371/journal.pcbi.1000213>.

4. Overcoming autofluorescence to assess GFP expression during normal physiology and aging in *Caenorhabditis elegans*

Alina C. Teuscher¹ and Collin Y. Ewald^{1*}

Bio Protoc. ; 8(14): . doi:10.21769/BioProtoc.2940.

When imaging old *C. elegans* the naturally increased autofluorescent age pigments in the *C. elegans* intestine consistently masked the GFP signal preventing the collection of reliable data. We developed a novel combination of a triple-band filter set used to separate the GFP signal from autofluorescence, displaying GFP in green and autofluorescence in yellow, which we describe here to provide a tool for fellow researchers. In order to demonstrate the filter sets efficiency we performed several example experiments, like e.g. the scoring the nuclear localization of SKN-1 transcription factor under oxidative stress conditions.

My contribution to this paper includes the design and performance of all experiments described as well as the manuscript writing in cooperation with CYE.

Published in final edited form as:

Bio Protoc. ; 8(14): . doi:10.21769/BioProtoc.2940.

Overcoming Autofluorescence to Assess GFP Expression During Normal Physiology and Aging in *Caenorhabditis elegans*

Alina C. Teuscher and Collin Y. Ewald*

Department of Health Sciences and Technology, Institute of Translational Medicine, Eidgenössische Technische Hochschule (ETH) Zürich, Schwerzenbach-Zürich, Switzerland

Abstract

Green fluorescent protein (GFP) is widely used as a molecular tool to assess protein expression and localization. In *C. elegans*, the signal from weakly expressed GFP fusion proteins is masked by autofluorescence emitted from the intestinal lysosome-related gut granules. For instance, the GFP fluorescence from SKN-1 transcription factor fused to GFP is barely visible with common GFP (FITC) filter setups. Furthermore, this intestinal autofluorescence increases upon heat stress, oxidative stress (sodium azide), and during aging, thereby masking GFP expression even from proximal tissues. Here, we describe a triple band GFP filter setup that separates the GFP signal from autofluorescence, displaying GFP in green and autofluorescence in yellow. In addition, yellow fluorescent protein (YFP) remains distinguishable from both the yellowish autofluorescence and GFP with this triple band filter setup. Although some GFP intensity might be lost with the triple band GFP filter setup, the advantage is that no modification of currently used transgenic GFP lines is needed and these GFP filters are easy to install. Hence, by using this triple band GFP filter setup, the investigators can easily distinguish autofluorescence from GFP and YFP in their favorite transgenic *C. elegans* lines.

Keywords

Microscopy; Filter set; Fluorescent protein; GFP; YFP; Autofluorescence; Gut granules; Lysosome-related organelles; Age-pigments; Lipofuscin; Aging; Transcription factor; SKN-1; HSF-1; *C. elegans*

Background

Major sources of autofluorescence include intracellular lysosome-derived granules, mitochondria (*i.e.*, autofluorescent molecules such as NAD(P)H and flavins), or extracellular collagen (Hermann *et al.*, 2005; Monici, 2005). During aging, autofluorescent materials such as lipofuscin and advanced glycation end-products (AGE) accumulate. In the nematode *C. elegans*, the autofluorescence of gut granules starts already during embryogenesis, reflecting the biogenesis of lysosome-related organelles (Hermann *et al.*, 2005). This prominent autofluorescence of these lysosome-related gut granules in the intestine continues throughout development and adulthood. The source of the autofluorescence, whether it is

*For correspondence: collin-ewald@ethz.ch.

lipofuscin, AGE, tryptophan metabolites, or something else, is still unclear. However, this autofluorescence increases during aging and the two main tissues that show the highest autofluorescence are the intestine and the uterus in *C. elegans* (Pincus *et al.*, 2016). With current fluorescent filter sets (TRITC, DAPI, FITC), three different autofluorescent wavelengths have been characterized in *C. elegans*. The red autofluorescence (visualized by TRITC) progressively increases with age, the blue autofluorescence (visualized by DAPI) peaks right before death, and the green autofluorescence (visualized by FITC) is a mixture from the red and blue autofluorescence (Pincus *et al.*, 2016).

The multicellular model organism *C. elegans* is transparent, allowing GFP fluorescence to be assessed *in vivo* non-invasively (Chalfie *et al.*, 1994). With commonly used GFP filter sets, for instance, FITC with an excitation center wavelength of 470 nm and a full bandwidth of 40 nm (470/40 nm), and emission range of 525/50 nm, the intestinal autofluorescence overlaps with the GFP signal. Previously, knockdowns by RNA interference (RNAi; *e.g.*, *tdo-2* RNAi) or gut *granule-loss* (*glo*) mutations (Hermann *et al.*, 2005; Coburn *et al.*, 2013), which either diminish or eliminate the intestinal autofluorescence, have been applied to the desired GFP transgenic *C. elegans* lines to overcome this problem. However, RNAi knockdowns or mutations that help to diminish autofluorescence alter gene function and might cause artifacts. In addition, there are transgenic GFP fusions of several stress response-regulating transcription factors (DAF-16::GFP, HSF-1::GFP, HLH-30::GFP, SKN-1::GFP) that are routinely used to assess cytoplasmic to nuclear translocation in intestinal cells as a proxy for their activation (Henderson and Johnson, 2001; Libina *et al.*, 2003; Kwon *et al.*, 2010; Lapierre *et al.*, 2013; Morton and Lamitina, 2013; Ewald *et al.*, 2015 and 2017b). Particularly, the transgenic SKN-1::GFP fusion is barely visible and is masked by intestinal autofluorescence even in larval *C. elegans* (Havermann *et al.*, 2014; Wang *et al.*, 2016; Hu *et al.*, 2017).

To overcome the problem of autofluorescence masking intestinal GFP, Oliver Hobert (<http://www.bio.net/mm/celegans/1998-November/001769.html>) and several other investigators in the *C. elegans* community had proposed the principle of this combination of GFP filter sets. Optimization of these GFP filter sets by the Blackwell lab made it possible to assess the subcellular localization of SKN-1 and other proteins that were difficult to visualize (An and Blackwell, 2003). Unfortunately, these previous filter sets are not on sale anymore. Here, we describe the currently and commercially available filters that can be used to rebuild these GFP-filter settings. In contrast to the single band FITC GFP filter set, the proposed triple band GFP filter set has a very narrow excitation bandwidth of 10 nm, which is right by the maximum peak for the S65C mutant GFP excitation (488 nm) that is commonly used in *C. elegans* (Boulin *et al.*, 2006; Heppert *et al.*, 2016). More importantly, the emission filter used here has a first pass-through (520/20 nm) for the light emitted close to the GFP emission peak (509 nm) and a second pass-through (595/40 nm) from the light around the autofluorescence emission, allowing the separation of GFP (visible in green) and autofluorescence (visible in yellow).

Materials and Reagents

1. 250 ml glass Erlenmeyer flask

2. 1.5 ml centrifuge tubes
3. Microscope slides (size: 76 mm x 26 mm, 1 mm thick; VWR, Thermo Fisher Scientific, catalog number: [631-1303](#))
4. Cover slip (size: 18 mm x 18 mm; VWR, catalog number: [631-1567](#))
5. Tape (MILIAN, catalog numbers: [140255B](#), [BA-5419-07](#))
6. *C. elegans* strains (available at Caenorhabditis Genetics Center [CGC] <https://cbs.umn.edu/cgc/home>) or if not available at CGC, can be requested directly from the research labs that generated them: N2 *C. elegans* wild-type Bristol, LD1 *Is007* [*Pskn-1::skn-1b/c::gfp*; pRF4 *rol-6 (su1006)*], LSD2022 *spe-9(hc88); jgIs5* [*Prol-6::rol-6::gfp*, *Pttx-3::gfp*], EQ87 *iqIs28* [pAH71 *Phsf-1::hsf-1::gfp*; pRF4 *rol-6 (su1006)*], BT24 *rhIs23* [*gfp::him-4*] III, NL5901 *pkIs2386* [*Punc-54::alpha-synuclein::YFP + unc-119(+)*]

Note: For culturing and handling C. elegans, please see Stiernagle (2006).

7. Agarose (Conda, catalog number: [8010](#))
8. KH₂PO₄ (Merck, catalog number: [1048731000](#))
9. Na₂HPO₄ (Sigma-Aldrich, catalog number: [S5136](#))
10. NaCl (Sigma-Aldrich, catalog number: [S3014](#))
11. MgSO₄ (Fisher Scientific, catalog number: [10316240](#))
12. Levamisole hydrochloride (Sigma-Aldrich, catalog number: [L0380000](#)) (2 mM) solved in M9 buffer

Note: Used here to paralyze worms; it is not recommended to use sodium azide (NaN₃) (Sigma-Aldrich, catalog number: [S2002-100G](#)) (20 mM, solved in M9 buffer).

13. Agarose pads (see Recipes)
14. M9 buffer (see Recipes) (Stiernagle, 2006; He, 2011)

Equipment

1. Autoclave
2. Microwave to heat up agarose
3. Heated water bath or heat block to keep agarose molten
4. For loading *C. elegans* onto agarose pads:

Stereomicroscope, worm pick, pipettes (Figure 1A) (Ewald *et al.*, 2017a)

5. Upright bright field fluorescence microscope (Tritech Research, model: [BX-51-F](#), Figure 1B)
6. Camera (The Imaging Source, model: [DFK 23UX236](#), with IC Capture 2.4 software)

It is important to use a color camera, since a monochrome camera is unable to distinguish between colors, so the filter set would be ineffective.

7. Triple band filter sets

Note: The triple band filter sets used here are from Chroma Technology Corp., but similar filter sets can be acquired from other manufacturers.

The triple band filter sets consist of the 69000 ET-DAPI/FITC/TRITC (69000x, 69000m, 69000bs, EX/EM 25 mm, ringed, DC 25.5 x 36 x 1 mm) (Chroma Technology, catalog number: 69000). However, the excitation filter 69000x is exchanged with an ET485/10x narrow band excitation filter (25 mm, ringed; Chroma Technology, catalog number: ET485/10x). The interpretation of the filter nomenclature for example for ET485/10x is: “ET” stands for magnetron sputtered exciter, “485” indicates the center wavelength of 485 nm and the “/10” indicates the full bandwidth of 10 nm (*i.e.*, +/- 5 nm from the center), and the “x” stands for excitation. Hence, the triple band filter set consists of the ET485/10x excitation filter, the 69000bs dichroic beam splitter, and the 69000m emission filter. The triple band filters are then assembled in a microscope filter cube. A schematic of this setup is shown in Figures 1C and 1D. A comparison between the filter set properties and the resulting images are shown in Figure 2. In brief, the 69000m emission filter allows light coming through from 520/20 nm (green) and from 595/40 (yellow to orange/red) but blocks the greenish to yellow light (535-572 nm), which is the key feature of the triple band filter set that allows distinguishing GFP from autofluorescence (Figure 2). This is in contrast to a GFP long-pass emission filter (ET500lp, > 500 nm), which allows all the light from green to red to pass through.

Software

1. IC Capture 2.4 software (<https://www.theimagingsource.com/support/downloads-for-windows/end-user-software/iccapture/>)
2. ImageJ (https://imagej.net/Image_Stitching)

Procedure

1. Prepare 2% agarose pads (adapted from <http://www.wormatlas.org/agarpad.htm>): Place three microscope slides next to each other. Place a piece of tape on the two outer slides (Figure 1E). To obtain a 2% agarose solution, add 1 g of agarose into 50 ml M9 buffer using a 250 ml glass Erlenmeyer flask.
2. Heat the solution until it is boiling and mix well to get all agarose into solution. To prevent the solution from solidifying, keep it at 65 °C, for example, in a heated water bath (see Note 1). Pipette a drop of the 2% agarose solution onto the middle of a slide and immediately place another microscope slide in a 90° angle on top of it, so that it is secured by the two stickered slides hovering over the middle one resulting in an even thickness of the solidifying agarose (Figure 1E, see Note 2). Wait for 1 min, then carefully remove the top microscope slide by sliding it off. After around 5 min, the pad is dry enough and can be used for microscopy.

3. Place a drop (10 μ l) of 1 mM levamisole (or tetramisole) dissolved in M9 buffer to paralyze *C. elegans* on the agarose pad. Add 10-20 *C. elegans* by picking them into the drop. Carefully cover the agarose pad with a coverslip.
4. Use a fluorescent microscope to take images of the prepared *C. elegans* (see Note 3).

Data analysis

1 Scoring nuclear localization of SKN-1 transcription factor

The transcription factor SKN-1 is the orthologue of the mammalian Nrf/CNC proteins (Nrf1, 2, 3) and is essential for oxidative stress response, protein and lipid homeostasis, and aging (Blackwell *et al.*, 2015). Assessing the activation of SKN-1 is important to gain insights into these cellular protective mechanisms. The *skn-1* gene encodes four protein isoforms (SKN-1a, b, c, d) (Blackwell *et al.*, 2015). The SKN-1b isoform is predominantly expressed in the ASI pair of sensory neurons and is important for dietary restriction-induced longevity in liquid (Bishop and Guarente, 2007). The SKN-1c isoform is predominantly expressed in the intestine and is important for oxidative stress response and longevity through reduced insulin/IGF-1 (Tullet *et al.*, 2008; Ewald *et al.*, 2015) and TOR signaling (Robida-Stubbs *et al.*, 2012).

The transgenic *C. elegans* line LD1 *IdIs007* [*Pskn-1::skn-1b/c::gfp*] (An and Blackwell, 2003) expresses both SKN-1 b and c isoforms. Under unstressed conditions, SKN-1::GFP is visible in ASI neurons, but barely visible in intestinal cells, where it is presumably predominantly localized in the cytoplasm. Under oxidative stress conditions, SKN-1::GFP translocates from the cytoplasm into the nuclei of intestinal cells (An and Blackwell, 2003). A major problem is the scoring of this SKN-1::GFP translocation, since autofluorescence emitted from the intestinal lysosome-related gut granules masks the weakly expressed SKN-1::GFP even during larval stages (Figure 3). The triple band filter sets proposed here allow GFP to appear in green and autofluorescence in yellow (Figures 3B and 3C). This facilitates scoring SKN-1::GFP nuclear localization in the intestinal nuclei.

The SKN-1::GFP scoring scheme as described in Robida-Stubbs *et al.* (2012) and Ewald *et al.* (2017b) is divided into four categories:

1. None: no GFP observed in intestinal nuclei;
2. Low: up to one-third of intestinal nuclei show GFP;
3. Medium: more than half of the intestinal nuclei show GFP;
4. High: all intestinal nuclei show GFP (Figure 4A).

An example result for scoring SKN-1::GFP localization under control (empty vector) and under reduced insulin/IGF-1 signaling conditions [*daf-2(RNAi)*] is shown in Figure 4B, and the corresponding number and percent distribution of *C. elegans* in each SKN-1::GFP scoring category is shown in Figures 4C and 4D, respectively. *C. elegans* has about 30-34 intestinal nuclei (McGee *et al.*, 2011) and in Figure 3B SKN-1::GFP is visible in all 34 nuclei when treated with *daf-2(RNAi)*. For each condition, it is recommended to score at

least 60 *C. elegans* (see Note 4). For statistical comparison, the Chi-square test can be applied. Importantly, upon oxidative stress, SKN-1::GFP can move into the nucleus within minutes (An and Blackwell, 2003; Kell *et al.*, 2007). For instance, sodium azide (NaN₃), an inhibitor of cytochrome oxidase and a compound commonly used to paralyze *C. elegans*, drives SKN-1::GFP into the nucleus within 3-6 min (Figure 5), depending on the concentration used (5-10 mM) (An and Blackwell, 2003). In addition, the intestinal autofluorescence increases within 10 min exposure to 10 mM sodium azide (Figure 5). Therefore, we recommend using either levamisole or tetramisole (a nicotinic acetylcholine receptor agonist that causes prolonged contraction of nematode muscles) to paralyze these transgenic SKN-1::GFP *C. elegans*.

2 Scoring HSF-1 transcription factor activation

Similarly, this triple band filter set can be used for scoring the activation of other transcription factors, such as HSF-1, DAF-16, HLH-30, and others. For the HSF-1 transcription factor, autofluorescence also plays an interfering role since heat shock increases autofluorescence of intestinal cells (Figure 6). Upon heat shock (1-20 min at 35 °C), HSF-1 tagged GFP (HSF-1::GFP) forms foci in the hypodermal nuclei, but the HSF-1::GFP foci are difficult to score in the intestinal nuclei (Chiang *et al.*, 2012; Morton and Lamitina, 2013). Figure 7 shows that the triple band filter set facilitates scoring of HSF-1::GFP foci in the intestinal nuclei, since autofluorescence appears yellowish. The HSF-1::GFP foci scoring is described elsewhere (Chiang *et al.*, 2012; Morton and Lamitina, 2013).

3 Scoring GFP-tagged proteins during old age

During aging, the *C. elegans* autofluorescence increases (Pincus *et al.*, 2016), making it more difficult to score levels and localization of GFP-fused proteins. Figure 8 shows transgenic animals that express a GFP-tagged HIM-4 fusion, which is localized to the basement membrane, either imaged with standard filter sets or with the triple band filter sets (on day 1 and day 8 of adulthood). Although some of the GFP signal might be lost with the triple band filter set, the GFP signal can be easily distinguished from the age-dependent autofluorescence.

4 Distinguishing YFP, GFP, and autofluorescence in a single image

We wondered whether the triple band filter set would be able to distinguish the fluorescence of YFP and GFP from the intestinal autofluorescence. To test this, we crossed transgenic NL5901 animals that express an α -synuclein-tagged YFP in body wall muscles with the LSD2022 animals, which express GFP in the AIY interneuron pair. Remarkably, YFP in the body wall muscles appears yellowish-green, GFP in the neuron appears aqua marine, and autofluorescence in the intestine appears yellowish (Figure 9).

Notes

1. The remaining of the 2% agarose kept at 65 °C in the heat bath can be aliquoted and stored for later re-use. Once the imaging session is completed, we usually aliquot the rest of molten agarose in 1 ml aliquots into 1.5 ml centrifuge tubes for

storage at room temperature for at least 2 months. These aliquots can be re-used by placing on a heating block at 95 °C for several minutes and then kept at 65 °C during the imaging session.

2. To pipet a drop of 2% agarose onto the microscope slide, cut the end of a pipetting tip to allow easier pipetting of the viscous agarose.
3. In general, *C. elegans* should not be kept longer than 15 min on the agar pad during an imaging session.
4. For the transgenic *C. elegans* line LD1 *IdIs007* [*Pskn-1::skn-1b/c::gfp*], nuclear localization of the fusion protein is preferably scored at the fourth larval stage (L4).

Recipes

1. Agarose pads for *C. elegans* immobilization and imaging
Add agarose in M9 buffer to obtain a final 2% agarose solution

Heat to dissolve agarose in solution and keep molten by placing it on a heat block at 65 °C
2. M9 buffer (Stiernagle, 2006; He, 2011)

Add 3 g KH₂PO₄, 7.52 g Na₂HPO₄, 5 g NaCl, 0.0493 g MgSO₄ to 1 L ddH₂O, then autoclave

Acknowledgments

We thank Keith Blackwell, Bob Goldstein, Andrew Papp, and Ewald lab members for her helpful discussions and comments on the manuscript. The triple band filter set configurations were adapted from the Blackwell lab. We thank Jaegal Shim for the *jpgIs5* and Ao-Lin Hsu for the EQ87 *C. elegans* strain. Some *C. elegans* strains were provided by the CGC, which is funded by NIH Office of Research Infrastructure Programs (P40 OD010440). This work was supported by Swiss National Science Foundation [PP00P3 163898] to A.C.T. and C.Y.E. The authors declare no conflict of interest.

Funding:

This work was supported by Swiss National Science Foundation [PP00P3 163898] to A.C.T. and C.Y.E.

References

1. An JH, Blackwell TK. SKN-1 links *C. elegans* mesendodermal specification to a conserved oxidative stress response. *Genes Dev.* 2003; 17(15):1882–1893. [PubMed: 12869585]
2. Bishop NA, Guarente L. Two neurons mediate diet-restriction-induced longevity in *C. elegans*. *Nature.* 2007; 447(7144):545–549. [PubMed: 17538612]
3. Blackwell TK, Steinbaugh MJ, Hourihan JM, Ewald CY, Isik M. SKN-1/Nrf, stress responses, and aging in *Caenorhabditis elegans*. *Free Radic Biol Med.* 2015; 88(Pt B):290–301. [PubMed: 26232625]
4. Boulin T, Etchberger JF, Hobert O. Reporter gene fusions. *Worm Book.* 2006:1–23.
5. Chalfie M, Tu Y, Euskirchen G, Ward WW, Prasher DC. Green fluorescent protein as a marker for gene expression. *Science.* 1994; 263(5148):802–805. [PubMed: 8303295]

6. Chiang WC, Ching TT, Lee HC, Mousigian C, Hsu AL. HSF-1 regulators DDL-1/2 link insulin-like signaling to heat-shock responses and modulation of longevity. *Cell*. 2012; 148(1–2):322–334. [PubMed: 22265419]
7. Coburn C, Allman E, Mahanti P, Benedetto A, Cabreiro F, Pincus Z, Matthijssens F, Araiz C, Mandel A, Vlachos M, Edwards SA, et al. Anthranilate fluorescence marks a calcium-propagated necrotic wave that promotes organismal death in *C. elegans*. *PLoS Biol*. 2013; 11(7):e1001613. [PubMed: 23935448]
8. Ewald CY, Landis JN, Porter Abate J, Murphy CT, Blackwell TK. Dauer-independent insulin/IGF-1-signalling implicates collagen remodelling in longevity. *Nature*. 2015; 519(7541):97–101. [PubMed: 25517099]
9. Ewald CY, Hourihan JM, Blackwell TK. Oxidative stress assays (arsenite and tBHP) in *Caenorhabditis elegans*. *Bio-protocol*. 2017a; 7(13):e2365. [PubMed: 29445761]
10. Ewald CY, Hourihan JM, Bland MS, Obieglo C, Katic I, Moronetti Mazzeo LE, Alcedo J, Blackwell TK, Hynes NE. NADPH oxidase-mediated redox signaling promotes oxidative stress resistance and longevity through *memo-1* in *C. elegans*. *Elife*. 2017b; 6:e19493. [PubMed: 28085666]
11. Havermann S, Chovolou Y, Humpf HU, Watjen W. Caffeic acid phenethyl ester increases stress resistance and enhances lifespan in *Caenorhabditis elegans* by modulation of the insulin-like DAF-16 signalling pathway. *PLoS One*. 2014; 9(6):e100256. [PubMed: 24964141]
12. He F. Common worm media and buffers. *Bio-protocol*. 2011; 1(7):e55.
13. Henderson ST, Johnson TE. *daf-16* integrates developmental and environmental inputs to mediate aging in the nematode *Caenorhabditis elegans*. *Curr Biol*. 2001; 11(24):1975–1980. [PubMed: 11747825]
14. Heppert JK, Dickinson DJ, Pani AM, Higgins CD, Steward A, Ahringer J, Kuhn JR, Goldstein B. Comparative assessment of fluorescent proteins for *in vivo* imaging in an animal model system. *Mol Biol Cell*. 2016; 27(22):3385–3394. [PubMed: 27385332]
15. Hermann GJ, Schroeder LK, Hieb CA, Kershner AM, Rabbits BM, Fonarev P, Grant BD, Priess JR. Genetic analysis of lysosomal trafficking in *Caenorhabditis elegans*. *Mol Biol Cell*. 2005; 16(7):3273–3288. [PubMed: 15843430]
16. Hu Q, D'Amora DR, MacNeil LT, Walhout AJM, Kubiseski TJ. The oxidative stress response in *Caenorhabditis elegans* requires the GATA transcription factor ELT-3 and SKN-1/Nrf2. *Genetics*. 2017; 206(4):1909–1922. [PubMed: 28600327]
17. Kell A, Ventura N, Kahn N, Johnson TE. Activation of SKN-1 by novel kinases in *Caenorhabditis elegans*. *Free Radic Biol Med*. 2007; 43(11):1560–1566. [PubMed: 17964427]
18. Kim TH, Kim DH, Nam HW, Park SY, Shim J, Cho JW. Tyrosylprotein sulfotransferase regulates collagen secretion in *Caenorhabditis elegans*. *Mol Cells*. 2010; 29(4):413–418. [PubMed: 20229090]
19. Kwon ES, Narasimhan SD, Yen K, Tissenbaum HA. A new DAF-16 isoform regulates longevity. *Nature*. 2010; 466(7305):498–502. [PubMed: 20613724]
20. Lapierre LR, De Magalhaes Filho CD, McQuary PR, Chu CC, Visvikis O, Chang JT, Gelino S, Ong B, Davis AE, Irazoqui JE, Dillin A, et al. The TFEB orthologue HLH-30 regulates autophagy and modulates longevity in *Caenorhabditis elegans*. *Nat Commun*. 2013; 4:2267. [PubMed: 23925298]
21. Libina N, Berman JR, Kenyon C. Tissue-specific activities of *C. elegans* DAF-16 in the regulation of lifespan. *Cell*. 2003; 115(4):489–502. [PubMed: 14622602]
22. McGee MD, Weber D, Day N, Vitelli C, Crippen D, Herndon LA, Hall DH, Melov S. Loss of intestinal nuclei and intestinal integrity in aging *C. elegans*. *Aging Cell*. 2011; 10(4):699–710. [PubMed: 21501374]
23. Monici M. Cell and tissue autofluorescence research and diagnostic applications. *Biotechnol Annu Rev*. 2005; 11:227–256. [PubMed: 16216779]
24. Morton EA, Lamitina T. *Caenorhabditis elegans* HSF-1 is an essential nuclear protein that forms stress granule-like structures following heat shock. *Aging Cell*. 2013; 12(1):112–120. [PubMed: 23107491]

25. Pincus Z, Mazer TC, Slack FJ. Autofluorescence as a measure of senescence in *C. elegans*: look to red, not blue or green. *Aging (Albany NY)*. 2016; 8(5):889–898. [PubMed: 27070172]
26. Preibisch S, Saalfeld S, Tomancak P. Globally optimal stitching of tiled 3D microscopic image acquisitions. *Bioinformatics*. 2009; 25(11):1463–1465. [PubMed: 19346324]
27. Robida-Stubbs S, Glover-Cutter K, Lamming DW, Mizunuma M, Narasimhan SD, Neumann-Haefelin E, Sabatini DM, Blackwell TK. TOR signaling and rapamycin influence longevity by regulating SKN-1/Nrf and DAF-16/FoxO. *Cell Metab*. 2012; 15(5):713–724. [PubMed: 22560223]
28. Stiernagle T. Maintenance of *C. elegans*. *Worm Book*. 2006:1–11.
29. Tullet JM, Hertweck M, An JH, Baker J, Hwang JY, Liu S, Oliveira RP, Baumeister R, Blackwell TK. Direct inhibition of the longevity-promoting factor SKN-1 by insulin-like signaling in *C. elegans*. *Cell*. 2008; 132(6):1025–1038. [PubMed: 18358814]
30. Wang Z, Ma X, Li J, Cui X. Peptides from sesame cake extend healthspan of *Caenorhabditis elegans* via upregulation of *skn-1* and inhibition of intracellular ROS levels. *Exp Gerontol*. 2016; 82:139–149. [PubMed: 27381188]

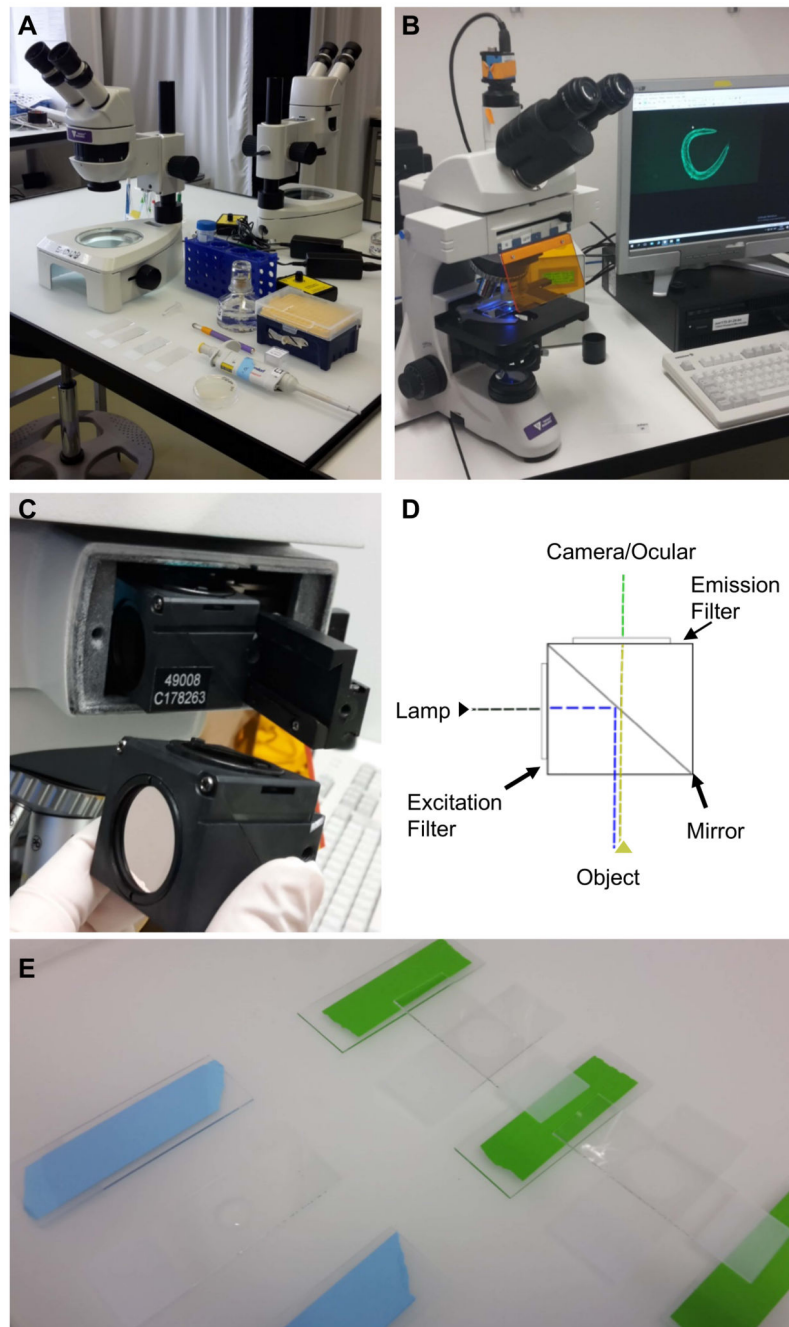


Figure 1. Equipment and experimental setup.

A. Equipment and utilities for mounting *C. elegans* on microscope slides. Shown from the top left: a stereoscope, M9 buffer in a falcon tube, levamisole in a 1.5 ml centrifuge tube, a pipette with tips, a worm-pick to mount *C. elegans* in the liquid droplet, microscope slides with 2% agarose pad, and *C. elegans* on culturing plate. B. Upright bright field fluorescence microscope setup; C. The filter cube and its position in the microscope; D. A schematic representation of the filter cube. The dashed lines indicate the pathway of the light through the filter cube, while the arrows indicate the filters and the mirror. E. Preparation of the 2%

agarose pad slides for microscopy. On the left side is a slide with a drop of 2% agarose dropped between two blue taped slides, while on the right side the agarose drop was already covered by another slide perpendicular to the green taped slides.

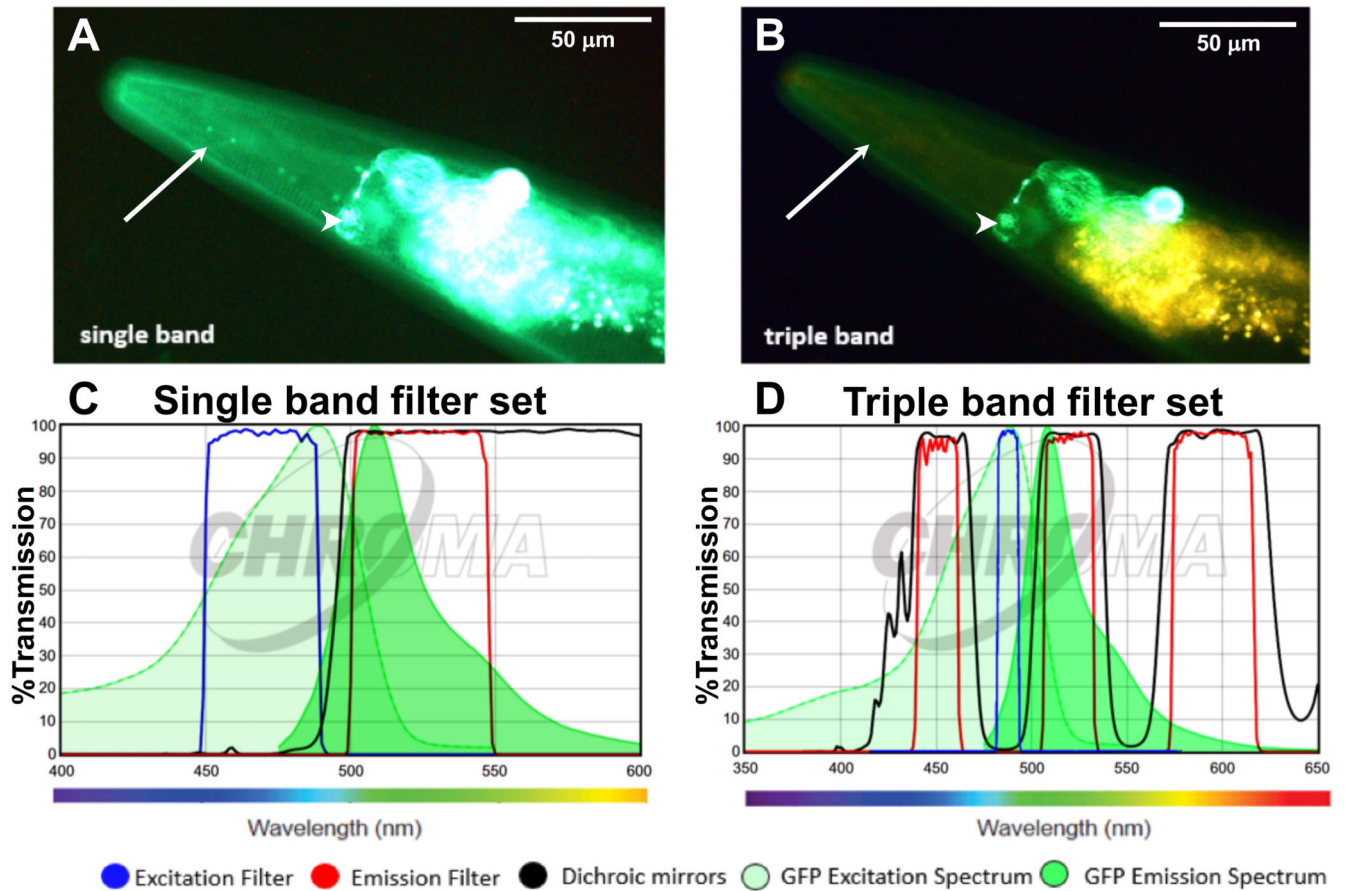


Figure 2. Applying the triple band filter set to distinguish between GFP signal and *C. elegans* autofluorescence.

A-B. The LSD2022 *C. elegans* strain expresses an integrated collagen::GFP transgene (ROL-6::GFP), which is visible in the cuticle (white arrow). In addition, the strain LSD2022 expresses GFP driven by the *ttx-3* promoter in the AIY interneuron pair (white arrowhead) (Kim *et al.*, 2010). A *C. elegans* worm (LSD2022) imaged with a commonly used single band filter set (A). The same animal imaged with the triple band filter set. Green is GFP and yellow is autofluorescence (B). C. Transmission graph of the single band filter set we used in (A) [49002-ET-EGFP (FITC/Cy2) by Chroma]; D. Transmission graph of the triple band filter setup used for (B). The triple band filter setup consists of a narrow band ET485/10x excitation filter, a 69000bs dichroic mirror filter, and a 69000m emission filter, which allows light coming through from 520/20 nm (green) and from 595/40 (yellow to orange/red). However, the 69000m emission filter blocks the greenish to yellow light (535-572 nm), which is the key feature that helps to distinguish GFP from autofluorescence. (C and D) The graphs are both adapted from www.chroma.com.

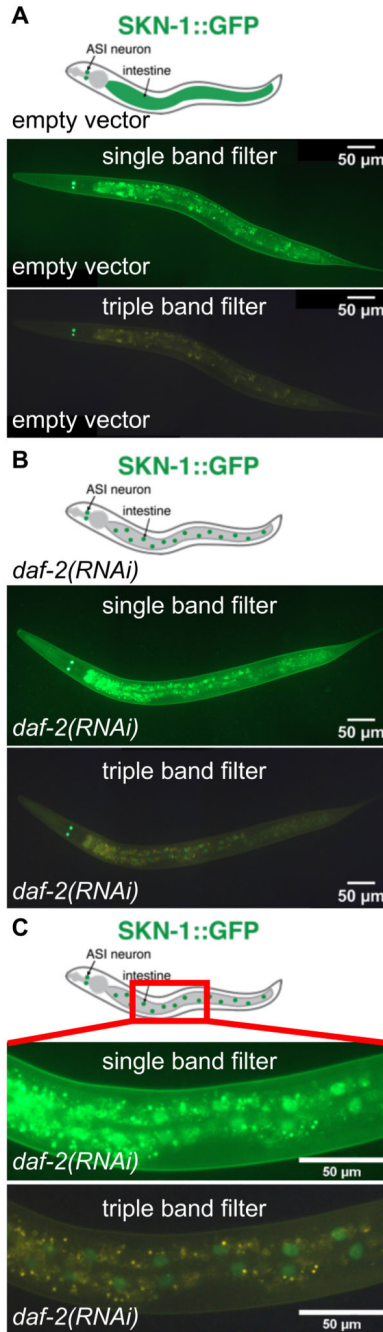


Figure 3. SKN-1::GFP nuclear localization.

In (A) and (B), the same transgenic LD1 *IdIs007* [*P_{skn-1}::skn-1b/c::gfp*] *C. elegans* (anterior to the left, ventral side down) at larval stage 4 (L4) is imaged with the single band filter set (middle panel; 1/30 sec exposure time) or the triple band filter set (bottom panel; 1/30 sec exposure time). Top panel shows schematic representation of SKN-1::GFP depicted in green. A. Transgenic LD1 *C. elegans* imaged at L4 larval stage fed with control RNAi bacteria carrying an empty vector (L4440), starting from the L1 larval stage. SKN-1::GFP is diffuse and barely visible in the intestine. Note that green signal observed in the intestine

here is mainly gut autofluorescence. B. Transgenic LD1 *C. elegans* imaged at L4 larval stage treated with *daf-2* RNAi (which reduces insulin/IGF-1 signaling), starting from the L1 larval stage. SKN-1::GFP is localized in the intestinal nuclei and prominently visible with the triple band filter sets by displaying the GFP in green and the autofluorescence in yellow.

Note: Treatment of daf-2(RNAi) does not increase skn-1 expression levels (Tullet et al., 2008; Ewald et al., 2015). (C) shows a magnified section (1/30 sec exposure time) indicated by the red box in the schematic (top panel). For (A) and (B), images were stitched together using ImageJ (https://imagej.net/Image_Stitching) (Preibisch et al., 2009).

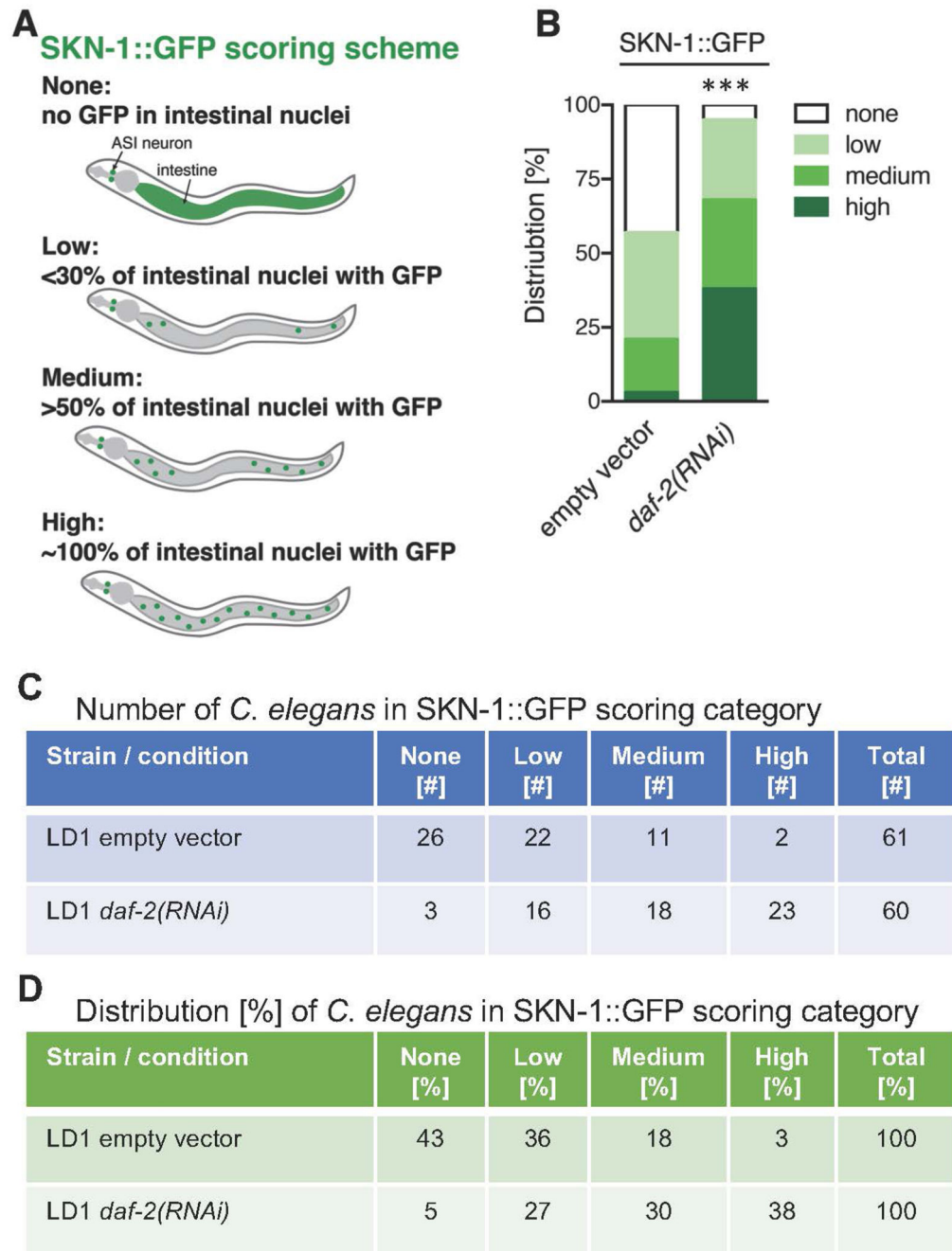


Figure 4. Quantification of SKN-1::GFP nuclear localization.

A. Schematic representation of SKN-1::GFP (green) scoring categories; B. Graphical representation of distribution of *C. elegans* found in the individual SKN-1::GFP scoring categories. LD1 transgenic L4 animals expressing a translational fusion of SKN-1 protein tagged with GFP [*IdIs007 (P_{skn-1}::skn-1b/c::gfp)*] were scored. C. Table of scoring data of the number of *C. elegans* in the SKN-1::GFP scoring categories; D. The data from (C) was used to calculate the distribution of the *C. elegans* found in SKN-1::GFP scoring categories

represented in percent, which is also graphical represented in (B). $N > 60$, one trial. *** < 0.0001 P value was determined by Chi^2 -test.

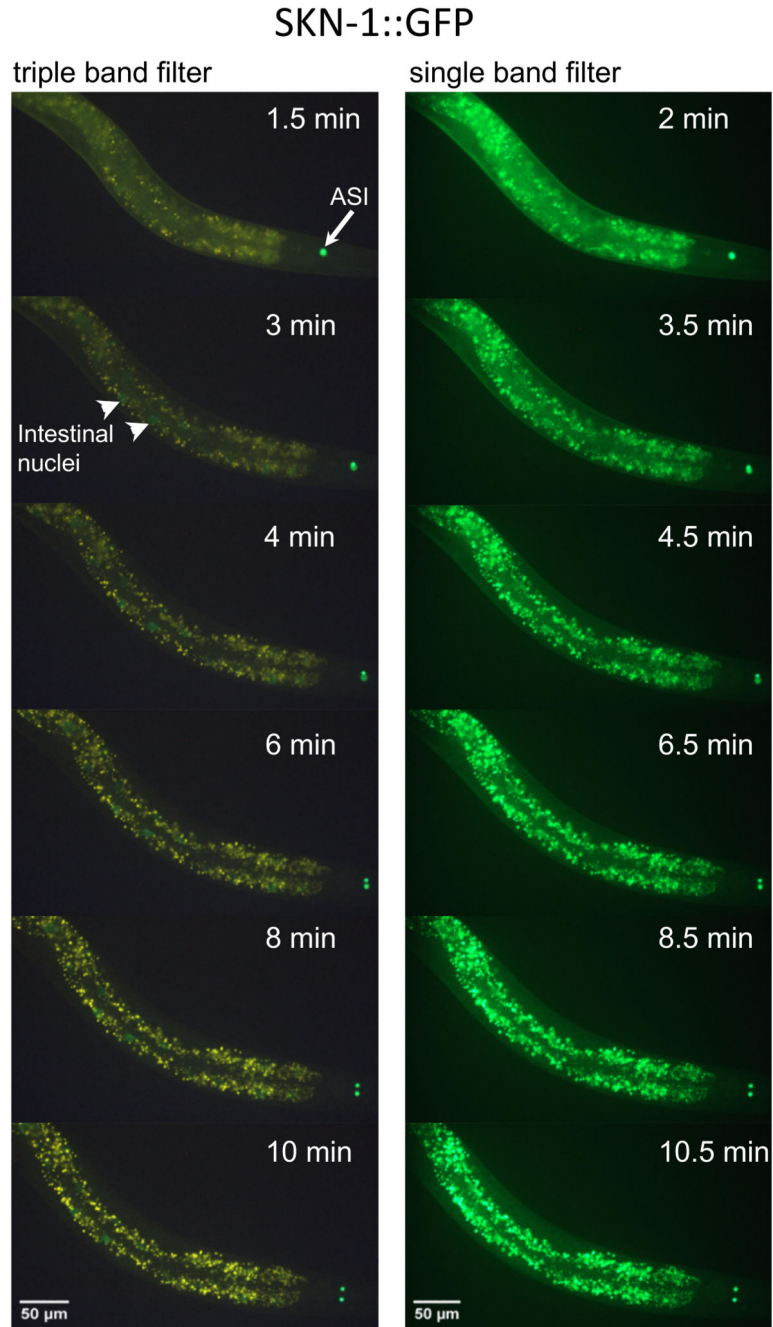


Figure 5. Time-course of SKN-1::GFP nuclear localization during oxidative stress. Shown is the same transgenic LD1 *C. elegans* (head to the right, ventral side down) at larval stage 4 (L4) imaged with the triple band filter set (left panel; 1/30 sec exposure time) and the single band filter set (right panel; 1/30 sec exposure time) over the time-course of 10.5 min treated with 10 mM sodium azide (NaN_3). After 3 min, SKN-1::GFP (white arrowhead) starts to become visible in intestinal nuclei when imaged with the triple band filter set (left panel). The white arrow indicates constitutively expressed SKN-1::GFP in the ASI neuron pair. Note that over time the intestinal autofluorescence also increases.

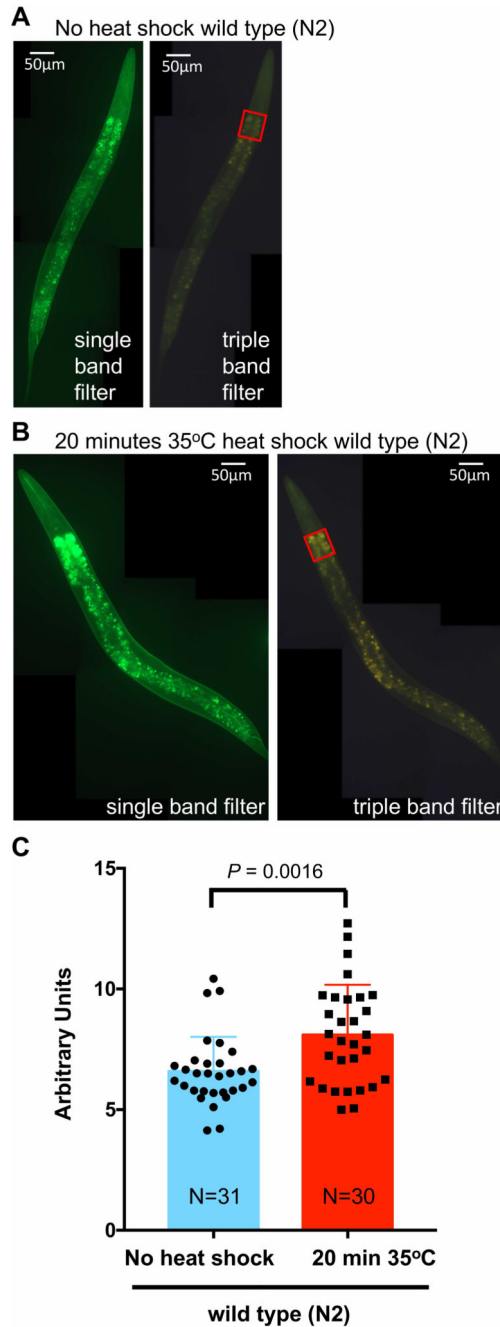


Figure 6. Heat shock increases intestinal autofluorescence.

A. Wild-type (N2) L4 *C. elegans* without heat shock, imaged with the single band filter set (left panel) and the triple band filter set. Anterior to the top, ventral side to the right. B. Wild-type (N2) L4 *C. elegans* with a 20 min heat shock at 35 °C, imaged with the single band filter set (left panel) and the triple band filter set. Anterior to the top, ventral side to the right. C. Using the triple band filter set, about 30 wild-type (N2) L4 *C. elegans* either not subjected to heat shock or treated with a 20 min heat shock at 35 °C were imaged. To quantify the intestinal autofluorescence, the pixel values of the same region of interest at the

anterior intestine [red rectangle shown in (A) and (B)] were measured and background was subtracted by placing the same rectangular area next to the *C. elegans* using ImageJ. The arbitrary unit was derived by first weighting each pixel and then normalizing to the measured area. In ImageJ, each pixel is given a value from 0 to 255 (dark to bright), which was multiplied with the number of pixels measured for a given pixel value. Then the sum of these weighted pixels was divided by the total number of pixels in the measured area. Data is represented as scatter dot plot (individual *C. elegans*) with the mean shown as a bar with standard deviation. *P* value was derived from an unpaired two-tailed *t*-test. For (A) and (B), images were stitched together using ImageJ (https://imagej.net/Image_Stitching) (Preibisch *et al.*, 2009).

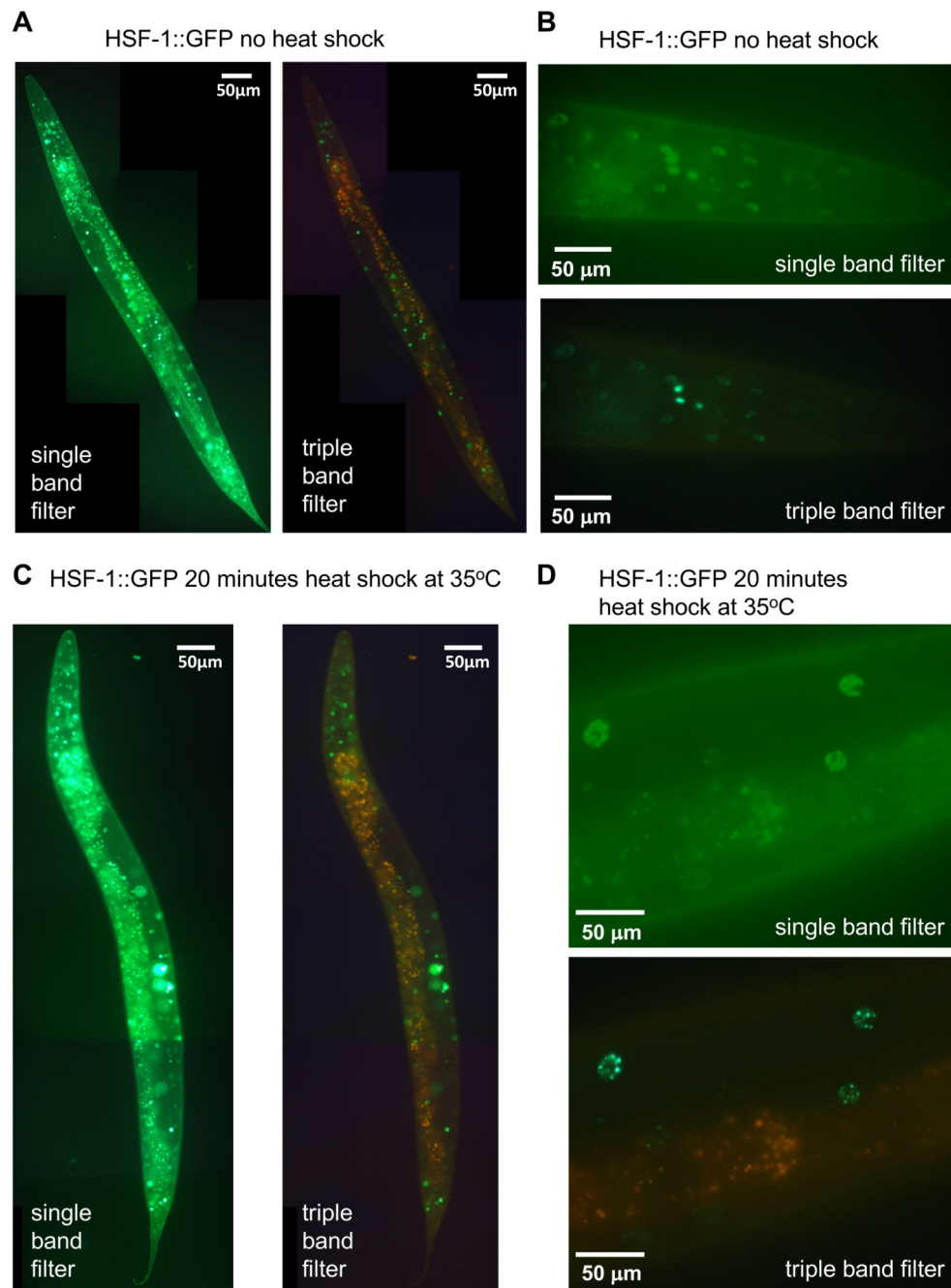


Figure 7. HSF-1::GFP nuclear foci formation upon heat shock.

A. Transgenic EQ87 *iqIs28 [hsf-1::gfp]L4 C. elegans* without heat shock, imaged with the single band filter set (left panel) and the triple band filter set (right panel). Anterior to the top, ventral side left. 1/30 sec exposure time). B. Head region of a transgenic animal without heat shock, imaged at a higher magnification with the single band filter set (left panel) and the triple band filter set (right panel; 1/55 sec exposure time). C. With a 20 min heat shock at 35 °C, imaged with the single band filter set (top panel) and the triple band filter set (bottom panel; 1/30 sec exposure time). D. Head region of a transgenic animal with a 20 min heat

shock at 35 °C, imaged at a higher magnification with the single band filter set (left panel) and the triple band filter set (right panel; 1/55 sec exposure time). For (A) and (C), images were stitched together using ImageJ (https://imagej.net/Image_Stitching) (Preibisch *et al.*, 2009).

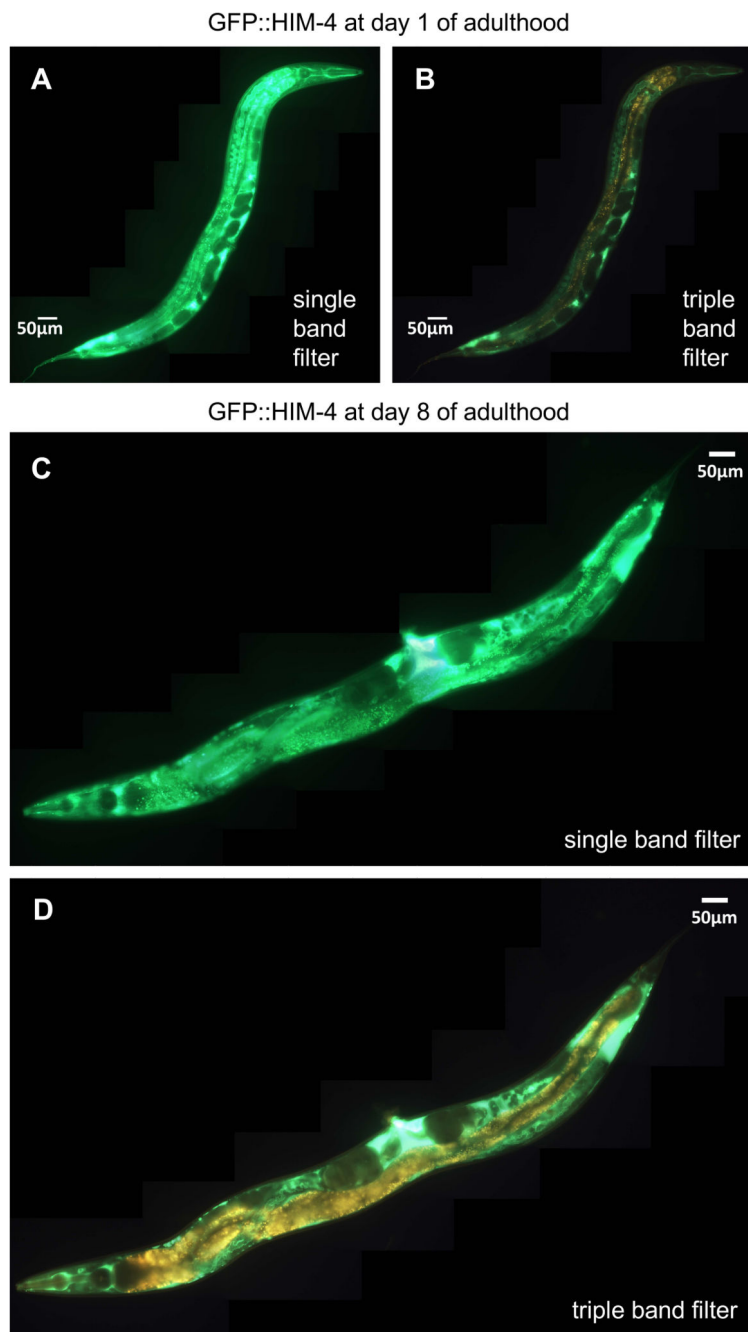


Figure 8. Autofluorescence increases with age masking GFP signal even from proximal tissues. In (A) and (B), the same transgenic BT24 *rhIs23* [*gfp::him-4*] *C. elegans* (anterior to the top, ventral side right) at day 1 of adulthood is imaged with the single band filter set (A; 1/30 sec exposure time) or the triple band filter set (B; 1/30 sec exposure time). In (C) and (D), another transgenic animal (anterior to the bottom, ventral side up) at day 8 of adulthood is imaged with the single band filter set (C; 1/30 sec exposure time) or the triple band filter set (D; 1/30 sec exposure time). For (A)-(D), images were stitched together using ImageJ (https://imagej.net/Image_Stitching) (Preibisch *et al.*, 2009).

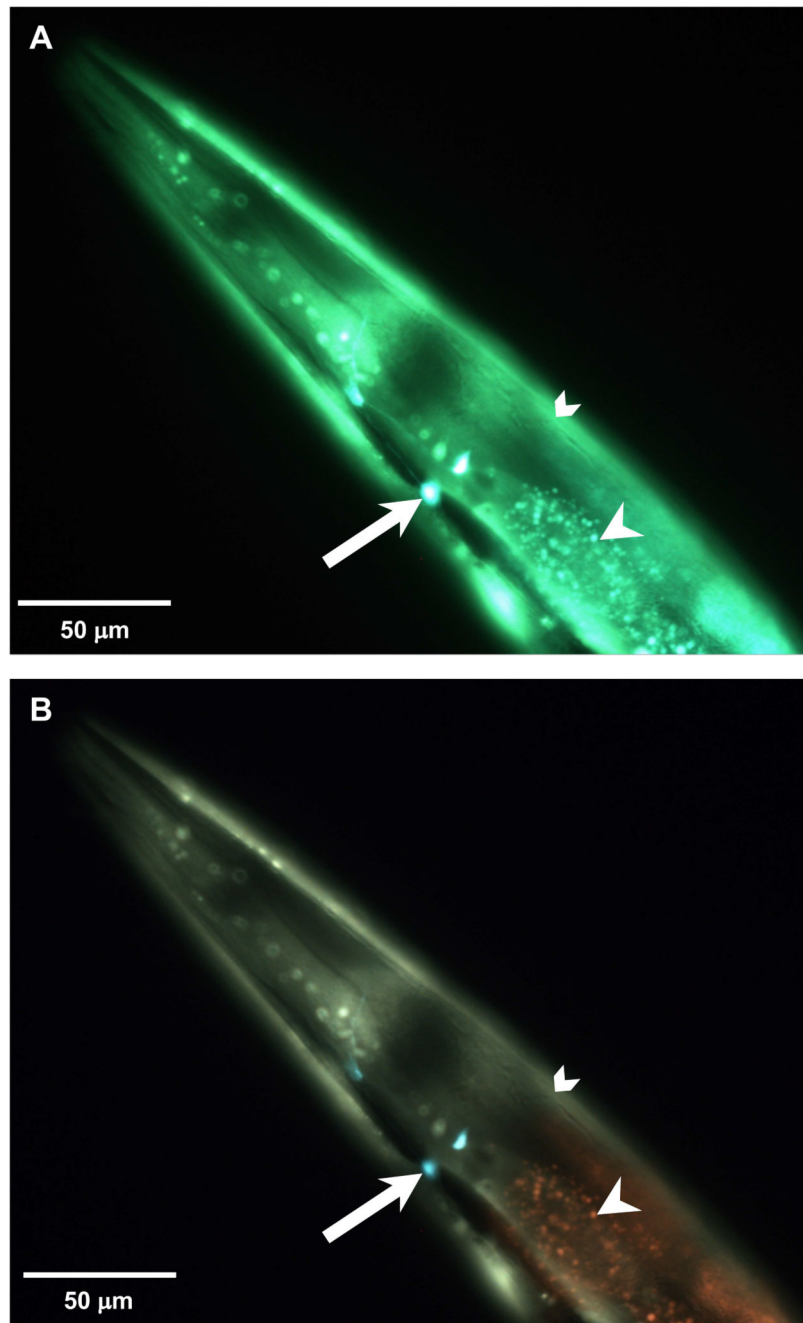


Figure 9. Triple band filter set allows a clear distinction of YFP from autofluorescence and from GFP.

(A and B) Head region of a double transgenic *C. elegans* at the eighth day of adulthood that expresses GFP driven by the *ttx-3* promoter in the AIY interneuron pair (white arrow) and α -synuclein-tagged YFP driven by the *unc-54* promoter in body wall muscles (chevron). The white arrowhead indicates intestinal autofluorescence. A. Imaged with the single band filter set. B. The same animal imaged with the triple band filter set. 1/120 sec exposure time.

5. Assessing collagen deposition during aging in mammalian tissue and in *Caenorhabditis elegans*

Alina C. Teuscher, Cyril Statzer, Sophia Pantasis, Mattia R. Bordoli, and Collin Y. Ewald¹

Methods Mol Biol . 2019;1944:169-188. doi: 10.1007/978-1-4939-9095-5_13.

It has previously been shown that the total collagen mass is declining during aging. In *C.elegans* collagen has been shown to be both sufficient to increase the lifespan of animals and required to attain the full lifespan extension in long-lived mutants. Therefore, methods to examine and quantify collagen levels in tissues and whole organisms are useful tools when researching the role of the matrisome in aging and longevity.

Here we describe a histological and a colorimetric approach to assess collagen levels in mammalian tissues and in the nematode *Caenorhabditis elegans*. For the estimation the total amount of collagen we describe the hydroxyproline measurement method on *C. elegans* and mammalian samples. To visualize collagen structures and potential turnover we introduce the polychrome Herovici's staining in mice and in *C. elegans*. Furthermore, we show how to harvest the cuticles of *C. elegans* specifically.

My contributions to this paper are the adaptation of the Herovici staining for mammal samples and its establishment in *C. elegans*, performing the cuticle isolation protocol and writing the manuscript together with my Co-authors. Due to the licensing agreement the publication could not be included into this thesis directly. For the final version we refer the reader to the published manuscript. A preliminary authors's manuscript version can be found on PubMed.

6. Mechanotransduction regulates extracellular matrix dynamics across tissue boundaries and influences longevity in *C. elegans*

6.1. Introduction

The ECM is a network composed of many large multidomain proteins linked together to form a stable structure. The ECM is essential for tissue geometry and integrity. ECM-cell interactions play an essential role in regulating many cellular functions, such as proliferation, differentiation, migration, and cell survival (Bonnans et al., 2014; Frantz et al., 2010; Hynes, 2009). ECM-cell interactions function as an anchor for cells and by signaling to cells through adhesion receptors. Furthermore, they are able to act as a signaling coreceptor and as a reservoir of growth factors and bioactive molecules (Lu et al., 2011). The compendium of all proteins that are part of the extracellular matrix or contribute to it is referred to as matrisome (Hynes and Naba, 2012; Teuscher et al., 2019a), while the complement of cell-cell and cell-matrix adhesion receptors in an organism are called adhesome (Whittaker et al., 2006).

When anchored to cells, the ECM can be a highly dynamic structure, being enzymatically remodeled to assure cellular function and needs (Bonnans et al., 2014; Ewald, 2020; Yue, 2014). This remodeling is crucial for morphogenesis during development, angiogenesis, bone development, wound repair, and maintaining stem cell niches (Bonnans et al., 2014).

Physical matrix properties can be sensed by cell-surface receptors like integrins that connect the ECM with the cytoskeleton (Charras and Sahai, 2014). Integrins integrate mechanical forces of the ECM-to-cell connection by initiating re-organization of the cytoskeleton or by triggering signaling cascades via small GTPases (Rho) or MAP kinase pathways (Humphrey et al., 2014). This leads to transcriptional gene expression changes and cellular adaptations (Humphrey et al., 2014; Hynes, 2009; Uhler and Shivashankar, 2017). Several ECM proteins encode “growth factor domains”, such as epidermal growth factor (EGF), which could act as ligands for growth receptors on the cell surface (Hynes, 2009). The presentation of these domains and other cryptic binding-domains also depends on mechanical stretching and unfolding or relaxing and coiling along the ECM proteins (Vogel, 2018). Thus, the composition of the ECM, the physical properties of the ECM, the anchoring to the cells, and the transduction of mechanical forces regulate cellular behavior and homeostasis.

Previous studies have already shown that the ECM plays a role in several age-dependent diseases and conditions like fibrosis, arthritis, osteoporosis, skin aging, and wound healing problems (Herrera et al., 2018; Mei Xiong et al., 2017; Shi et al., 2019; Sroga and Vashishth, 2012). Long-lived mutant mice showed extended preservation of connective tissue elasticity and integrity during aging (Flurkey et al., 2002; Wilkinson et al., 2012). A “young” ECM was

able to restore senescent human cell cultures to a youthful state (Choi et al., 2011). Furthermore, it could be shown that core matrisome proteins are required and sufficient to increase the lifespan of *C. elegans* (Ewald et al., 2015).

Longevity pathways might slow aging by activating collagen and ECM remodeling, slowing the age-related decline in ECM integrity (Ewald, 2020). How the ECM is generally regulated/maintained during aging is still unknown. Also, how the age-related decline in the biosynthesis of ECM proteins impacts matrix composition and whether there are any functional consequences on cellular integrity and homeostasis *in vivo* is largely unexplored.

6.2. Results

The ECM *C.elegans* atlas suggests a decline of cuticular collagen but not basement membrane components during aging

The expression of collagens and extracellular matrix genes is known to decline over time and is considered a common signature of aging (Budovskaya et al., 2008; Ewald, 2020; de Magalhães et al., 2009). However, mRNA and even protein levels might not represent actual collagen or core-matrisome proteins incorporated into extracellular matrices. ECM proteins have to be expressed by cells, secreted into the ECM space, and incorporated into the matrix. Therefore, we cannot draw direct conclusions from expression or protein levels to functional proteins without including protein locations. ECM genes are known to be expressed from different tissues, including body wall muscles, hypodermis, pharynx, intestine, gonad, and neurons, to form and incorporate into *C. elegans*' basement membranes, cuticle, and other pericellular structures (Figure 1A, 1B) (Graham et al., 1997; Kramer, 2005).

To investigate the plasticity and dynamics of ECM compositions, we first established an *in-vivo* atlas of the matrisome and adhesome to collect data about ECM gene expression and extracellular ECM protein levels and patterns during the development and aging of *C. elegans*. For this, we used all publicly available transcriptional and translational transgenic animals and generated some ourselves. We then analyzed the fluorescence patterns at different developmental stages. We made images of eggs, early larval stages (L1-L3), day 1 of adulthood, and day 8 of adulthood to include aging (Fig.1 C). We analyzed 37 strains in total, 15 of them were expression/transcriptional, and 22 were protein-fusion/translational reporter strains (Fig. 1 D-H).

As mentioned, collagens and other ECM genes have been shown to be generally downregulated during aging (Budovskaya et al., 2008; Ewald, 2020; de Magalhães et al., 2009). We could confirm this observation for most of the examined cuticular collagens (COL-10, COL-120, COL-129, COL-144). By contrast, the basement membrane collagen type IV (*let-*

2, *emb-9*) and hemicentin (*him-4*) have continued or even increased expression during aging (Fig. 1 F; Supp. Fig. 1-2).

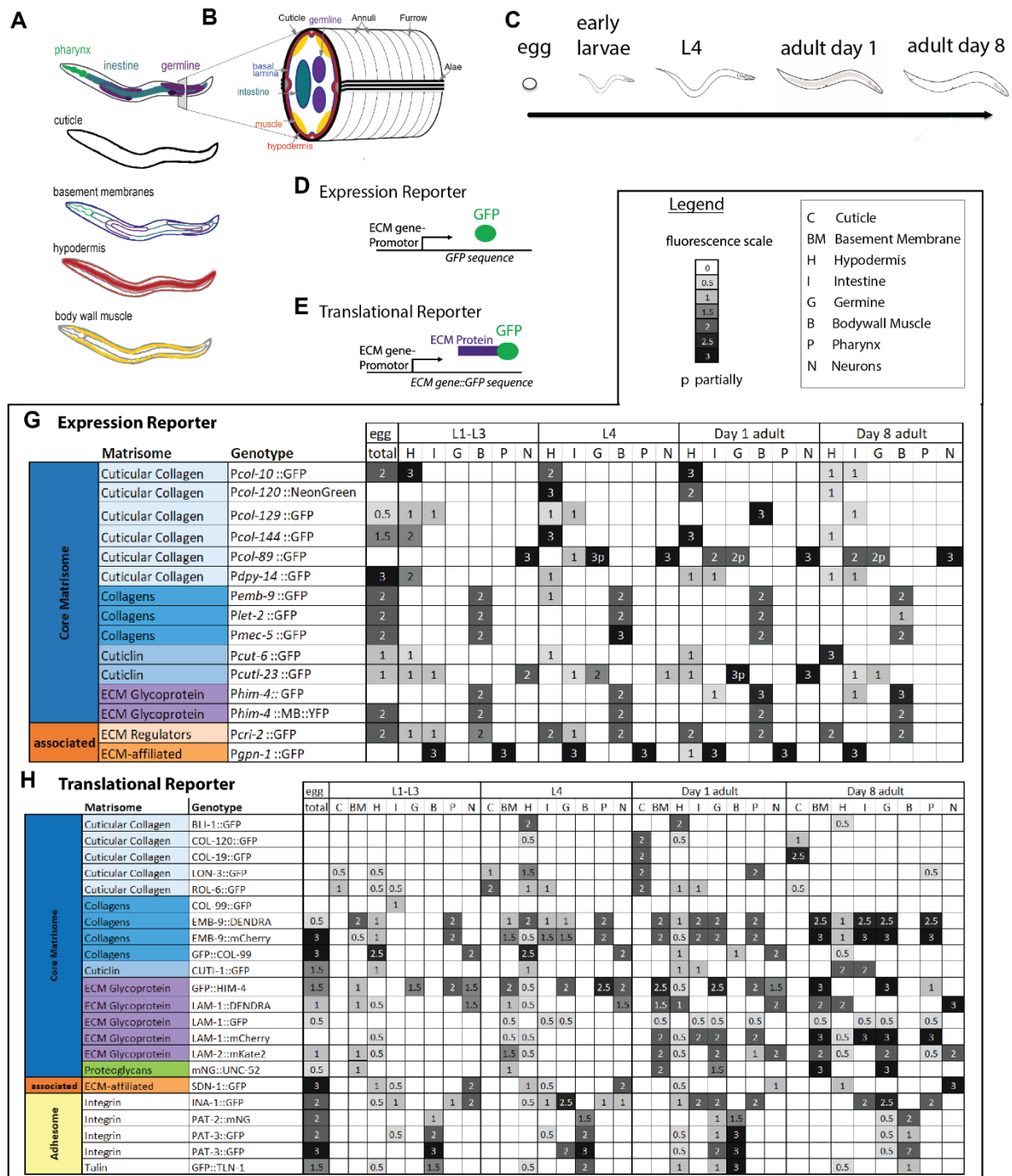


Figure 4: Matrisome and adhesome atlas during development and aging.

(A) Schematic representations of *C. elegans* tissues and ECMs. For orientation, some tissues are highlighted. (B) Schematic cut through *C. elegans*. On the outside are the annuli, furrows, and the alae of the cuticle (black). Below the cuticle is the hypodermis, The basal lamina (basement membranes), and the muscles.

(C) Overview of the different stages that were imaged for the atlas. (D) Schematic of expression reporter: GFP expression is controlled by an ECM gene promoter (E) Schematic of translation fusion reporter: ECM gene promoter drives the expression of the ECM genes fused to a GFP coding sequence. (F, G) Overview tables of the matrisome/adhesome atlas. Microscope images were taken of fluorescent *C. elegans* strains in different developmental stages and tissues to assess expression, protein location, and levels of ECM and adhesome genes. The strain-specific fluorescent levels were rated on a fluorescence scale from 0-3 in 0.5 steps. With the exception of the egg stage, the fluorescence levels are indicated for different tissues of *C. elegans*. (F) Overview table of

expression reporter stains to monitor expression levels during development and aging. (G) Overview table of translational fusion strains to assess protein levels and location during development and aging.

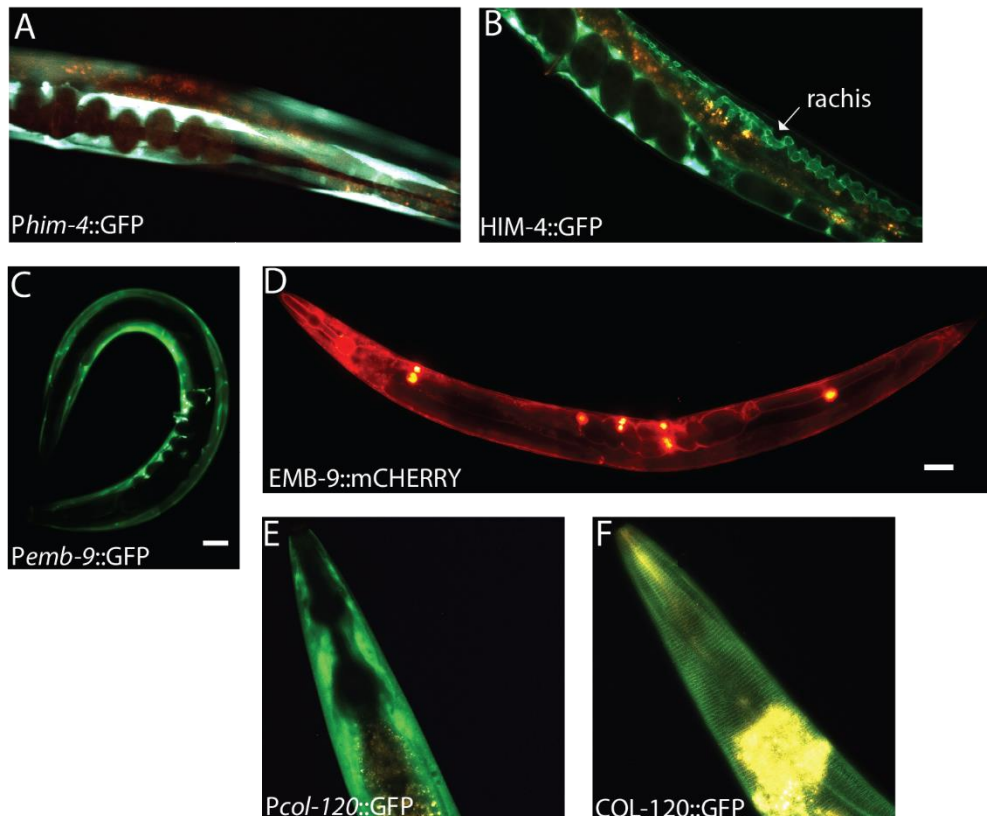


Figure 5: Example images of the matrisome and adhesome atlas

(A) GFP visualizes the expression of hemicentin (*him-4*) in the body wall muscle of *C. elegans*. (B) GFP::HIM-4 fusion protein is visible in the basement membrane and germline, especially in the rachis. The rachis is a central canal in the germline connecting the germ cells, (C) *emb-9* expression in the body wall muscles. (D) EMB-9::mCherry fusion protein localized in the basement membranes. The six bright dots are coelomocytes, phagocytic leukocytes, that are likely discarding misfolded EMB-9. (E) Expression of *col-120* in the hypodermis. (F) COL-120::GFP fluorescence in the animal's cuticle.

Next, we used the translational reporter strains to determine the incorporation of collagens and matrisome proteins into ECMs (Fig. 1 G). Here, we found that basement membrane-localized collagen type IV (EMB-9), hemicentin (HIM-4), laminin (LAM-1), and perlecan (UNC-52) increased in abundance during aging (Fig. 1G). On the other hand, cuticular collagens levels decreased during aging (Fig. 1G, Supp. Fig. 3-5).

During our examination, we confirmed that ECM glycoprotein hemicentin *him-4* is expressed in body wall muscles and incorporated into the basement membranes surrounding pharynx, gonads, hypodermis, and neurons (Fig. 2 A-B) (Vogel and Hedgecock, 2001). Similarly, basement membrane collagen type IV (EMB-9) is expressed in body wall muscles and hypodermis to form basal laminae surrounding intestine, gonads, pharynx, and parts of body wall muscles and hypodermis (Fig.2 C-D). We confirmed that the cuticular-predicted collagen *col-120* is expressed from the hypodermis to get incorporated into the cuticle (Fig. 2 E-F) (Teuscher et al., 2019a). We found that most cuticular collagens are predominantly expressed in the hypodermis and incorporated into the cuticle. The exceptions in our atlas are *col-89* and

col-129 that were also expressed in neurons and body wall muscles (Fig. 1 F-H; Supp. Fig. 1-5).

Taken together, we established the first ECM atlas associated with aging. We observed differences in ECM plasticity and dynamics for cuticle components compared to basement membrane components during aging. Using reporter lines, we confirmed observations from several expression data sets. We further see a correlation of transcriptional and translational activity, reflecting actual ECM protein content being incorporated into pericellular matrices during aging.

Lifespan extension slows the progressive loss of cuticular collagen

Interventions that increase lifespan were shown to prolong collagen gene expression and show an almost two-fold higher collagen content based on hydroxyproline levels during older ages (day 8 of adulthood) (Ewald et al., 2015)(Fig. 1 G). However, whether these increases results in proper incorporation into ECMs was not shown so far. Our first approach was to use the trichrome Herovici staining for collagens in *C. elegans* (Teuscher et al., 2019b). We found no apparent changes in staining inside the animals, like on the basement membrane. However, the cuticles preserve a brighter blue collagen staining during older ages (day-8-of adulthood) in long-lived *glp-1 (e2141)* mutant animals, still looking like young cuticles (Supp. Fig. 6-7).

Since we could show that most cuticular collagen levels decreased over the adult lifespan (Fig. 1 G, Supp. Fig. 3-5), we next wanted to know if longevity interventions could maintain higher levels of those collagens in the ECM during aging.

In order to quantify collagen levels incorporated into ECMs, we had some challenges to overcome. One was the continuous increase of autofluorescent age-pigments from the *C. elegans* intestine that masked the fluorescence from GFP signal, especially in all our cuticular collagen-GFP fusion strains, as they all display a weak GFP signal. We suspect that this is due to low protein levels of single cuticular collagens. We were able to separate the GFP signal from autofluorescence with a novel combination of a triple-band filter set (Teuscher and Ewald, 2018). Although some GFP intensity might be lost, the autofluorescent signal does not bleed into the GFP signal, thereby separating GFP autofluorescence (Fig. 2F). Furthermore, we had to subtract the yellow signal from the images before we could quantify the fluorescence intensity.

For quantification, we focused on three cuticular collagens (COL-120, LON-3, ROL-6), for which the expression and protein levels declined during aging, and on cuticular collagen COL-19, for which the mRNA but not the protein levels decreased (Budovskaya et al., 2008) (Fig. 1 H, Fig 3 D). We knocked down insulin/IGF-1 receptor *daf-2* by RNAi to slow aging and found

that these animals showed higher COL-120, LON-3, and ROL-6 incorporation into the cuticle during older ages (day-5 and/or 8 of adulthood) compared to control RNAi treatment (Fig. 2B-D, F). The levels of COL-19 were not changed upon *daf-2* (RNAi) treatment (Fig. 2 E-F).

These results suggest that COL-19 stays in the ECM throughout the animals' life after they were incorporated into the ECM during early adulthood (day 1), as its protein levels stay stable, while its expression declines. By contrast, other cuticular collagens, such as ROL-6, COL-120, and LON-3 seemed to disappear from the ECM during aging, a process that was slowed in long-lived animals. This begged the question if collagens are faster replaced in long-lived animals or if they stay longer in the cuticle.

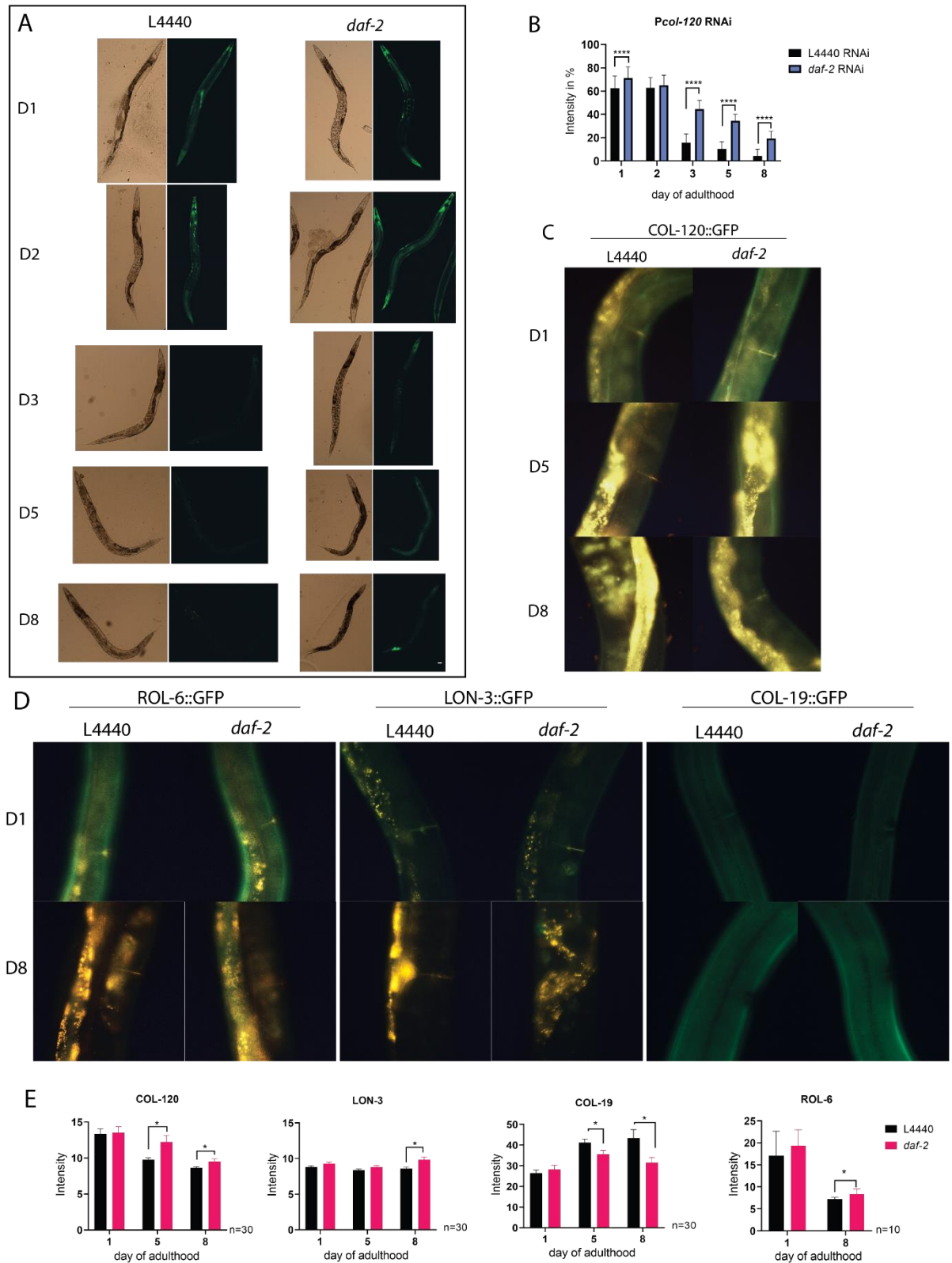


Figure 6: Expression and protein levels of cuticular collagens decline slower in long-lived *C. elegans*

(A) Time course of *Pcol-120::NeonGreen* animals fed with *daf-2* RNAi or the empty RNAi vector control L4440 bacteria. (B) Quantification of the *Pcol-120::NeonGreen* time course. Three rounds, each $n=20$, were quantified using a visual grading scale system with values from 0 - 3 in 0.5 steps. Error bars represent SDs. (C) Images of *COL-120::GFP* animals fed with *daf-2* RNAi or the empty RNAi vector control L4440 bacteria during aging, taken

at day 1, day 5, and day 8 of adulthood. (D) Images of ROL-6::GFP, LON-3::GFP, and COL-19::GFP animals fed with *daf-2* RNAi or the empty RNAi vector control L4440 bacteria during aging, taken at day 1 and day 8 of adulthood. (E) Fluorescence intensity quantification of three rounds of *daf-2* or L4440 RNAi experiments on translational cuticular collagen reporter strains. The green fluorescence intensities of images of either 30 or 10 (ROL-6) animals were quantified. The data are represented as mean \pm SD. **** indicates P-value \leq 0.0001 determined by using a two-way ANOVA.

Is cuticular collagen turned over during aging, and is this turnover maintained longer in the ECM in long-lived animals?

To determine whether collagens are turned over during aging, we translationally fused the photoconvertible fluorophore Dendra2 to the cuticular collagen COL-120. We selected COL-120 because it was shown to be required for *daf-2* induced longevity and increased the lifespan of *C. elegans* when overexpressed (Ewald et al., 2015). Newly synthesized Dendra2 emits green fluorescence, but upon UV irradiation, the Dendra2 tag becomes irreversibly photoconverted and emits red fluorescence (Mizuno et al., 2003). If the green Dendra2 that was fused to COL-120 is photoconverted to red in early adulthood and a few days later photoconverted areas get checked again for the red to green signal ratio, we could use the ratio to confirm and quantify the amount of turned over COL-120 (Fig. 4A). Since *col-120* biosynthesis is strongest at L4 to day 1 of adulthood based on expression levels and then markedly declines (Fig. 1F, 3A), we decided to photoconvert at day 2 of adulthood. We photoconverted two areas, head and mid-body areas, per animal at day 2 of adulthood and then quantified the changes two days later (Fig. 4, A-C). For quantification, the red and green signals were measured in the photoconverted areas (or to be photoconverted areas). To exclude potential differences in COL-120 levels in the animals, we also measured two areas close to the treated area in the same *C. elegans* for normalization (one above and one below). We then calculated the normalized green-to-red ratio of each of these three areas per animal and timepoint. (Fig. 4, D, E; Supp. Fig. 8 A-B). If green protein replaces the red one, the differences between the photo switched areas and the surrounding areas should decline. However, we could not see a significant turnover in our experiments.

During the experiments, we noticed that the animals had red fluorescence before photoconversion, which was not described in other studies using Dendra2. However, Dendra2 was developed to function inside cells, not extracellularly. Also, the fact that cuticular collagens like COL-120 form heterotrimers could have an influence on the conformation and therefore on the fluorescence of Dendra2. Looking at our raw data, we could also see that the red fluorescence didn't increase after photoconversion on day 2 of adulthood. It seems we primarily photobleached the GFP signal and measured only the GFP that came back two days later instead of converting it from green to red. Another difficulty performing the experiment was the handling of the animals: we had to image each animal separately to re-identify them two days after the photoconversion. Also, we had to get the worms back from the imaging slide after the

photoconversion, so we had to make sure that we only mildly paralyze them and carefully move them back on the plate. Another problem arose during imaging of the animals on day 4, as we had to find the photoconverted area again. In many cases, we could not relocate the area, likely because the animals were laying on the wrong side, and we had to ignore these animals for the experiment. Another point to consider is the generally low fluorescence level of translational cuticular collagen reporters. In most young adults, fluorescent reporter strains show no autofluorescence (Fig. 2; Sup. Fig. 2). In the strains that translate a cuticular collagen fused to GFP, we can already see the autofluorescence in young animals, as we had to increase the fluorescence signal a lot to make it visible under the microscope (Fig. 3). The presumably low protein levels of single cuticular collagens could make it difficult to visualize a turn-over because not much material gets exchanged. One solution, for example, could be to tag cuticular collagens that are turned over in greater levels, like COL-144, to increase the signal. With COL-120 we also face the problem that its expression declines rapidly after day 2 (Fig. 3), likely leading to a lower turnover rate after day 2, if we have one, also impairing the detectability of such a mechanism.

It could still be that *daf-2* RNAi has a higher collagen expression and that these collagens are just staying longer in the cuticle (Fig. 4 D, E).

We could not show the existence of a cuticular collagen turnover in the cuticle of *C. elegans*, so we cannot exclude the likely possibility that collagens are higher expressed and remain longer in the *C. elegans* cuticle.

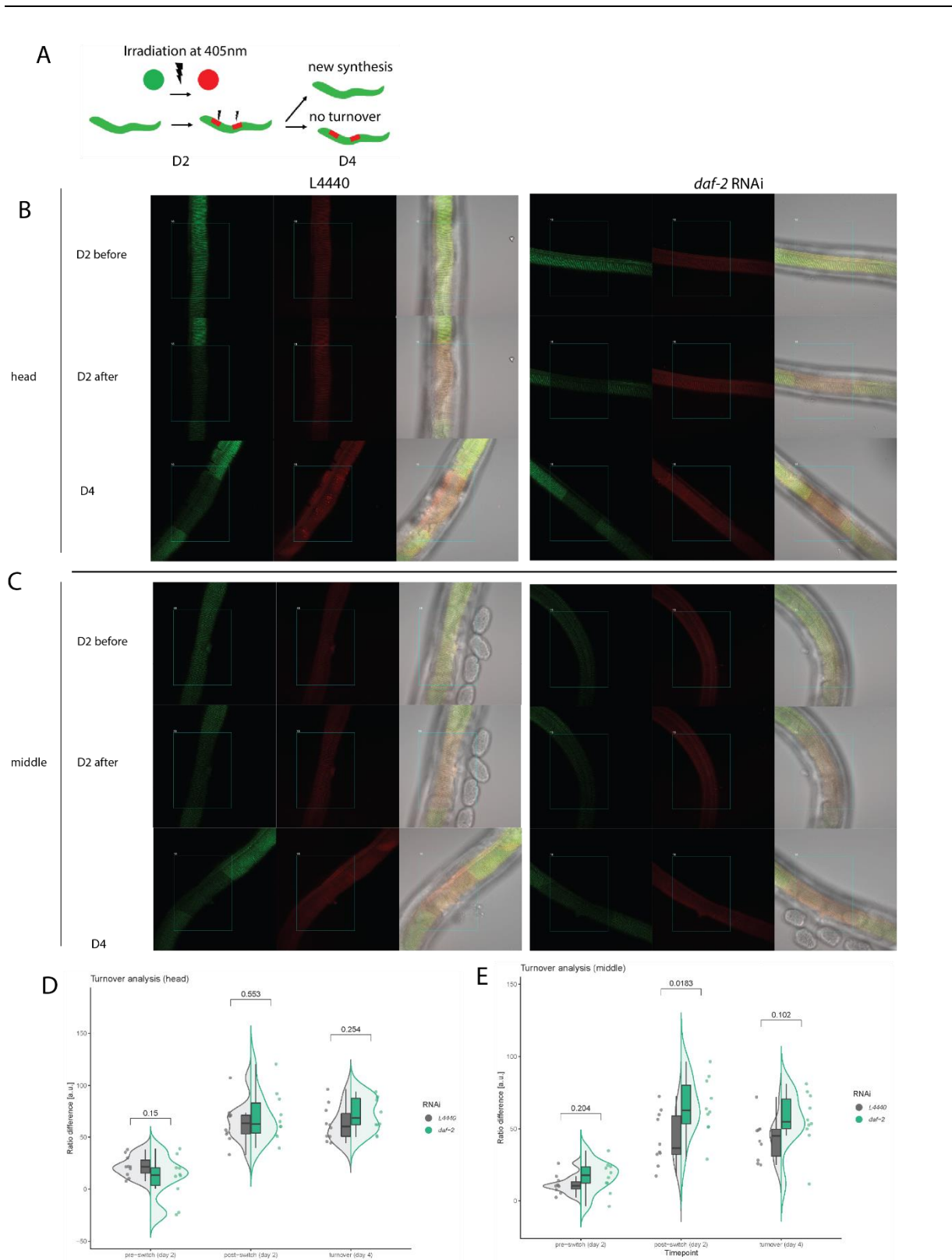


Figure 7: No significant turnover measurable in COL-120::Dendra2 strain

(A) Scheme for collagen turnover experiment using a *C. elegans* strain carrying the photoconvertible fluorophore Dendra2 fused with COL-120. (B-C) Images of LSD1062 (*P_{col-120}::col-120::dendra2*) *C. elegans* treated with L4440 RNAi as empty control or lifespan-extending *daf-2* RNAi. Images were taken on day 2 of adulthood, before and after photoconversion, and two days later, on day 4 of adulthood. Photoconverted areas are highlighted with a rectangle (B) images of the area just below the head region (C) Images of the middle area around the vulva of *C. elegans*. (D, E) Analysis of the images for a potential turnover of COL-120::Dendra2. The data points shown represent the relative difference of the photoconverted area to the surrounding non-treated area in percentage. N=10 per strain. Plots were done by Cyril Statzer.

Screening for regulators of prolonged collagen expression

In order to find regulators of the prolonged collagen expression by longevity interventions during aging, we carried out a targeted RNAi screen. We used *col-144* promoter-driven GFP *C. elegans* reporter strains (*Pcol-144::GFP*), which showed a progressive decline in fluorescence between day 1 to day 8 of adulthood, modeling the typical decline of most cuticular collagen expressions during aging (Fig. 1 G)(Budovskaya et al., 2008; Ewald, 2020; Ewald et al., 2015).

For our screen (Fig. 5, A), we used two strains carrying the *Pcol-144::GFP* and either a *spe-9* (*hc88*) or a *glp-1*(*e2141*) mutation. *spe-9*(*hc88*) is temperature sensitive and leads to sterility due to defective sperm production when the animals are moved to 25°C during development but has a normal lifespan and shows the same decline in *col-144* expression as the wild type (Fig. 5, B). *glp-1*(*e2141*) mutants only develop the somatic part of the gonad, leading to an elongated lifespan (Berman and Kenyon, 2006) and extended collagen *col-144* expression (Fig. 5, B). To validate screening hits and to include another type of longevity-promoting mutant, we crossed *spe-9*(*hc88*) mutants with long-lived *daf-2*(*e1370*) animals.

We aimed to identify two types of regulators by RNAi screening: First, negative regulators that, when knocked down, would result in higher *Pcol-144::GFP* levels at day 8 of adulthood, which would suggest prolonged collagen maintenance. Second, regulators that are required for prolonged collagen expression in long-lived mutant backgrounds. When those regulators are knocked down, higher *Pcol-144::GFP* levels at day 8 of adulthood would be abolished in long-lived animals.

We screened through most *C. elegans* kinases (382 out of 438 kinases), about one-third of all transcription factors (330 out of 934 genes), and 190 metabolism genes (Fig. 5C). We decided to generate a matrisome library based on our *C. elegans* matrisome (Teuscher et al., 2019a) containing 625 out of the 719 matrisome genes (Fig. 5 C). Furthermore, a whole-genome RNAi screen has been previously performed for pathogen infections, but they used *col-12* promoter as a control (Zugasti et al., 2016). We re-analyzed their screening data for enhancer or suppressor of *col-12* expression during young adulthood and chose 133 genes that might affect prolonged collagen expression during aging until day 8 adulthood (Fig. 5 C). Lastly, we performed a literature search for ECM regulators across species and selected 98 genes. In total, we screened 1758 genes in more than three replicates and found 254 hits. These hits were once again revalidated in a two-pass system. In the first pass was a retesting with *spe-9* and *glp-1* animals, and in the second pass, candidate genes were validated in addition in *daf-2* (*e1370*) longevity background. We ended up with 107 confident hits (Fig. 5 C).

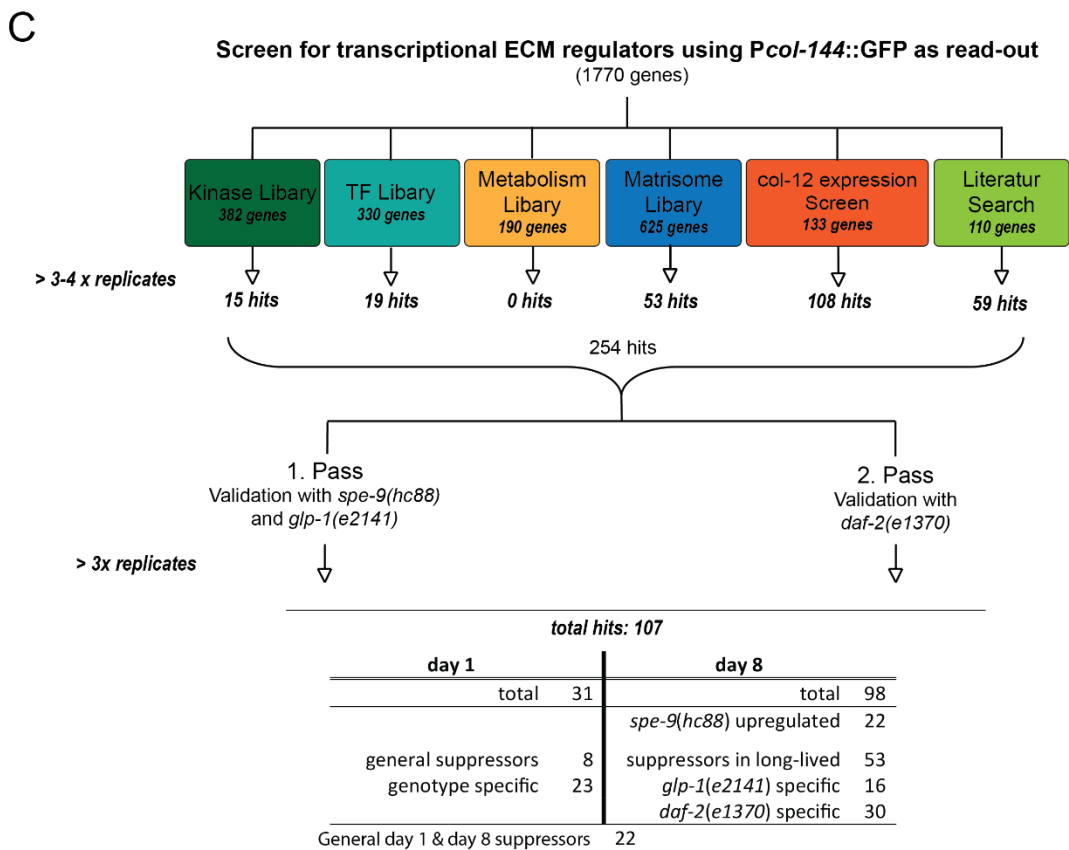
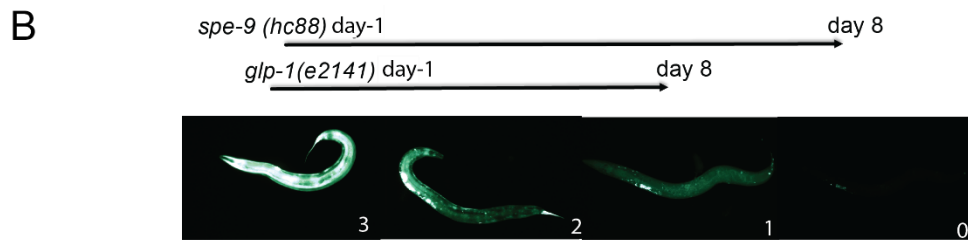
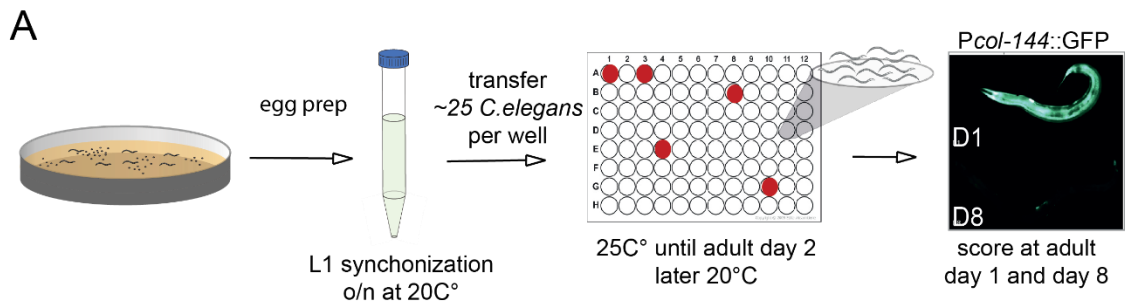


Figure 8: RNAi screen for transcriptional ECM regulators

(A) Workflow of the RNAi screen. *C. elegans* eggs were extracted by bleaching and synchronized overnight. On the next day, they were transferred to the screening plates. The fluorescence of the animals were scored on day 1 and day 8 of adulthood (B) Scoring scheme for the Pcol-144::GFP *C. elegans*. Above is the usual decline of the fluorescence of two mutant backgrounds: *spe-9(hc88)* and *glp-1(e2141)*. (C) Schematic overview of the RNAi screen. We screened several RNAi libraries, a list of selected genes from a previously performed whole-genome RNAi screen with *col-12* expression (Zugasti et al. 2016), and a list of genes from the literature. We used two *C. elegans* strains carrying the Pcol-144::GFP reporter in either a *spe-9(hc88)* or a long-lived *glp-1(e2141)* background. The hits were re-validated in *spe-9(hc88)* and *glp-1(e2141)* and additionally in *daf-2(e1370)* animals. The table lists the number of hits per condition and categories.

We found that RNAi against some transcription factors, such as *daf-16/FOXO*, *pqm-1*, and *xbp-1*, which are required for longevity, downregulates *Pcol-144::GFP* fluorescence in the longevity mutant backgrounds (Supp. Table 1-2). We also identified known longevity-promoting genes that prolonged *Pcol-144::GFP* expression (e.g., *sams-1*, *pat-4*, Supp. Table 1-2).

We used the online tool WormCat (Holdorf et al., 2020) and our matrisome list to annotate our screen hits and sort them into gene ontology (GO) term categories. We found that by far the most hits were hit (49 out of 107) were genes of the matrisome, followed by genes involved in signaling, autophagy, adhesome genes, metabolism, and transcription factors (Table 1, Supp. Table 1-2).

Next, we asked, which gene ontology terms are over-represented among the genes which regulate the *col-144* promoter in our long-lived strains (*glp-1* only, as *daf-2* testing didn't involve enough genes because we used the mutant only in our final validation round with 254 genes). We, therefore, performed an enrichment analysis, which first compared the hits in both backgrounds and then analyzed which categories were enriched compared to the data set of all screened genes. The enrichment analysis implicates the entire axis of the nucleus to ECM signal transduction to be involved in *col-144* promoter regulation (Supp. Fig 9 A). We found the ECM, cytoskeleton, and the cytoplasm in general, as well as multiple membrane-resident GO terms. Autophagy (mitophagy, macroautophagy, and autophagosome) and muscle cell processes are among the most-enriched biological functions (Supp. Fig. 9 B and Supp. Fig 10). In terms of molecular function, the structural aspects are the most over-represented within our gene target list (Supp. Fig. 9 C).

We were surprised that so many matrisome and adhesome genes, which are involved either in muscle or matrix attachment, were found in our screen (Table 1, Supp. Table 1-2). We, therefore, mapped these candidates in an anatomical model displaying the four layers of cuticle attached to the hypodermis attached to the basement membrane attached to the body wall muscles (Figure 6). We found that knocking down genes that were previously described to form or remodel the cuticle either function as an enhancer (green) or suppressor (red) of prolonged collagen expression (Figure 6, Supp. Table 1-2). In general, proteins linking the cuticle through the hypodermis and basement membrane to the muscle seemed to be required for prolonged collagen expression. This includes genes that are part of the hemidesmosome like fibrous organelles (*mup-4/* matrilin, *vab-10/* dystonin, *let-805/* myotactin-fibronectin repeats) and genes coding for basement membrane proteins (*emb-9/* collagen type IV, *unc-52/* perlecan, *epi-1/* laminin alpha, *lam-2/* laminin gamma) (Fig. 6, Supp. Table 1-2). By contrast, knockdown of genes that form the adhesome parts in the muscle that are anchoring the muscle to the basement membrane (*pat-2/* integrin alpha, *unc-112/* pleckstrin, *pat-4/* integrin-linked kinase, *pxl-1/* paxilin, *pat-10/* troponin C) upregulated and prolonged *Pcol-144::GFP*

expression in the hypodermis (Figure 6, Supp. Table 1-2). Most strikingly, all these genes are components that are either required for enabling or transmitting mechanical forces (mechanotransduction).

Table 1: Confident hits of RNAi screen for transcriptional ECM regulators sorted by gene ontology categories.

For the categorization, we used the WormCat online tool (Holdorf et al., 2020)

Category	Number	Percentage
Matrisome	49	45.8%
Signaling	12	11.2%
Autophagy	9	8.4%
Adhesome	6	5.6%
Metabolism	6	5.6%
Transcription factor	6	5.6%
Proteolysis	3	2.8%
Stress response	3	2.8%
Unknown	3	2.8%
Development	2	1.9%
Muscle function	2	1.9%
Nucleic acid-binding	2	1.9%
Chaperone	1	0.9%
Cytoskeleton	1	0.9%
Neuronal function	1	0.9%
Protein modification	1	0.9%
Total	107	100%

Many basement membrane genes like *emb-9*, *let-2*, *lam-1* and *lam-2*, as well as the integrins *pat-2* and *pat-3* and genes responsible for the dense body proteins that are expressed in the body wall muscle. Still, their knockdown remotely regulates the expression of *col-144* in the hypodermis. This is clear evidence for cross-tissue communication. Mechanotransduction could be the key player in this cross-tissue signaling because so many hits we found are involved in this process.

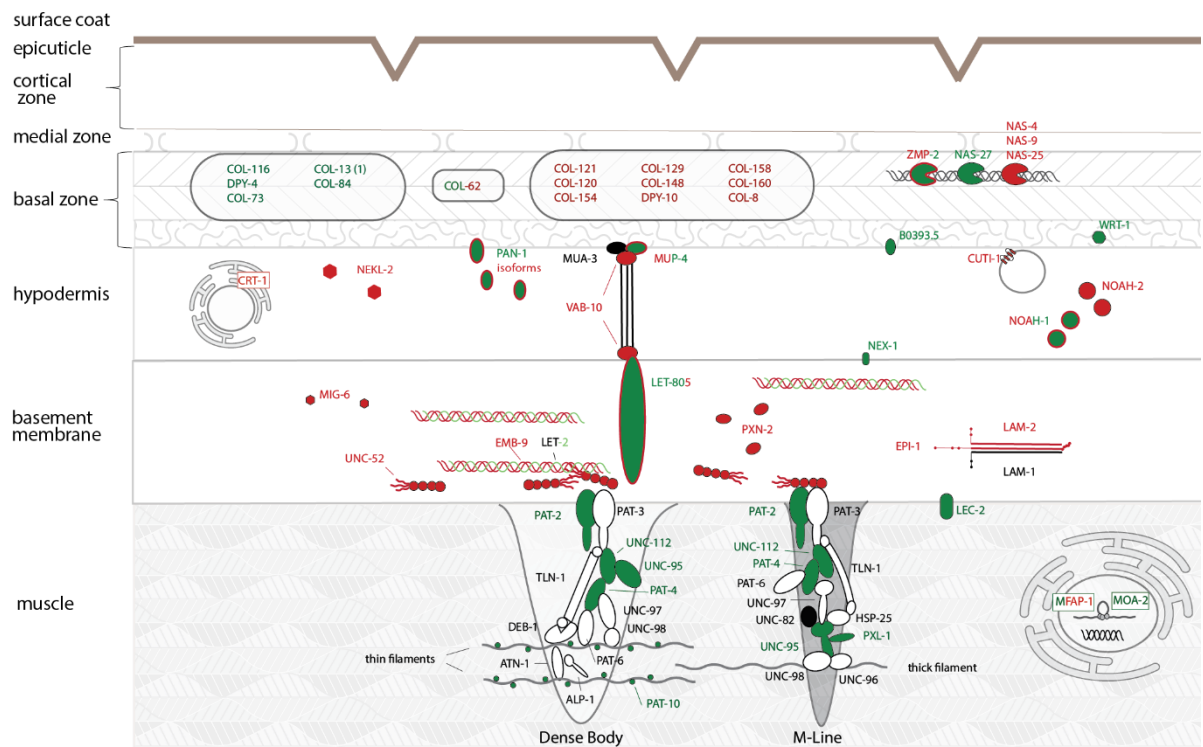


Figure 9: Overview of screen hits located in a body-wall cross-section of *C. elegans*

The hits of the screen are shown in the predicted layers. Knockdown of green marked hits led to an upregulation of the *Pcol-144::GFP* reporter signal (potential suppressors/inhibitors) in at least one of the screened strains, while knockdown against the red ones led to a downregulation (potential activators). The green and red marked proteins showed an upregulation in some of the strains but downregulation in others. The proteins in black were also tested but did not show a significant up- or downregulation, while the white ones were not included in the screen. The surface coat, epicuticle, cortical zone, medial zone, and basal zone belong to the cuticle. The proteins in the three bubbles in the basal layer are collagens. Their exact location in the cuticle is unknown so far. ZMP-2, NAS-27/4/9/25 are metalloproteinases. B0393.5 is an ortholog of human SNED1 protein, while WRT-1 is a hedgehog-signaling molecule. In the hypodermis, CRT-1 is a chaperone controlling the folding of extracellular matrix protein UNC-52. The kinase NEKL-2 is required for molting. PAN-1 is involved in molting and has three different isoforms; one is transmembrane, while another is predicted to be cytosolic. Hemidesmosome-like junctions in the hypodermis consist of MUA-3, MUP-4, the intermediate filaments, VAB-10 and LET-805, which reach through the membrane into the basement membrane. NEX-1 is an ortholog of human ANXA13 (annexin A13). CUTI-1 is predicted to be involved in the tethering and fusion of vesicles. NOAH-1 and NOAH-2 are both involved in molting. MIG-6 in the basement membrane shows similarity papilin and lacunin, while UNC-52 is a perlecan, that is likely binding to the integrins PAT-2 and PAT-3. EMB-9 and LET-2 are the two *C. elegans* type IV collagens. The peroxidase *pxn-2* is described to play an important role in basement membrane integrity. EPI-1, LAM-1, and LAM-2 form together with the one of the two *C. elegans* isoforms ($\alpha\beta$) and which is present on the pharynx, intestine, body wall muscle, and hypodermis. PAT-2(α) and PAT-3(β) are the two Integrins that are connecting the dense bodies and the M-lines to the basement membrane. In the muscles, we show the proteins that together build the dense body holding the thin actin filaments and the M-line holding the thick myosin filaments, which together are responsible for the attachment of the muscle to the basement membrane. MFAP-1 and MOA-2 are both responsible for alternative splicing.

Excluding developmental effects by rescreening hits starting RNAi treatment in L4 stage

For our screen, the animals were placed on the plates in L1, so they were exposed to the RNAi treatment during most of their development. As some of the genes also play an important role during development, animals treated with RNAi against those genes displayed developmental phenotypes, like larval arrest or dumpy (short and fat) phenotypes. Therefore, we rescreened hits of our mechanotransduction model that caused developmental phenotypes and waited

until L4 until we shifted them to RNAi plates. Fifteen genes were tested again with our *spe-9* and *glp-1* screenings strains expressing *Pcol-144::GFP*. Out of the 15, 7 showed upregulation on day 8 in the *spe-9* background (*nekl-2*, *dpy-10*, *col-120*, *noah-1*, *tln-1*, *lam-2*, *unc-95*) while we had 4 upregulated genes in the *glp-1* background (*nekl-2*, *col-120*, *let-805*, *unc-112*) (Supp. Table 3 and 4). There was no significant change on day 1, likely due to the short timespan since the start of the treatment, as RNAi needs at least 24 h to become effective. Interestingly the effect of the RNAi against the two collagens *dpy-10* and *col-120* changed compared to the screen on L1 animals. Starting from L1, the knockdown of *col-120* (in *glp-1*) or *dyp-10* (*glp1* and *daf-2*) caused downregulation of *col-144* expression, while in L4 animals it led to an upregulation of *col-144* in *spe-9* animals and for *col-120* also in *glp-1* mutants. Because RNAi has no effect on already existing proteins, RNAi treatment starting at L4 only reduces proteins that are being synthesized in adulthood, which could lead to different regulatory effects on the expression of *col-144* gene. Many others did not cause a significant change in *col-144* expression as they did in the L1 screen.

This differences in results could be due to the characteristics of RNAi. RNAi can only knock down RNA. As mentioned, when the corresponding proteins are synthesized mainly in the larval stages, RNAi in L4 or adults will not show any effect at all. Furthermore, RNAi by feeding in *C. elegans* is slow and needs at least 1 to 2 days to be effective (Ahringer, 2006). Sometimes it is even recommended to wait until the next generation to get a stronger knockdown. Nematodes, like *C. elegans* have an additional RNAi pathway, which is not present in mammals: the siRNA can act as a primer for a dsRNA-dependent RNA polymerase (RdRP), leading to the formation of a new dsRNA and an enhancement of the RNAi effect over time (Sijen et al., 2001).

Validation of screen hits and testing for potentially important signaling pathways by examining the influence of mutations on *col-144* expression

As RNAi could have off target effects, we wanted to validate important genes of the mechanotransduction system by crossing loss-of-function mutants of those genes into our *Pcol-144::GFP* screening strain. The *Pcol-144::GFP* fluorescence of these newly crossed strains was then monitored from day 1 to day 8 of adulthood and compared to the *col-144* expression in a wild-type background.

The perlecan *unc-52* is an important part of the mechanotransduction from the muscle to the cuticle. *unc-52(e699, su250)* is a temperature-sensitive mutation of perlecan in *C. elegans*. Starting at day 2 of adulthood mutants experience progressive paralyzation at 15°C. At 25°C, the mutants show complete loss of function (Ben-Zvi et al., 2009). The expression of *col-144*

at 20°C shows a slight but significant upregulation in the *unc-52* mutants during aging (Fig. 7 A, B), which confirms *unc-52* as a hit in our screen. Interestingly, we can already see an accumulation of GFP fluorescence in dots on day 1, which becomes even more evident over time (Fig. 7, B). *col-144* is expressed in the hypodermis, which consists of a small number of multinucleate syncytia, as most epidermal cells fuse during mid-embryogenesis. Without a properly functioning *unc-52*, something appears to stop the GFP from floating freely through the hypodermis syncytium of *C. elegans*.

The integrin α -subunit gene *pat-2* was a hit in our screen with the RNAi treatment causing an upregulation of *col-144* expression at day 8 in long-lived *glp-1* animals. Therefore, we also wanted to test if the sole integrin β -subunit influenced *col-144* expression. We tested two mutants of the integrin PAT-3, which is part of the integrin heterodimer anchoring the muscle cells to the basement membrane. Both mutants lead to a strong upregulation of *col-144* in old *C. elegans* compared to the control (Fig. 7, E-F). Therefore, we could show that both integrins forming the heterodimer at the muscle membrane regulate *col-144* expression during aging.

In our screen, we could link *col-144* expression to mechanotransduction, but we also wanted to check for signaling pathways working together or in parallel with mechanotransduction to regulate *col-144* expression. We, therefore, used mutants of genes that are part of potential pathways, as they were previously described to be either involved in the regulation of collagens and/or in longevity and also crossed them with our *Pcol-144::GFP* screening strain.

Transforming Growth Factor- β (TGF- β) superfamily signaling plays a crucial part in cell-to-cell communication. It is involved in many different processes, like defining and maintaining cell identity and embryonic body plan. *C. elegans* contains five members of TGF- β ligand family, with two of them, *daf-7* and *dbl-1*, signaling through a canonical receptor-Smad signaling pathway (Gumienny and Savage-Dunn, 2013). The DAF-7/TGF- β -related ligand is expressed in the pair of ASI sensory neurons (Ren et al., 1996) and acts as a systemic signal for autophagy regulation in *C. elegans* (Zhang et al., 2019). It was previously shown to increase the lifespan of *C. elegans* when *daf-7* is downregulated, and that this increase requires the FOXO transcription factor *daf-16* of the insulin signaling pathway (Shaw et al., 2007). *dbl-1*, which is expressed by ventral cord motor neurons (Suzuki et al., 1999) and is the ligand of the TGF- β pathway also known as Sma/Mab pathway (Padgett et al., 1998). This pathway regulates the innate immunity and body size of *C. elegans* (Gumienny and Savage-Dunn, 2013). It was previously shown that DBL-1 genetically acts with the UNC-52/perlecan in directing migrating distal tip cells (Merz et al., 2003). Furthermore, DBL-1/BMP signaling determines body size through the transcriptional regulation of cuticle collagen genes. However, the signaling is bidirectional as these cuticular collagens are also able to regulate *dbl-1* gene activity, forming a contact-independent feedback loop (Madaan et al., 2018, 2020). Both genes were also defined as a part of the matrisome. Mutants of *daf-7* displayed a strong and *dbl-1* a

slight but significant upregulation of *col-144* (Fig. 7 C-F). Interestingly mutants of the type I receptor for the Sma/Mab pathway, *sma-6*, showed a much higher upregulation compared to its ligand *dbl-1* (Fig. 7 E-F).

The STAT family protein STA-2 and were shown to induce the expression of antimicrobial peptides (AMPs) in the epidermis in response to fungal infection or injury (Dierking et al., 2011, Pujol et al., 2008b, Pujol et al., 2012). During molting, when the cuticle gets replaced and the trans-epidermal hemidesmosome-like fibrous organelles get disrupted on the apical side. It was shown that this disruption triggers lysosomal activation via ELT-3 and the STAT family protein STA-2, facilitating ECM remodeling essential for larval development (Miao et al., 2020). It was also shown that the GATA transcription factors circuit consisting of *elt-3*, *elt-5* and *elt-6* is able to control aging in *C. elegans* and that one of *elt-3* downstream targets is *col-144* (Budovskaya et al., 2008). Therefore, we also tested the effect of *sta-2* mutants on the expression of *col-144*. Again, we found a clear upregulation in old animals.

F09A5.2 is a putative tyrosine-protein kinase that was a hit in our screen, and that was previously associated with lifespan increase in *C. elegans* (Rikke et al., 2000), here we could show that *col-144* expression is clearly upregulated during aging in a F09A5.2 mutant background.

Both the TGF beta signaling pathway and the *elt* GATA transcription factor family show very promising results and were previously connected to the regulation of longevity and aging. It would be interesting to evaluate the interactions with our mechanotransduction model. Especially *dbl-1* could be an interesting candidate.

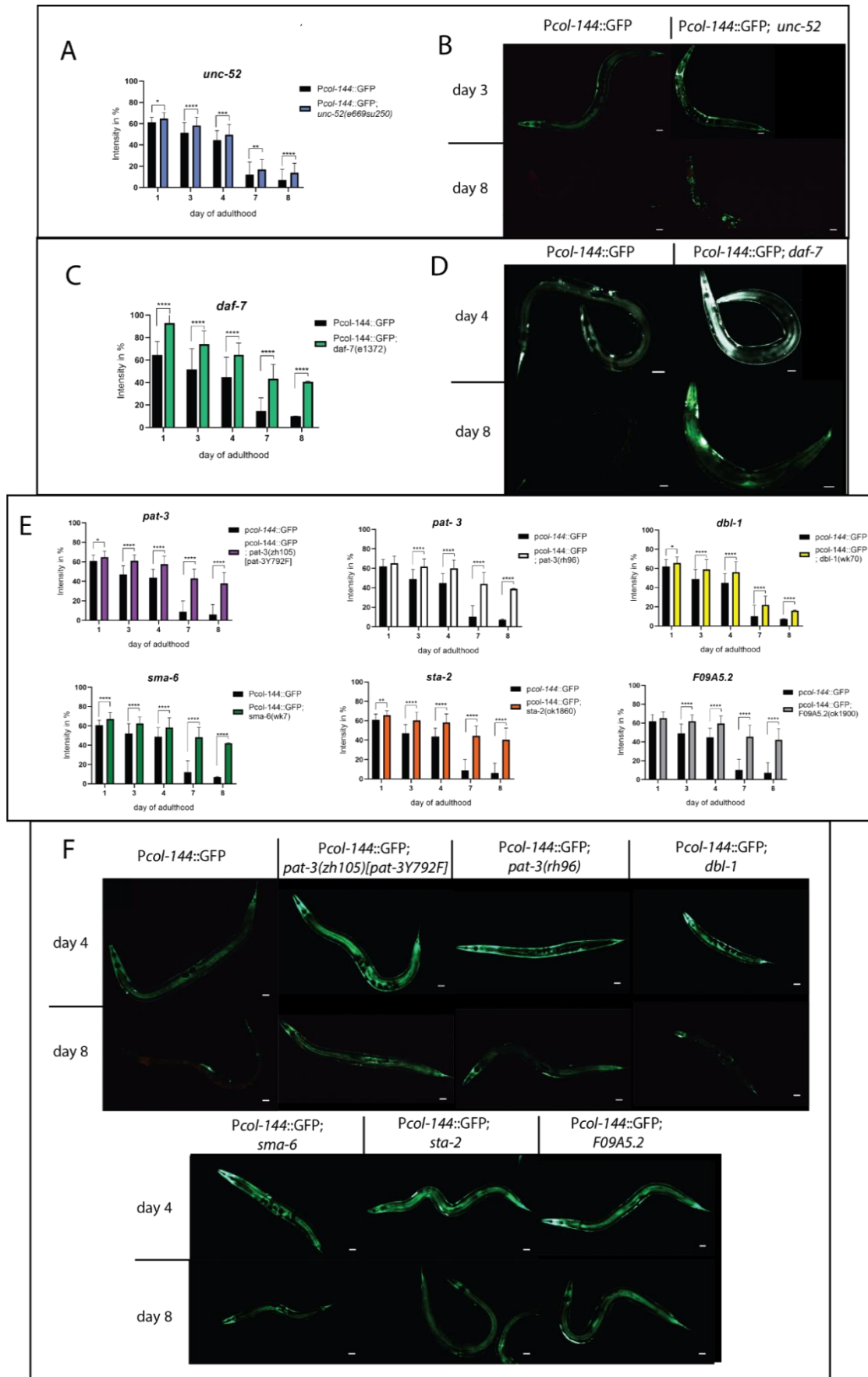


Figure 10: Validation and examination of potential *col-144* regulators

(A) Quantification of *Pcol-144::GFP* fluorescence in *unc-52* temperature-sensitive mutants at semi-permissive 20°C during aging. Three rounds, each n=20. (B) fluorescent images of *Pcol-144::GFP; unc-52(e669su250)* mutants at day 3 and 8 of adulthood at 20°C compared with *Pcol-144::GFP* in wild-type background. (C) quantification of *Pcol-*

144::GFP fluorescence in *daf-7(e1372)* mutants from day 1 to day 8 of adulthood at 20°C. Three rounds, each n=30. (D) fluorescent images of *Pcol-144::GFP; daf-7(e1372)* mutants at day 4 and 8 of adulthood at 20°C compared with *Pcol-144::GFP* in wild-type background. (E) quantification of *Pcol-144::GFP* fluorescence in *pat-3(zh105)*, *pat-3(rh96)*, *dbl-1(wk70)*, *sma-6(wk7)*, *sta-2(ok1860)*, *F09A5.2(ok1900)* mutant backgrounds during aging at 20°C. Each graph represents three independent rounds, each n=30. (F) fluorescent images of strains quantified at day 4 and day 8 compared with *Pcol-144::GFP* in wild-type background at 20°C. All time courses were quantified using a visual grading scale system with values from 0 – 4. Error bars in the figure display the standard deviation

Potential disassociation of basement membrane components with integrins during aging

The linkage of the muscle to the basement membrane is the necessary first step in order to allow mechanotransduction from the muscle up to the cuticle. It was shown previously that perlecan *unc-52* is required for this force transmission and that integrins bind to the basement membrane via *unc-52* (Battaglia et al., 1993; Bix and Iozzo, 2008). Perlecan *unc-52*, on the other hand, is able to bind to type IV collagens (*emb-9* and *let-2*) and laminins linking the muscle to the structural network of the basement membrane (Gotenstein et al., 2018; Jiang and Couchman, 2003) (Figure 6).

We hypothesized that maybe during aging, this close association might progressively decline. To address this, we assessed co-localization of collagen EMB-9 tagged with mCherry and integrin receptor PAT-3 tagged with GFP (Figure 8).

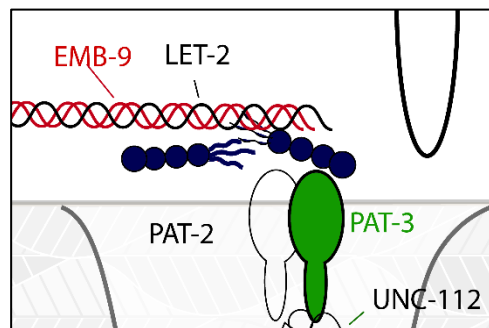


Figure 11: Location of fluorescently tagged type IV collagen and integrin in our co-localization experiment

The mCherry tagged EMB-9 in a heterotrimer with LET-2 the basement membrane binds via the blue labeled perlecan *unc-52* to the integrin heterodimer PAT-2/PAT-3::GFP in the muscle membrane

Our images showed a possible progressive disassociation of EMB-9 with PAT-3 co-localization during day 1 to 8 of adulthood (Figure 9A), as the ratio of the yellow signal, which shows the close proximity of GFP and mCherry signal visually declines in older animals. At the moment, we are working on a way to quantify the signals from both fluorescence channels to calculate the overlap, together with Prof. Dr. Orcun Goskel.

We wondered what the source of this potential dissociation could be. During aging, protein homeostasis rapidly collapses, and temperature-sensitive mutations in perlecan result in paralyzed *C. elegans* starting at day 2 of adulthood at 15°C, a phenotype accelerating on

higher temperatures (Ben-Zvi et al., 2009). We found that temperature-sensitive perlecan *unc-52(e699, su250)* at semi-permissive temperature 20°C accelerated the disassociation of EMB-9 with PAT-3 co-localization during day 1 to 8 of adulthood (Fig. 9A, 9B). More obvious is the massive decline in PAT-3 levels in *unc-52(e699, su250)* mutants, which could also be an alternative explanation for the increase in disassociation. We can confirm the requirement of UNC-52 to localize PAT-3 at the basal muscle membrane, which was previously described, as we see PAT-3::GFP signal floating freely in the *unc-52* mutants (Mullen et al., 1999) (Fig. 9 B). We are still working on the quantification of this experiment, also in collaboration with Prof. Orcun Goskel. This result might suggest that mechanical-coupling declines during aging and a disruption of this system could increase the effect.

If loss of protein homeostasis underlies this, then reducing Insulin/IGF-1 signaling with *daf-2(RNAi)*, which improves protein homeostasis (Henis-Korenblit et al., 2010) should rescue disassociation of EMB-9 with PAT-3 co-localization. Our next step would therefore be to treat *C. elegans* with *daf-2* RNAi and check for a level of co-localization of EMB-9 with PAT-3 co-localization at day 3 and/or day 8 of adulthood compared to control treatment.

Through personal communication with Cyril Statzer, who measured the lifespan of *C. elegans* mutants on *daf-2* RNAi with wild type animals as control using the lifespan machine (Stroustrup et al., 2013), we know that the temperature-sensitive *unc-52(e699, su250)* mutation abolished the lifespan extension effect of *daf-2* RNAi, while it didn't influence the lifespan of control animals significantly (unpublished data). These results show that *unc-52*, a core protein of our mechanotransduction model, is required for longevity. As the loss of *unc-52* overtime does not influence the lifespan on control RNAi compared to wildtype, it certainly does reduce their quality of life by causing paralysis.

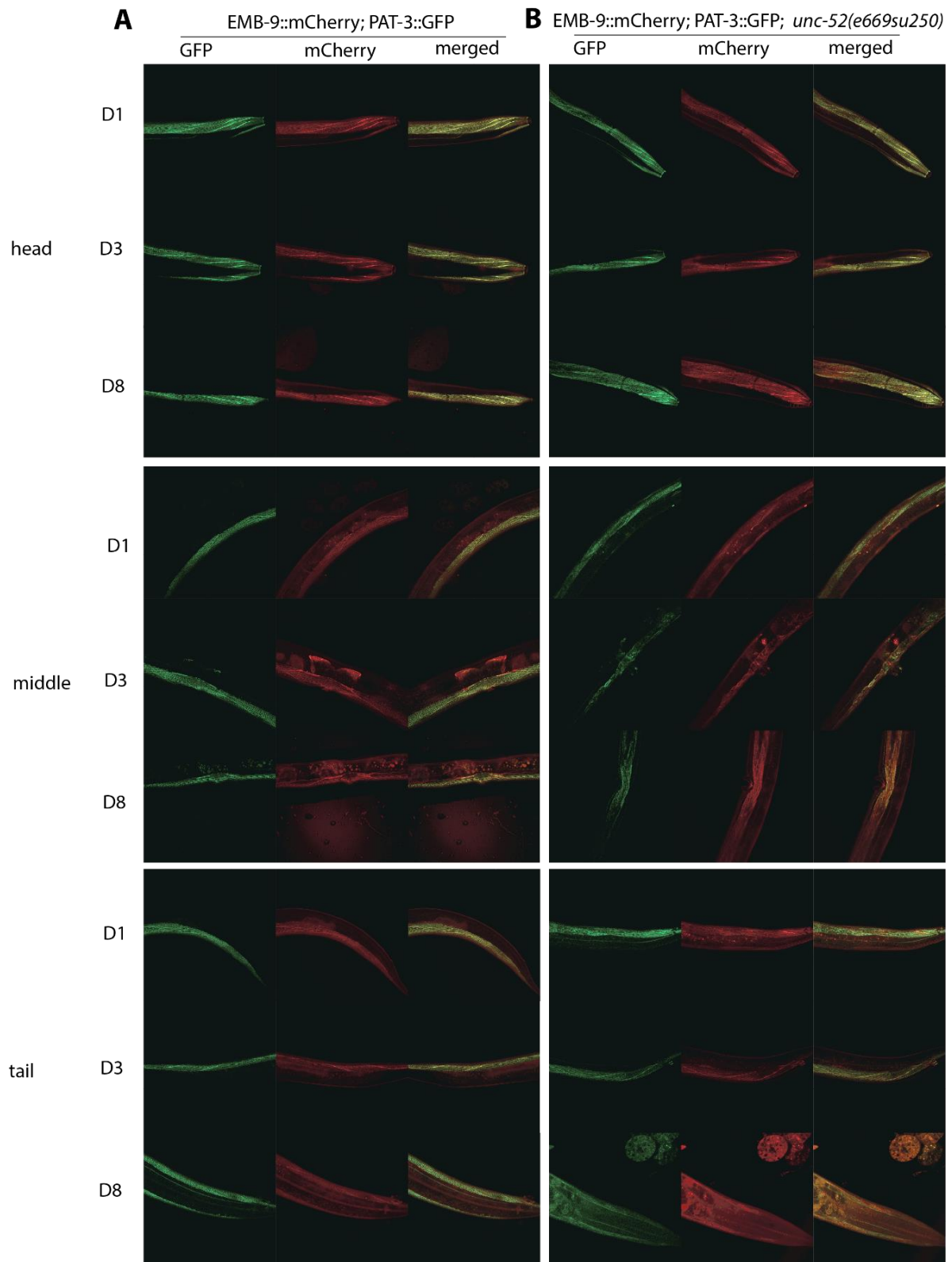


Figure 12: EMB-9 and PAT-3 co-localization during aging via UNC-52

Confocal images of the head, vulva, and tail region of EMB-9::mCherry; PAT-3::GFP strains during aging (A) EMB-9::mCherry; PAT-3::GFP images on D1, D3, and D8 of adulthood in the head, middle, and tail region of the animal. (B) EMB-9::mCherry; PAT-3::GFP in *unc-52* mutant background. Images were taken on D1, D3 and D8 of adulthood in different regions of the animal.

6.3. Discussion

The extracellular environment influences cell behavior. To fully understand age-related changes in cellular function, we need to consider the impact of the loss of structural support, loss of barrier function, and loss of cell-to-cell communication due to age related changes in the ECM. (Birch, 2018).

Previous studies showed that a functional and better maintained ECMs plays an important role in longevity (Ewald, 2020; Ewald et al., 2015). We, therefore, asked how the ECM is generally regulated/maintained during aging and how a more robust or better maintained enhanced ECM might be able to extent the lifespan of *C. elegans*.

Our results showed that the individual ECMs of *C. elegans* change differently with age. The majority of basement membrane proteins remain stable on the transcriptional and translational level while a subset incrementally increases during aging. On the other hand, cuticular collagen mRNA and protein levels strongly decline with age. Interestingly, pro-longevity treatments robustly increase the level of cuticular collagen expression. In doing so, they directly oppose the characteristic age-associated demise of cuticular collagens. Currently, the evidence of whether cuticular collagens are more efficiently replaced in longevity or whether they are deposited in higher amounts remains elusive.

Our *col-144* promotor activation screen revealed that proteins of the mechanotransduction system play a central role in controlling the expression of cuticular collagens during aging. The mechanotransduction system links the body wall muscles to the cuticle and mediates inter-tissue communication. Of key importance for the transduction of mechanical signals is the interaction between perlecan/UNC-52 and the integrin PAT-2/PAT-3 heterodimer. We could implicate a progressive disassociation of these proteins with the aging state of the animal, highlighting their potential role in multiple aging phenotypes. Furthermore, several genes of this mechanotransduction system and screen hits were previously linked to longevity. The cuticular collagens (*col-12*, *col-120*, *col-144*) that were shown to be upregulated by longevity treatments, required or even sufficient for longevity are at one end of the axis (Budovskaya et al., 2008; Ewald et al., 2015). The perlecan *unc-52* is required for longevity (Cyril Statzer, unpublished data). By contrast, downstream of integrin, down regulation of the integrin-linked kinase *pat-4* downregulation was shown to increase lifespan through the activation of stress response genes, without effecting muscle integrity (Kumsta et al., 2014). This suggests that mechanotransduction does not only play a role in collagen expression, but also for longevity.

In the following paragraphs, we discuss the results, conclusions, and limitations of this work in more detail.

To examine whether the age-related decline in the biosynthesis of ECM proteins impacts matrix composition and has any functional consequences on cellular integrity and homeostasis *in vivo*, we characterized the aging-associated changes in ECM protein expression and levels during aging and longevity. We found different dynamics of the two major ECMs of *C. elegans*. Basement membrane components were steadily expressed during aging, while their protein levels were stable or increased, whereas cuticular collagens expression declined, and some collagens were remodeled out of the aging cuticle. We could see a correlation of transcriptional and translational activity, reflecting actual ECM protein content incorporated into pericellular matrices during aging. Longevity treatments were able to slow the progressive decline of cuticular collagens.

To follow up, we asked if long-lived animals have more collagen turnover or if they better maintain existing collagens. We could not find significant evidence for an active turnover mechanism for cuticular collagen (*col-120*) in *C. elegans*. However, we generally see higher collagen content and expression in *daf-2* RNAi treatment during aging (Fig. 3)(Ewald et al., 2015), which points more towards higher expression levels and/ or less removal from the cuticle.

In our screen for regulators of longevity-promoting prolonged collagen expression, we hit two major categories. First, autophagy, which is important to maintain collagen mass (Chen et al., 2019), suggesting a potential role in collagen maintenance during aging and longevity. And second, matrisome and adhesome components. These components are important for *C. elegans* to be able to move, as they form the connection, which transduces the force from the muscle to the cuticle. The body wall muscles are anchored to a thin sheet of basement membrane, which is connected via hemidesmosomal-like and fibrous organelles through the hypodermis to the outer cuticle that acts as a soft exoskeleton (Fig. 6). Our hits were in all these connecting components. We identified 15 cuticular collagens and 5 matrix metalloproteases that remodel the cuticle. We found *mup-4*, *mua-3* and *vab-10*/plakin, the apical and basal parts of the hemidesmosomal-like structure, which connects the cuticle through the hypodermis via *let-805*/myotacin to the basement membrane. *unc-52*/perlecan can directly bind to integrin (PAT-2/3) in the muscle membranes, which form focal adhesions and initiate downstream signaling (Gieseler, 2017). These connecting molecular components were previously shown to transduce mechanical forces from the muscle to remodel the hemidesmosomes-like junctions in the hypodermis and to cytoskeleton re-arrangement required for embryo elongation (Labouesse, 2012; Zhang et al., 2011). Thus, our screen implicated components of this mechanotransduction adhesome complex in regulating collagen gene expression.

We performed a targeted RNAi screen to identify genes involved in ECM remodeling. RNAi is an inexpensive and relatively simple and, therefore fast method to knock down the expression

level of a gene post-transcriptionally (Fire et al., 1998; Tissenbaum, 2015). However, RNAi can have off-target effects and are not effective in some neurons because they lack the transmembrane protein SID-1, which is essential for the systemic RNAi effect by distributing dsRNA in the whole organism (Asikainen et al., 2005; Calixto et al., 2010). Therefore, we decided to validate our screen using loss-of-function mutations. Furthermore, we could only find genes that have an effect if knocked down and not the ones showing an effect when they are overexpressed or have a gain of function mutation or have partially impaired functions. In the *C. elegans* research field, two major RNAi feeding libraries are available, covering 80% of the genome of the nematode. Since it would take quite a long time to screen through all 20,470 genes of *C. elegans* with our approach, we used a targeted approach. We informed ourselves on gene clusters that were more likely to change - or cause change to - the ECM during aging. For example, the matrisome library, which consists of the entirety of the known ECM genes, that were available as RNAi clones. However, using just a subset of all *C. elegans* genes leads to a preselection bias, as we can only find genes in the libraries we selected. We used two approaches to limit this bias. We performed an enrichment analysis, which showed an increase in structural matrisome and autophagy compared to the initial screening list, even with the preselection bias. Additionally, we used data from a whole genome screen of the Ewbank lab. Previous experiments showed that *col-12* RNAi was reducing the lifespan expanding effect of *daf-2*, *glp-1* and *eat-2* mutants (Ewald et al., 2015), showing the importance of *col-12* for longevity. To follow up on this observation we reanalyzed data from an Ewbank lab screen (Zugasti et al., 2016). We used their control data to search for genes that could potentially up- or downregulate *col-12* and included them in our screen. With this we wanted to reduce our bias for some gene classes as this data comes from a whole genome screen, as well as the usage of just one collagen reporter in our screen by including hits from a screen using another longevity-related cuticular collagen reporter. Some interesting hits in this *col-12* regulator screen were *mup-4* (hemidesmosome-like junction), *emb-9* (basement membrane), the transcription factor *elt-3*, and *col-144*, together with nine other cuticular collagens. Because our results are limited to the assessment on *col-144* and *col-12*, it would be interesting to validate our screening hits with other cuticular collagens involved in longevity. In our next experiments, we wanted to test our hypothesis of the involvement of mechanotransduction in collagen regulation during aging. We observed a possible disassociation of the basement-membrane collagen from the integrin receptor during aging. Notably, we showed that changes affecting protein homeostasis of basement-membrane protein perlecan (UNC-52) might be responsible for this age-dependent dissociation. As the longevity induced by *daf-2* RNAi is abolished in *unc-52* mutants, we conclude that during aging, cell attachment to the ECM via cell-surface receptors might become weakened, resulting in an uncoupling or loss of mechanotransduction, which impairs inter-tissue signaling important for longevity.

One of the key proteins in mechanotransduction is perlecan/UNC-52. We found that perlecan increases in abundance in basement membranes during aging (Fig. 1H). However, whether these perlecans are functional is not known, as there are at least two key processes that could lead to improper perlecan production and function during aging. First, perlecan mRNA needs to be correctly alternatively spliced by mechanosensory splicing factor *mec-8* (Lundquist et al., 1996; Spike et al., 2002) and mRNA splicing fidelity declines during aging (Heintz et al., 2017). Second, non-essential and temperature-sensitive mutations in perlecan result in an age-dependent paralysis phenotype at 15°C, which was attributed to the collapse of the protein homeostasis in early adulthood in *C. elegans* (Ben-Zvi et al., 2009). Furthermore, mutants of CRT-1/calreticulin, a molecular chaperone that assists the folding of UNC-52/perlecan, show 50% reduced UNC-52 protein levels (Zahreddine et al., 2010; Zhang and Labouesse, 2010). *crt-1* expression declines during aging (Walther et al., 2015), probably leading to more misfolded UNC-52. *crt-1* was also a hit in our RNAi screen (Fig. 6; Supp. Table 2). Longevity interventions improve protein homeostasis (Balch et al., 2008; Dhondt et al., 2016; Visscher et al., 2016), and it was shown that the age-dependent perlecan-paralysis was slowed down in long-lived *glp-1*-mutants (Cohen-Berkman et al., 2020). This suggests that perlecan homeostasis declines during aging, a process improved by longevity interventions.

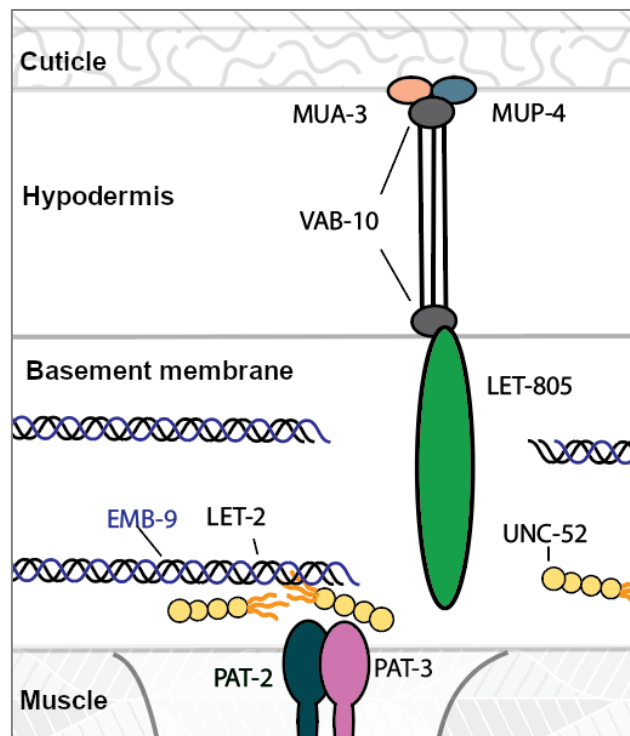


Figure 13: Overview mechanical linkage of the cuticle to the muscle in *C. elegans*

In cuticle in the upper part is linked via hemidesmosome-like fibrous organelles in the hypodermis that consists of MUA-3, MUP-4, VAB-10, Intermediate filaments and LET-805, which reaches into the basement membrane. In the basement membrane, the perlecan UNC-52 binds to the collagen type IV collagen heterotrimer of EMB-9 and LET-2 and likely also to the Integrin PAT-2/PAT-3, which anchors the basement membrane to the dense bodies and M-lines in the muscle. All proteins in the scheme except MUA-3 were hits in our RNAi screen (Fig. 6) or in the mutant time course experiments (Fig.7)

A similar process for perlecan was shown in human keratinocyte cultures and skin samples. Age-related changes on dermal-epidermal junctions, which primarily consist of laminins, type IV collagen, nidogens, and perlecan, lead to decreased contact with keratinocytes, impairing epidermal homeostasis, and renewal. Aged keratinocytes can form only a thin and poorly organized epidermis. The supplementation of these cells with purified perlecan reversed the effect leading to a renewed well-differentiated ECM (Dos Santos et al., 2016).

Another key component of *C. elegans* mechanotransduction are the integrins. The communication between cells and the ECM was shown to predominately pass through integrins (Kechagia et al., 2019). They connect the extracellular space to the cytoskeleton and establish a mechanotransduction axis in nearly all mammalian cell types (Ross et al., 2013). While perlecans and collagens are structural proteins and therefore static, integrins can transduce signals by changing their conformation, which can be influenced by external mechanical forces (Askari et al., 2009). The signal transduction can be in either direction, referred to as either “inside-out” or “outside-in” signaling (Harburger and Calderwood, 2009). Activated integrins cluster together and bind extracellular ligands, while the β -integrin cytoplasmic tail recruits cytoplasmic adaptor proteins to focal adhesion sites through phosphorylation. (Margadant et al., 2012; Nieswandt et al., 2007; Rognoni et al., 2016; Tadokoro et al., 2003).

Consistent with our screen findings, a previous study demonstrated that mutations in muscle focal adhesion components show an uncoordinated movement phenotype (*Unc*; *unc-95/paxilin*, *unc-97/pinch*, *unc-52/perlecan*) and upregulate cuticular collagen as well as *dpy-18/prolyl-4-hydroxylase* expression, an enzyme which stabilizes collagen bundles (Broday et al., 2007). By contrast, mutations in muscle myosin *unc-54*, important for muscle contraction, or mutations in *unc-13*, important for neurotransmitter release, did not induce cuticular collagen expression (Broday et al., 2007). Together with our results, this suggests a mechanotransductional control of collagen expression across tissues.

Mutations in collagens that localize to the cuticle furrows between the annuli, such as *dpy-7* and *dpy-10* (Page and Johnstone, 2007), resulting in disorganized cuticular structure (Essmann et al., 2017). Mutations in these furrow-localized collagens, but not other cuticular collagens, elicit a variety of stress response pathways, including osmolarity stress response, oxidative detoxification stress response, hypoxia stress response, antimicrobial stress response, and activating autophagy (Dodd et al., 2018; Lamitina et al., 2006; Vozdek et al., 2018; Wheeler and Thomas, 2006; Zhang et al., 2019). Since the cuticle functions as a barrier to the outside, physical damage to this ECM mobilizes the intracellular stress response to improve cellular protection. Longevity interventions improve cuticle morphology (Essmann et al., 2020; De Haes et al., 2014). Interestingly, we found that *col-120*, which is required and sufficient for longevity (Ewald et al., 2015), to localize to these furrows, and COL-120 levels in

these furrows was maintained for longer in long-lived animals during aging (Fig. 3, C). Other collagens that are stably integrated into the cuticular ECM (Figure 1H, Fig.3, D), such as *col-19*, localize to the annuli but not to the furrows and are not required nor sufficient for longevity (Ewald et al., 2015). Thus, the cuticular furrows might respond to environmental insults, and the ECM composition at these furrows between the annuli is dynamic and altered during aging. This localized ECM dynamic also declines partially through uncoupling of the overarching mechanotransduction apparatus connecting muscle, basement membrane, hypodermis and cuticle.

It would be interesting to follow up by further determining potential pathways that work together or in parallel with mechanotransduction to regulate collagen expression. We found three especially interesting candidates in our mutant *Pcol-144::GFP* time-course experiments.

The first two are part of the TGF- β superfamily. The downregulation of the DAF-7/TGF- β -related ligand was shown to increase the lifespan of *C. elegans* via *daf-16* (Shaw et al., 2007) and acts as a systemic signal for autophagy regulation (Zhang et al., 2019). Autophagy-related genes were one of the highly enriched gene categories in our screen (s. Supp. Fig. 9-10). The second one is also a TGF- β signaling pathway, also known as the Sma/Mab pathway (Padgett et al., 1998), which uses *dbl-1* as ligand. *dbl-1* was shown to regulate innate immunity and body size of *C. elegans* (Gumienny and Savage-Dunn, 2013) and additionally, the regulation of the body size was also connected through an contact independent transcriptional feedback loop with cuticular collagens (Madaan et al., 2018, 2020). Furthermore, *dbl-1* genetically interacts with UNC-52/perlecan in directing distal tip cell migration (Merz et al., 2003).

The third candidate is the STA-2/*elt-3* signaling, which is involved in the innate immune response. STA-2 was shown to physically interact with MUP-4, an apical protein of the hemidesmosome-like junction. The disturbance of the apical part of the hemidesmosome-like junctions by molting or damage of the cuticle was shown to detach STA-2. This detachment triggers the activation of antimicrobial peptide (AMP) production as well as activation of lysosomes via ELT-3 (Miao et al., 2020; Zhang et al., 2015). *elt-3* expression declined during aging and was shown to be required for oxidative stress response and longevity induced by *skn-1* overexpression (Hu et al., 2017). *elt-3* was also shown to regulate collagen gene expression in response to environmental stimuli (Mesbahi et al., 2020). *elt-5* and *elt-6* repress *elt-3* expression, while their own expression is increasing with age. RNAi against both *elt-5* and *elt-6* were shown to elongate the lifespan of *C. elegans*. All three together represent a GATA transcription factors circuit that regulates many downstream genes that change expression during aging, including *col-144* (Budovskaya et al., 2008).

In human aging skin, collagen biosynthesis decreases due to fibroblast senescence and lower mechanical stimulation or transduction capacity (Varani et al., 2006). Mechanical stimulation depends on the physical properties and composition of the ECM and drives collagen synthesis in fibroblasts (Chiquet, 1999; Wang and Thampatty, 2006). We speculate that this mechanical feed-forward loop might be interpreted by integrin-based focal adhesions. A previous *in-silico* study found focal adhesions as a central network associated with human longevity (Wolfson et al., 2009). Furthermore, the levels of collagen COL17A1, which is part of hemidesmosomes expressed from epidermal stem cells, determines stem cell maintenance and skin aging in mice and human 3D *in-vitro* models (Liu et al., 2019). This suggests conserved roles of mechanical forces on focal adhesion and hemidesmosomes in aging and longevity.

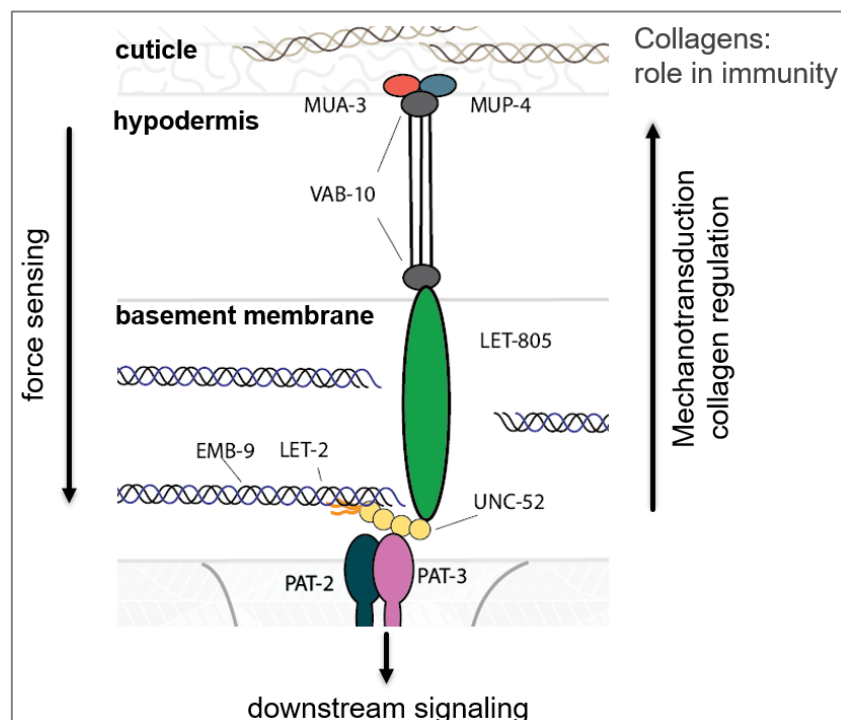


Figure 14: Hypothesis: Mechanical signaling across tissues regulates collagen expression

In this model the mechanical linkage over integrins, through perlecan/UNC-52 and the basement collagens to the hemidesmosome-like junctions is responsible not only for mechanotransduction, but also collagen regulation. While the same system is also able to sense forces in the cuticle and can change downstream signaling.

Based on our experimental results and literature research, we hypothesized that the expression of collagens in the cuticle is regulated through the same mechanical linkage that is responsible for the mechanical force transduction from the muscle to the cuticle. This system consists of the hemidesmosome-like junction, basement collagens, perlecan/UNC-52 and the integrins PAT-2/PAT-3 and is able to sense age-dependent changes in the forces transmitted from the cuticle and the cuticles composition. This force sensing changes the downstream integrin signaling and, therefore, affects longevity and healthy aging. Finding ways to enhance or protect this system during aging could be an important pro-longevity mechanism (Fig. 14).

In summary, we identified a novel function of integrin-based focal adhesions in regulating the homeostasis of a distant ECM across basement membrane and adjacent tissues to be essential to promote longevity. We provide evidence that the composition of the basement membrane and the cuticle of *C. elegans* undergo dynamic changes during aging and that these seemingly independent changes are at least in part linked via mechanical tension coupling. Our study implicates the importance of mechanotransduction for longevity *in vivo*. Our understanding of tissue and organismal aging may benefit from the further characterization of the effects of structural integrity, mechanotransduction, and ECM composition on cellular homeostasis.

6.4. Material and Methods

Strains

Caenorhabditis elegans strains were grown on NGM plates with OP50 *Escherichia coli* bacteria at 20°C as described (Stiernagle, 2006). The Bristol N2 was used as wild-type strain (Brenner, 1973). We received most strains from the Caenorhabditis Genetics Center [CGC]. BC10074 *dpy-5(e907)* I; *sEx10074*[*Pemb-9::GFP* + *pCeh361*], BC11902 *dpy-5(e907)* I; *sEx11902* [*Pcol-129::GFP* + *pCeh361*], BC12229 *dpy-5(e907)* I; *sEx10002* [*Pcutl-23::GFP* + *pCeh361*], BC12275 *dpy-5(e907)* I; *sEx12275* [*Pcut-6::GFP::GFP* + *pCeh361*], BC12533 *dpy-5(e907)* I; *sEx12533* [*Pcol-89::GFP* + *pCeh361*], BC12900 *dpy-5(e907)* I; *sIs11600* [*Pmec-5::GFP*+ *pCeh361*], BC13149 *dpy-5(e907)* I; *sEx13149* [*Phim-4::GFP* + *pCeh361*], BC13560 *dpy-5(e907)* I; *sIs13559* [*col-59::GFP* + *pCeh361*], BC13623 *dpy-5(e907)* I; *sEx13623* [*Pcri-2::GFP* + *pCeh361*], BC13861 *dpy-5(e907)* I; *sIs13252* [*Plet-2::GFP* + *pCeh361*], BC14295 *dpy-5(e907)* I; *sEx14295* [*Pgpn-1::GFP*+ *pCeh361*], BT24*rhIs23* [*GFP::HIM-4*] III, CH1445 *unc-119(ed3)* III; *cgEx198* [*BLI-1::GFP* + *unc-119(+)*], HS428 *dpy-22(os26)* X; *osEx89* [*COL-10::GFP* + *dpy-22(+)*], MH2051 *kuls55*[*LON-3::GFP* + *unc-119(+)*]; pYSL3G3, NG2517 *him-5(e1490)* V; [*INA-1::GFP* + *rol-6(su1006)*], NK248 *unc-119(ed4)* III; *qyls10* [*LAM-1::GFP* + *unc-119(+)*] IV, NK2583 *unc-52(qy80)*; [*NeonGreen::UNC-52*], NK358 *unc-119(ed4)* III; *qyls43* [*PAT-3::GFP* + *INA-1(genomic)* + *unc-119(+)*], NK364 *unc-119(ed4)* III; *qyls46* [*EMB-9::mCherry* + *unc-119(+)*], NK651 *unc-119(ed4)* III; *qyls108* [*LAM-1::Dendra* + *unc-119(+)*], NK696 *unc-119(ed4)* III; *qyls127* [*LAM-1::mCherry* + *unc-119(+)*], NK860 *unc-119(ed4)* III; *qyls161* [*EMB-9::Dendra* + *unc-119(+)*], NK2446 *qy41*[*lam-2::mKate2*] X, NK2479 *qy49*[*pat-2::2xmNG*] III, RP247 *trIs30* [*Phim-4::MB::YFP* + *Phmr-1b::DsRed2* + *Punc-129nsp::DsRed2*], TP12 *kals12* [*COL-19::GFP*], WS3403 *opIs170* [*SDN-1::GFP::unc-54* 3'UTR + *lin-15(+)*], WT30 *unc-119(ed3)* III; *wtEx30* [*CUTI-1::GFP* + *unc-119(+)*], TJ1060 *spe-9(hc88)* I; *rff-3(b26)* II, CB4037 *glp-1(e2141)* III, LD1036 *daf-2(e1370)*; *him-8(e1489)*.

The strains AH3437 *zh117* [GFP::TLN-1] and AH4617 *zh115* [PAT-3::GFP] III (Walser et al., 2017) were gifts from Alex Hajnal's lab.

The following strain were gifts from the lab that generated them *jgls5* [ROL- 6::GFP;TTX-3::GFP] (Kim et al., 2010), TU1 *unc-119(ed3)III*; [Pcol-99[16655]::S0001_pR6K_Amp_2xTY1ce_EGFP_FRT_rpsl_neo_FRT_3xFlag] dFRT::unc-119 (Tu et al., 2015), VH2847 *hdl/s73* [col-99::GFP, *pha-1(+)*] (Taylor et al., 2018).

The last group of strain was generated by crossing or injection in our lab. LSD1106 *pha-1(e2123)* III; *xchEx105* [Pcol-120::NeonGreen; *pha-1(+)*], LSD2001 *xchls001* [Pcol-144:: GFP; *pha-1(+)*], LSD2043 *xchls012* [(pRedFlp-Hgr) (col-120 [30044]::S0001 pR6K Amp 2xTY1ce EGFP FRT rpsl neo FRT 3xFlag) dFRT::unc-119-Nat]; pRF4 *rol-6(su1006gf)*, LSD2117 *xchls016* [Pcol-19::GFP], LSD2002 *spe-9(hc88)* I ; *xchls001* [Pcol-144:: GFP; *pha-1(+)*], LSD2003 *glp-1(e2141)* III ; *xchls001* [Pcol-144:: GFP; *pha-1(+)*], LSD2122 *spe-9(hc88)* I; *daf-2(e1370)* III; *xchls001* [Pcol-144:: GFP; *pha-1(+)*], LSD1061 *xchEx062*[pcol-120::col-120::dendra2; *pha-1 (+)*]; *pha-1(e2123)III*, LSD2125 *xchls001*[Pcol-144:: GFP; *pha-1(+)*] X; *F09A5.2(ok1900)* X, LSD2131 *xchls001*[Pcol-144:: GFP; *pha-1(+)*] X; *elt-7(ok835)*, LSD2191 *xchls001*[Pcol-144:: GFP; *pha-1(+)*] X; *unc-52(e669su250)*, LSD2193 *xchls001*[Pcol-144:: GFP; *pha-1(+)*] X ; *sta-2(ok1860)* V, LSD2194 *xchls001*[Pcol-144:: GFP; *pha-1(+)*] X; *sma-6(wk7)* II, LSD2195 *xchls001*[Pcol-144:: GFP; *pha-1(+)*] X; *dbl-1(wk70)* V, LSD2196 *xchls001*[Pcol-144:: GFP; *pha-1(+)*] X; *pat-3(zh105)*[*pat-3Y792F*], LSD2197 *xchls001*[Pcol-144:: GFP; *pha-1(+)*] X; *pat-3(rh96)* III, LSD2198 *xchls001*[Pcol-144:: GFP; *pha-1(+)*] X , LSD2147 *qyls46*[*Pemb-9::emb-9::mCherry + unc-119(+)*] ; *pat-3(zh115)*[*pat-3::gfp*]; *unc-119(ed4)* III, LSD2161 *qyls46*[*Pemb-9::emb-9::mCherry + unc-119(+)*]; *unc-52(e669su250)* II ; *pat-3(zh115)*[*pat-3::gfp*]; *unc-119(ed4)* III

Cloning of transgenic constructs

The plasmid pXCH8 (Pcol-120::NeonGreen) was built and purchased from Vectorbuilder. The promotor sequence originates from *col-120* fosmid clone WRM0622A_D10(pRedFlp-Hgr)(col-120[30044]::S0001_pR6K_Amp_2xTY1ce_EGFP_FRT_rpsl_neo_FRT_3xFlag)dFRT::unc-119-Nat from the TransgeneOme Project (Sarov et al., 2012), while the plasmid DG398 (Slot2 ENTRY vector for mNeonGreen::3xFlag) (Hostettler et al., 2017) serves as backbone.

Generation of transgenic lines

LSD1106 *pha-1(e2123)* III; *xchEx105* [Pcol-120::NeonGreen; *pha-1(+)*]. Generated by injecting 50 ng/μl pXCH8 (Pcol-120::NeonGreen) with 50 ng/μl pBX (*pha-1 (+)*) co-injection

marker into *pha-1(e2123)*III mutants. LSD1107 *xchEx017* [*Pcol-120::NeonGreen*; *Pcol-12::DsRed*]. Generated by injecting 50 ng/μl pXCH8 (*Pcol-120::NeonGreen*) with 50 ng/μl *Pcol-12::DsRed* into N2.

LSD2001 *xchIs001* [*Pcol-144::GFP*; *pha-1(+)*] was generated by integration of *daf-2(e1370)* III; Ex[*pCol-144pro::GFP*; *pha-1(+)*] via UV light irradiation and 8 x outcrossing with N2 animals (Evans, 2006). Afterward, we checked for the presence or the absence of *daf-2* mutation, by placing the animals on 25° to induce the dauer phenotype in the *daf-2* mutants. Ex[*pCol-144pro::GFP*; *pha-1(+)*] originates from the SD1216 strain (Budovskaya et al., 2008).

The strain LSD2043 *xchIs012* [(*pRedFlp-Hgr*) (*col-120* [30044]::S0001 *pR6K Amp 2xTY1ce EGFP FRT rpsI neo FRT 3xFlag*) *dFRT::unc-119-Nat*]; *pRF4 rol-6(su1006gf)* was generated by microinjecting 1 ng/μl of WRM0622A_D10 fosmid (<https://transgeneome.mpi-cbg.de/transgeneomics/index.html>) together with 50 ng/μl *pRF4 rol-6(su1006gf)* into N2. The *xchEx001* strain was then stably integrated into the genome via UV light irradiation and outcrossed 8 times.

We obtained the strain LSD2117 *xchIs016* [*Pcol-19::GFP*] by injecting 50 ng/μl pJA1 [*Pcol-19::GFP*] (gift by Ann Rougvie) into N2, followed by UV irradiation and 8 times outcrossing.

LSD1061 was generated by injecting 50ng/μl pXCH4 (*Pcol-120::col-120::dendra2*) together with 50ng/μl pBX (*pha-1 (+)*) into LSD9 (*pha-1(e2123)*III). For selection and maintenance of transgenic animals, the *C. elegans* were placed at 25°C.

Imaging of Matrisome Atlas and Collagen::GFP strains

Unless indicated differently, animals were kept on NGM plates. For the atlas images, the stages egg-L4 were selected from a mixed plate under the stereoscope and immediately imaged. As preparation for the imaging of day 1 and day 8 of adulthood animals, L4 animals were transferred from NGM plates on plates containing 50 μM FUDR and imaged when they reached the respective age. For imaging we used the BX-51-F Tritech™ Research bright field fluorescence microscope with a DFK 23UX236 camera, IC Capture 2.4 software, and a triple-band filter from Chroma Technology Corp (described in Teuscher and Ewald, 2018). We used 2mM Levamisole hydrochloride solved in M9 buffer to immobilize the animals for imaging.

Analysis of Collagen::GFP fluorescence intensity

For the analysis of our Collagen::GFP strains we used a Python script by Elisabeth Jongsma and Dr. Jeliasko Jeliaskov in ImageJ [to be published]. The code is designed to measure the GFP intensity in *C. elegans* animals while ignoring the autofluorescence of the gut. The program takes the area of interest selected from the digital image and compares the intensities

for the green and red channel within each pixel. *C. elegans* autofluorescence appears as yellow in the images, a blend of red and green. To remove the autofluorescence without affecting the GFP signal, the red channel intensities are subtracted from the green. Furthermore, signals below a certain intensity threshold are regarded as background noise and also ignored. The program then counts all remaining pixels with intensities in the green channel and adds up the total intensity (it also gives the number of pixels and the mean intensity per pixel). The resulting image can be printed to check if the thresholds were placed properly. The data was further analyzed and visualized using GraphPad Prism 8.2.0. P-values were calculated using a two-way ANOVA.

Imaging and photoconversion of COL-120::Dendra2 in *C.elegans*

For the RNAi experiments, L4 animals were placed on respective RNAi plates for one generation. To age synchronize the animals, only L4 *C. elegans* of the F1 generation were selected and moved to fresh RNAi plates containing 50 μ M FUDR. The animals were imaged on day 2 and day 4 of adulthood, with the photoconversion being performed only on the second day of adulthood. For imaging, they were transferred into a drop of M9 onto 2mm thick, 3% agar pads on microscope slides. For the confocal images, an Olympus FluoView 3000 microscope was used. On day 2, images of the region behind the pharynx and of the vulva region were taken, both before and after the dendra2 photoconversion. Before photoconversion, dendra2's excitation maxima are at 490 and the emission maxima at 507 nm, similar to EGFP; after photoconversion, they change to 553 and 573 nm, in the red spectrum. In this study dendra2 was photoconverted by using 2% power of the 405nm laser for 6 sec with 8 μ /s at a resolution of 1024x 1024 (Evrogen, 2006; Gurskaya et al., 2006). For the analysis performed by Prof. Orcun Goksel the total signal intensity per mask was computed, separately for green and red. We then calculated the green-to-red ratio of each of these areas per animal and timepoint and used the ratios of the two outside areas as normalization for the respective inside area. The data was further analyzed and visualized using R (R Core Team, 2019). P-values were calculated using the Students T-test.

Herovici Staining

The two strains with temperature sensitive mutation for sterility, TJ1060 *spe-9(hc88)* I; *rrf-3(b26)* II and CB4037 *glp-1(e2141)* III were grown at 25°C until day 2 of adulthood. On day 1 or day they were washed off plate and treated as described in Teuscher et al., 2019a.

RNAi libraries

For the screen, we worked with 5 RNAi bacteria libraries containing selected RNAi clones to knock-down specific gene classes or categories. The kinase library, two transcription factor libraries (bZip and TXN-factor Libraries) and the metabolism library were a generous gift from Gary Ruvkun (Harvard Medical School). We constructed our Matrisome library in a similar matter, based on our definition of the *C. elegans* Matrisome (Teuscher et al., 2019a). The library contains 652 RNAi clones of the 719 of *C. elegans* Matrisome genes. For the missing 67 genes, no RNAi clones were available. The bacteria were picked from either the ORF-RNAi or the Ahringer RNAi libraries (both available from Source BioScience). Bacteria glycerol stocks of the clones were pipette into 96-well plates each also containing control wells with control bacteria clones (L4440, *daf-2*, *bli-3*, *daf-16*, *skn-1*, *gfp*, *col-144*) and some empty wells (LB mixed with glycerol).

The same was done for the two validation screen libraries. Validation library I consisted of hits from the previous screen rounds, together with selected clones of hits from the *col-12* expression screen performed by the Ewbank lab (Zugasti et al., 2016) and selected clones of genes from our literature research. Validation library II, consisted of hits from the Validation library I screen.

RNAi screen

The screen was performed on 96-well plates, each well containing 150 µl NGM with 100 µg/ml Ampicillin and 1mM IPTG, seeded with 8 µl concentrated RNAi bacteria. The bacteria were grown overnight in 96-deep-well plates in 800 µl LB containing 100 µg/ml Ampicillin and 12.5 µg/ml Tetracyclin. On the next morning, another 700µl LB with Ampicillin and Tetracyclin was added. After four additional hours of growth, the plates were centrifuged, the supernatant discarded and each well filled up with 35 µl LB containing 100 µg/ml Ampicillin and 1mM IPTG, enough to seed up to 4 96-well NGM plates. For the preparation of the worms we used plates containing gravid adult *C. elegans*. We age synchronized the animals at stage L1, by bleach killing everything except the eggs protected by their shells (egg prep) and letting them hatch in M9 medium with cholesterol, without food, so they stage arrest until all eggs were hatched. The next day we placed 25 animals of our screening strains in wells of 96-well containing Normal Growth Medium (NGM), each plate was seeded with one of the clones from the 96-well library plates. They grew up at 25°C until day 2 of adulthood, as this temperature is needed to activate *glp-1* and *spe-9* mutations during development and making them sterile, later moving them to 20°C. The plates were scored on adulthood day 1 and day 8 under a fluorescence stereoscope and the fluorescence of the animals was graded on a scale from 0- . The result was counted as a hit when the average of the three to four replicates was at least 0.5 (lowest visible difference) over the control.

Enrichment analysis

Genes that displayed significant *col-144* promotor activation in the long-lived *glp-1* background compared to the normal-lived *spe-9* genotype (see Supp Table 1-2) were subjected to an enrichment analysis using the R programming language (Henry and Wickham, 2019; Wickham, 2011). In this overrepresentation test, the gene ontology (GO) terms enriched among the hits (68) were compared to the GO terms of all genes that were assessed in the screen (1770) (Carlson, 2018; Yu et al., 2012). The Benjamini & Hochberg method was used for multiple testing correction and an adjusted p-value threshold of 0.05 was applied.

Time-course measurements of fluorescent expression reporter strains

The strains for time course measurements (Fig.7) were placed as L4s on plates containing 50 μ M FUDR and were scored on the indicated days (Fig.7) under a fluorescence stereoscope. For each animal the fluorescence was graded on a scale from 0-3 in 0.5 steps. Per measuring round 20-30 *C. elegans* were used. The data was further analyzed and visualized using GraphPad Prism 8.2.0. P-values were calculated using a two-way ANOVA.

EMB-9/PAT-3 co-localization experiments

For the imaging of a potential co-localization of the EMB-9::mCherry and PAT-3::GFP in *C.elegans*, the animals were placed as L4s on plates containing 50 μ M FUDR. Images were taken on day 1, day 3 and day 8 of adulthood using an Olympus FluoView 3000 microscope. For the RNAi experiments, the animals were placed as eggs on plates seeded with control L4440 RNAi or *daf-2* RNAi bacteria. The RNAi NGM plates contained 100 μ g/ml Ampicillin and 1mM IPTG. The L4 animals were moved to RNAi NGM plates that additionally contained 50 μ M FUDR.

Acknowledgments

The authors acknowledge the support of the Scientific Center for Optical and Electron Microscopy ScopeM of the Swiss Federal Institute of Technology ETHZ and especially want to thank Tobias Schwarz, Elisabeth Jongsma and Dr. Jeliuzko Jeliuzkov for their Phyton script for the analysis of our collagen::GFP strains. Prof. Orcun Goksel for his help in analyzing the dendra turnover and EMB-9::mcherry; PAT-3::GFP images. For the support in the making of graphs we want to thank Dr. Cyril Statzer. Thank you also to Prof. Alex Hajnal for support with the matrisome library and strains.

6.5. References

- Ahringer, J. (2006). Reverse genetics. WormBook.
- Asikainen, S., Vartiainen, S., Lakso, M., Nass, R., and Wong, G. (2005). Selective sensitivity of *Caenorhabditis elegans* neurons to RNA interference. *Neuroreport* 16.
- Askari, J.A., Buckley, P.A., Mould, A.P., and Humphries, M.J. (2009). Linking integrin conformation to function. *J. Cell Sci.* 122.
- Battaglia, C., Aumailley, M., Mann, K., Mayer, U., and Timpl, R. (1993). Structural basis of $\beta 1$ integrin-mediated cell adhesion to a large heparan sulfate proteoglycan from basement membranes. *Eur. J. Cell Biol.* 61.
- Ben-Zvi, A., Miller, E.A., and Morimoto, R.I. (2009). Collapse of proteostasis represents an early molecular event in *Caenorhabditis elegans* aging. *Proc. Natl. Acad. Sci. U. S. A.* 106.
- Berman, J.R., and Kenyon, C. (2006). Germ-cell loss extends *C. elegans* life span through regulation of DAF-16 by *kri-1* and lipophilic-hormone signaling. *Cell* 124.
- Bix, G., and Iozzo, R. V. (2008). Novel interactions of perlecan: Unraveling Perlecan's role in angiogenesis. *Microsc. Res. Tech.* 71.
- Bonnans, C., Chou, J., and Werb, Z. (2014). Remodelling the extracellular matrix in development and disease. *Nat. Rev. Mol. Cell Biol.* 15.
- Brenner, S. (1973). The genetics of *Caenorhabditis elegans*.
- Budovskaya, Y. V., Wu, K., Southworth, L.K., Jiang, M., Tedesco, P., Johnson, T.E., and Kim, S.K. (2008). An *elt-3/elt-5/elt-6* GATA Transcription Circuit Guides Aging in *C. elegans*. *Cell* 134, 291–303.
- Calixto, A., Chelur, D., Topalidou, I., Chen, X., and Chalfie, M. (2010). Enhanced neuronal RNAi in *C. elegans* using SID-1. *Nat. Methods* 7.
- Carlson, M. (2018). *org.Ce.eg.db: Genome wide annotation for Worm. R Packag. Version 3.7.0.*
- Charras, G., and Sahai, E. (2014). Physical influences of the extracellular environment on cell migration. *Nat. Rev. Mol. Cell Biol.* 15.
- Chen, Y.L., Tao, J., Zhao, P.J., Tang, W., Xu, J.P., Zhang, K.Q., and Zou, C.G. (2019). Adiponectin receptor PAQR-2 signaling senses low temperature to promote *C. elegans* longevity by regulating autophagy. *Nat. Commun.* 10.
- Chiquet, M. (1999). Regulation of extracellular matrix gene expression by mechanical stress. *Matrix Biol.* 18.
- Choi, H.R., Cho, K.A., Kang, H.T., Lee, J. Bin, Kaeberlein, M., Suh, Y., Chung, I.K., and Park, S.C. (2011). Restoration of senescent human diploid fibroblasts by modulation of the extracellular matrix. *Aging Cell* 10, 148–157.
- Cohen-Berkman, M., Dudkevich, R., Ben-Hamo, S., Fishman, A., Salzberg, Y., Ben-Asher, H.W., Lamm, A.T., and Henis-Korenblit, S. (2020). Endogenous siRNAs promote proteostasis and longevity in germlineless *C. Elegans*. *Elife* 9.
- Dodd, W., Tang, L., Lone, J.C., Wimberly, K., Wu, C.W., Consalvo, C., Wright, J.E., Pujol, N., and Choe, K.P. (2018). A damage sensor associated with the cuticle coordinates three core environmental stress responses in *caenorhabditis elegans*. *Genetics* 208.
- Essmann, C.L., Elmi, M., Shaw, M., Anand, G.M., Pawar, V.M., and Srinivasan, M.A. (2017). In-vivo high resolution AFM topographic imaging of *Caenorhabditis elegans* reveals previously unreported surface structures of cuticle mutants. *Nanomedicine Nanotechnology, Biol. Med.*

- Essmann, C.L., Martinez-Martinez, D., Pryor, R., Leung, K.Y., Krishnan, K.B., Lui, P.P., Greene, N.D.E., Brown, A.E.X., Pawar, V.M., Srinivasan, M.A., et al. (2020). Mechanical properties measured by atomic force microscopy define health biomarkers in ageing *C. elegans*. *Nat. Commun.* 11.
- Evans, T. (2006). Transformation and microinjection. *WormBook*.
- Evrogen (2006). Green to red photoswitchable fluorescent protein Dendra2. *Biotechniques* 1–4.
- Ewald, C.Y. (2020). The Matrisome during Aging and Longevity: A Systems-Level Approach toward Defining Matreotypes Promoting Healthy Aging. *Gerontology* 66.
- Ewald, C.Y., Landis, J.N., Abate, J.P., Murphy, C.T., and Blackwell, T.K. (2015). Dauer-independent insulin/IGF-1-signalling implicates collagen remodelling in longevity. *Nature* 519, 97–101.
- Fire, A., Xu, S., Montgomery, M.K., Kostas, S.A., Driver, S.E., and Mello, C.C. (1998). Potent and specific genetic interference by double-stranded RNA in *caenorhabditis elegans*. *Nature* 391.
- Flurkey, K., Papaconstantinou, J., Miller, R.A., and Harrison, D.E. (2002). Lifespan extension and delayed immune and collagen aging in mutant mice with defects in growth hormone production. *Proc. Natl. Acad. Sci.* 98, 6736–6741.
- Frantz, C., Stewart, K.M., and Weaver, V.M. (2010). The extracellular matrix at a glance. *J. Cell Sci.* 123, 4195–4200.
- Gieseler, K. (2017). Development, structure, and maintenance of *C. elegans* body wall muscle. *WormBook*.
- Gotenstein, J.R., Koo, C.C., Ho, T.W., and Chisholm, A.D. (2018). Genetic suppression of basement membrane defects in *caenorhabditis elegans* by gain of function in extracellular matrix and cell-matrix attachment genes. *Genetics* 208.
- Graham, P.L., Johnson, J.J., Wang, S., Sibley, M.H., Gupta, M.C., and Kramer, J.M. (1997). Type IV collagen is detectable in most, but not all, basement membranes of *Caenorhabditis elegans* and assembles on tissues that do not express it. *J. Cell Biol.* 137.
- Gumienny, T.L., and Savage-Dunn, C. (2013). TGF- β signaling in *C. elegans*. *WormBook*.
- Gurskaya, N.G., Verkhusa, V. V., Shcheglov, A.S., Staroverov, D.B., Chepurnykh, T. V., Fradkov, A.F., Lukyanov, S., and Lukyanov, K.A. (2006). Engineering of a monomeric green-to-red photoactivatable fluorescent protein induced by blue light. *Nat. Biotechnol.* 24.
- De Haes, W., Frooninckx, L., Van Assche, R., Smolders, A., Depuydt, G., Billen, J., Braeckman, B.P., Schoofs, L., and Temmerman, L. (2014). Metformin promotes lifespan through mitohormesis via the peroxiredoxin PRDX-2. *Proc. Natl. Acad. Sci. U. S. A.* 111.
- Harburger, D.S., and Calderwood, D.A. (2009). Integrin signalling at a glance. *J. Cell Sci.* 122.
- Heintz, C., Doktor, T.K., Lanjuin, A., Escoubas, C.C., Zhang, Y., Weir, H.J., Dutta, S., Silva-García, C.G., Bruun, G.H., Morantte, I., et al. (2017). Splicing factor 1 modulates dietary restriction and TORC1 pathway longevity in *C. elegans*. *Nature* 541.
- Henis-Korenblit, S., Zhang, P., Hansen, M., McCormick, M., Lee, S.-J., Cary, M., and Kenyon, C. (2010). Insulin/IGF-1 signaling mutants reprogram ER stress response regulators to promote longevity. *Proc. Natl. Acad. Sci.* 107, 9730–9735.
- Henry, L., and Wickham, H. (2019). purrr: Functional Programming Tools. R package version 0.3.3. R Packag. Version 0.3.2.

-
- Herrera, J., Henke, C.A., and Bitterman, P.B. (2018). Extracellular matrix as a driver of progressive fibrosis. *J. Clin. Invest.* 128.
- Holdorf, A.D., Higgins, D.P., Hart, A.C., Boag, P.R., Pazour, G.J., Walhout, A.J.M., and Walker, A.K. (2020). WormCat: An online tool for annotation and visualization of *Caenorhabditis elegans* genome-scale data. *Genetics* 214.
- Hostettler, L., Grundy, L., Käser-Pébernard, S., Wicky, C., Schafer, W.R., and Glauser, D.A. (2017). The bright fluorescent protein mNeonGreen facilitates protein expression analysis in vivo. *G3 Genes, Genomes, Genet.* 7, 607–615.
- Hu, Q., D'Amora, D.R., Macneil, L.T., Walhout, A.J.M., and Kubiseski, T.J. (2017). The oxidative stress response in *Caenorhabditis elegans* requires the GATA transcription factor ELT-3 and SKN-1/Nrf2. *Genetics* 206.
- Humphrey, J.D., Dufresne, E.R., and Schwartz, M.A. (2014). Mechanotransduction and extracellular matrix homeostasis. *Nat. Rev. Mol. Cell Biol.* 15.
- Hynes, R.O. (2009). The extracellular matrix: Not just pretty fibrils. *Science* (80-.). 326, 1216–1219.
- Hynes, R.O., and Naba, A. (2012). Overview of the matrisome-An inventory of extracellular matrix constituents and functions. *Cold Spring Harb. Perspect. Biol.* 4.
- Jiang, X., and Couchman, J.R. (2003). Perlecan and Tumor Angiogenesis. *J. Histochem. Cytochem.* 51.
- Kanehisa, M. Autophagy - other - *Caenorhabditis elegans* (nematode).
- Kechagia, J.Z., Ivaska, J., and Roca-Cusachs, P. (2019). Integrins as biomechanical sensors of the microenvironment. *Nat. Rev. Mol. Cell Biol.* 20.
- Kim, T.H., Kim, D.H., Nam, H.W., Park, S.Y., Shim, J., and Cho, J.W. (2010). Tyrosylprotein sulfotransferase regulates collagen secretion in *Caenorhabditis elegans*. *Mol. Cells* 29, 413–418.
- Kramer, J.M. (2005). Basement membranes. *WormBook*.
- Kumsta, C., Ching, T.T., Nishimura, M., Davis, A.E., Gelino, S., Catan, H.H., Yu, X., Chu, C.C., Ong, B., Panowski, S.H., et al. (2014). Integrin-linked kinase modulates longevity and thermotolerance in *C. elegans* through neuronal control of HSF-1. *Aging Cell* 13.
- Labouesse, M. (2012). Role of the extracellular matrix in epithelial morphogenesis: A view from *C. elegans*. *Organogenesis* 8.
- Lamitina, T., Huang, C.G., and Strange, K. (2006). Genome-wide RNAi screening identifies protein damage as a regulator of osmoprotective gene expression. *Proc. Natl. Acad. Sci. U. S. A.* 103.
- Liu, N., Matsumura, H., Kato, T., Ichinose, S., Takada, A., Namiki, T., Asakawa, K., Morinaga, H., Mohri, Y., De Arcangelis, A., et al. (2019). Stem cell competition orchestrates skin homeostasis and ageing. *Nature* 568.
- Lu, P., Takai, K., Weaver, V.M., and Werb, Z. (2011). Extracellular Matrix degradation and remodeling in development and disease. *Cold Spring Harb. Perspect. Biol.* 3.
- Lundquist, E.A., Herman, R.K., Rogalski, T.M., Mullen, G.P., Moerman, D.G., and Shaw, J.E. (1996). The *mec-8* gene of *C. Elegans* encodes a protein with two RNA recognition motifs and regulates alternative splicing of *unc-52* transcripts. *Development* 122.
- Mackinnon, A.C., Qadota, H., Norman, K.R., Moerman, D.G., and Williams, B.D. (2002). *C. elegans* PAT-4/ILK functions as an adaptor protein within integrin adhesion complexes. *Curr. Biol.* 12.

-
- Madaan, U., Yzeiraj, E., Meade, M., Clark, J.F., Rushlow, C.A., and Savage-Dunn, C. (2018). BMP signaling determines body size via transcriptional regulation of collagen genes in *Caenorhabditis elegans*. *Genetics* 210.
- Madaan, U., Faure, L., Chowdhury, A., Ahmed, S., Ciccarelli, E.J., Gumienny, T.L., and Savage-Dunn, C. (2020). Feedback regulation of BMP signaling by *Caenorhabditis elegans* cuticle collagens. *Mol. Biol. Cell* 31, 825–832.
- de Magalhães, J.P., Curado, J., and Church, G.M. (2009). Meta-analysis of age-related gene expression profiles identifies common signatures of aging. *Bioinformatics* 25, 875–881.
- Margadant, C., Kreft, M., De Groot, D.J., Norman, J.C., and Sonnenberg, A. (2012). Distinct roles of talin and kindlin in regulating integrin $\alpha 5\beta 1$ function and trafficking. *Curr. Biol.* 22.
- Mei Xiong, Z., O'Donovan, M., Sun, L., Young Choi, J., Ren, M., and Cao, K. (2017). Anti-Aging Potentials of Methylene Blue for Human Skin Longevity. *Sci. Rep.* 7.
- Merz, D.C., Alves, G., Kawano, T., Zheng, H., and Culotti, J.G. (2003). UNC-52/Perlecan affects gonadal leader cell migrations in *C. elegans* hermaphrodites through alterations in growth factor signaling. *Dev. Biol.* 256.
- Mesbahi, H., Pho, K.B., Tench, A.J., Guerrero, V.L.L., and MacNeil, L.T. (2020). Cuticle collagen expression is regulated in response to environmental stimuli by the GATA transcription factor ELT-3 in *Caenorhabditis elegans*. *Genetics* 215.
- Miao, R., Li, M., Zhang, Q., Yang, C., and Wang, X. (2020). An ECM-to-Nucleus Signaling Pathway Activates Lysosomes for *C. elegans* Larval Development. *Dev. Cell* 52.
- Mizuno, H., Mal, T.K., Tong, K.I., Ando, R., Furuta, T., Ikura, M., and Miyawaki, A. (2003). Photo-induced peptide cleavage in the green-to-red conversion of a fluorescent protein. *Mol. Cell* 12.
- Mullen, G.P., Rogalski, T.M., Bush, J.A., Gorji, P.R., and Moerman, D.G. (1999). Complex patterns of alternative splicing mediate the spatial and temporal distribution of perlecan/UNC-52 in *Caenorhabditis elegans*. *Mol. Biol. Cell* 10.
- Nieswandt, B., Moser, M., Pleines, I., Varga-Szabo, D., Monkley, S., Critchley, D., and Fässler, R. (2007). Loss of talin1 in platelets abrogates integrin activation, platelet aggregation, and thrombus formation in vitro and in vivo. *J. Exp. Med.* 204.
- Padgett, R.W., Das, P., and Krishna, S. (1998). TGF- β signaling, Smads, and tumor suppressors. *BioEssays* 20.
- Page, A.P., and Johnstone, I.L. (2007). The cuticle. *WormBook*.
- R Core Team (2019) (2019). R: A language and environment for statistical computing. Accessed 1st April 2019.
- Ren, P., Albert, P., and Riddle, D. (1996). Expression of DAF-7 in ASI neurons. *Worm Breeders Gaz.* 14.
- Rikke, B.A., Murakami, S., and Johnson, T.E. (2000). Paralogy and orthology of tyrosine kinases that can extend the life span of *Caenorhabditis elegans*. *Mol. Biol. Evol.* 17.
- Rognoni, E., Ruppert, R., and Fässler, R. (2016). The kindlin family: Functions, signaling properties and implications for human disease. *J. Cell Sci.* 129.
- Ross, T.D., Coon, B.G., Yun, S., Baeyens, N., Tanaka, K., Ouyang, M., and Schwartz, M.A. (2013). Integrins in mechanotransduction. *Curr. Opin. Cell Biol.* 25.
- Dos Santos, M., Michopoulou, A., André-Frei, V., Boulesteix, S., Guicher, C., Dayan, G., Whitelock, J., Damour, O., and Rousselle, P. (2016). Perlecan expression influences the keratin 15-positive cell population fate in the epidermis of aging skin. *Aging (Albany, NY)*. 8.

-
- Sarov, M., Murray, J.I., Schanze, K., Pozniakovski, A., Niu, W., Angermann, K., Hasse, S., Rupprecht, M., Vinis, E., Tinney, M., et al. (2012). A genome-scale resource for in vivo tag-based protein function exploration in *C. elegans*. *Cell* 150.
- Shaw, W.M., Luo, S., Landis, J., Ashraf, J., and Murphy, C.T. (2007). The *C. elegans* TGF- β Dauer Pathway Regulates Longevity via Insulin Signaling. *Curr. Biol.* 17.
- Shi, Y., Hu, X., Cheng, J., Zhang, X., Zhao, F., Shi, W., Ren, B., Yu, H., Yang, P., Li, Z., et al. (2019). A small molecule promotes cartilage extracellular matrix generation and inhibits osteoarthritis development. *Nat. Commun.* 10.
- Sijen, T., Fleenor, J., Simmer, F., Thijssen, K.L., Parrish, S., Timmons, L., Plasterk, R.H.A., and Fire, A. (2001). On the role of RNA amplification in dsRNA-triggered gene silencing. *Cell* 107.
- Spike, C.A., Davies, A.A., Shaw, J.E., and Herman, R.K. (2002). MEC-8 regulates alternative splicing of *unc-52* transcripts in *C. elegans* hypodermal cells. *Development* 129.
- Sroga, G.E., and Vashishth, D. (2012). Effects of bone matrix proteins on fracture and fragility in osteoporosis. *Curr. Osteoporos. Rep.* 10.
- Stiernagle, T. (2006). Maintenance of *C. elegans*. *WormBook* 1–11.
- Suzuki, Y., Yandell, M.D., Roy, P.J., Krishna, S., Savage-Dunn, C., Ross, R.M., Padgett, R.W., and Wood, W.B. (1999). A BMP homolog acts as a dose-dependent regulator of body size and male tail patterning in *Caenorhabditis elegans*. *Development* 126.
- Tadokoro, S., Shattil, S.J., Eto, K., Tai, V., Liddington, R.C., De Pereda, J.M., Ginsberg, M.H., and Calderwood, D.A. (2003). Talin binding to integrin β tails: A final common step in integrin activation. *Science* (80-.). 302.
- Taylor, J., Unsoeld, T., and Hutter, H. (2018). The transmembrane collagen COL-99 guides longitudinally extending axons in *C. elegans*. *Mol. Cell. Neurosci.* 89, 9–19.
- Teuscher, A., and Ewald, C. (2018). Overcoming Autofluorescence to Assess GFP Expression During Normal Physiology and Aging in *Caenorhabditis elegans*. *Bio-Protocol* 8.
- Teuscher, A.C., Jongsma, E., Davis, M.N., Statzer, C., Gebauer, J.M., Naba, A., and Ewald, C.Y. (2019a). The in-silico characterization of the *Caenorhabditis elegans* matrisome and proposal of a novel collagen classification. *Matrix Biol. Plus* 1–13.
- Teuscher, A.C., Statzer, C., Pantasis, S., Bordoli, M.R., and Collin, Y. (2019b). Assessing collagen deposition during aging in mammalian tissue and in *Caenorhabditis elegans*. *Methods Mol. Biol.* 1944, 169–188.
- Tissenbaum, H.A. (2015). Using *C. elegans* for aging research. *Invertebr. Reprod. Dev.* 59, 59–63.
- Tu, H., Huhtala, P., Lee, H.M., Adams, J.C., and Pihlajaniemi, T. (2015). Membrane-associated collagens with interrupted triple-helices (MACITs): Evolution from a bilaterian common ancestor and functional conservation in *C. elegans*. *BMC Evol. Biol.* 15, 1–21.
- Uhler, C., and Shivashankar, G. V. (2017). Regulation of genome organization and gene expression by nuclear mechanotransduction. *Nat. Rev. Mol. Cell Biol.* 18.
- Varani, J., Dame, M.K., Rittie, L., Fligiel, S.E.G., Kang, S., Fisher, G.J., and Voorhees, J.J. (2006). Decreased collagen production in chronologically aged skin: Roles of age-dependent alteration in fibroblast function and defective mechanical stimulation. *Am. J. Pathol.* 168.
- Vogel, V. (2018). Unraveling the Mechanobiology of Extracellular Matrix. *Annu. Rev. Physiol.* 80.
- Vogél, B.E., and Hedgecock, E.M. (2001). Hemicentin, a conserved extracellular member of

the immunoglobulin superfamily, organizes epithelial and other cell attachments into oriented line-shaped junctions. *Development* 128.

Vozdek, R., Long, Y., and Ma, D.K. (2018). The receptor tyrosine kinase HIR-1 coordinates HIF-independent responses to hypoxia and extracellular matrix injury. *Sci. Signal.* 11.

Walser, M., Umbricht, C.A., Fröhli, E., Nanni, P., and Hajnal, A. (2017). β -Integrin dephosphorylation by the Density-Enhanced Phosphatase DEP-1 attenuates EGFR signaling in *C. elegans*. *PLoS Genet.* 13, 1–22.

Walther, D.M., Kasturi, P., Zheng, M., Pinkert, S., Vecchi, G., Ciryam, P., Morimoto, R.I., Dobson, C.M., Vendruscolo, M., Mann, M., et al. (2015). Widespread proteome remodeling and aggregation in aging *C. elegans*. *Cell* 161.

Wang, J.H.C., and Thampatty, B.P. (2006). An introductory review of cell mechanobiology. *Biomech. Model. Mechanobiol.* 5.

Wheeler, J.M., and Thomas, J.H. (2006). Identification of a novel gene family involved in osmotic stress response in *Caenorhabditis elegans*. *Genetics* 174.

Whittaker, C.A., Bergeron, K.F., Whittle, J., Brandhorst, B.P., Burke, R.D., and Hynes, R.O. (2006). The echinoderm adhesome. *Dev. Biol.* 300.

Wickham, H. (2011). tidyverse: Easily Install and Load the “Tidyverse.” *Bioinformatics* 27.

Wilkinson, J.E., Burmeister, L., Brooks, S. V., Chan, C.C., Friedline, S., Harrison, D.E., Hejtmančík, J.F., Nadon, N., Strong, R., Wood, L.K., et al. (2012). Rapamycin slows aging in mice. *Aging Cell* 11, 675–682.

Wolfson, M., Budovsky, A., Tacutu, R., and Fraifeld, V. (2009). The signaling hubs at the crossroad of longevity and age-related disease networks. *Int. J. Biochem. Cell Biol.* 41.

Yu, G., Wang, L.G., Han, Y., and He, Q.Y. (2012). ClusterProfiler: An R package for comparing biological themes among gene clusters. *Omi. A J. Integr. Biol.* 16.

Yue, B. (2014). Biology of the extracellular matrix: An overview. *J. Glaucoma* 23.

Zahreddine, H., Zhang, H., Diogon, M., Nagamatsu, Y., and Labouesse, M. (2010). CRT-1/Calreticulin and the E3 Ligase EEL-1/HUWE1 Control Hemidesmosome Maturation in *C. elegans*. *Development. Curr. Biol.* 20.

Zhang, H., and Labouesse, M. (2010). The making of hemidesmosome structures in vivo. *Dev. Dyn.* 239.

Zhang, H., Landmann, F., Zahreddine, H., Rodriguez, D., Koch, M., and Labouesse, M. (2011). A tension-induced mechanotransduction pathway promotes epithelial morphogenesis. *Nature* 471.

Zhang, Y., Li, W., Li, L., Li, Y., Fu, R., Zhu, Y., Li, J., Zhou, Y., Xiong, S., and Zhang, H. (2015). Structural Damage in the *C. elegans* Epidermis Causes Release of STA-2 and Induction of an Innate Immune Response. *Immunity* 42.

Zhang, Y., Qi, L., and Zhang, H. (2019). TGF β -like DAF-7 acts as a systemic signal for autophagy regulation in *C. elegans*. *J. Cell Biol.* 218.

Zugasti, O., Thakur, N., Belougne, J., Squiban, B., Kurz, C.L., Soulé, J., Omi, S., Tichit, L., Pujol, N., and Ewbank, J.J. (2016). A quantitative genome-wide RNAi screen in *C. elegans* for antifungal innate immunity genes. *BMC Biol.* 14, 1–25.

7. Conclusion and Outlook

The ECM is a structural framework essential for tissue growth, remodeling, and maintenance by stabilizing structures and providing the needed elasticity. However, it is also a major communication layer between the environment and individual cells. Most studies focus on changes within cells; however, the ECM also deteriorates during aging. Interestingly longevity treatments seem to slow down the aging process partly through higher collagen expression levels. In this work, we identified regulators that modulate collagen expression during aging.

We found mechanotransduction to be a regulator of collagen during aging and found evidence that mechanotransduction and its maintenance play a role for healthy aging and longevity. However, the results still leave certain open questions or could benefit from further experiments.

Major hits of the screen could be validated using additional expression reporters for cuticular collagens, like *col-120* or *col-12*, which were previously connected with longevity to demonstrate that the regulation is not restricted to just *col-144*. Furthermore, it would be beneficial to test the RNAi or mutants of important screen hits. These assessments could involve lifespan, oxidative stress, or health assays like acoustic force field trap assay and swimming assays to strengthen the link between longevity and healthy aging.

Currently, co-localization experiments of EMB-9, integrin, and UNC-52 are still ongoing. We also plan to test if improved protein homeostasis would influence the EMB-9 PAT-3 disassociation by treating the double reporter strain with *daf-2* RNAi in wild-type or *unc-52* mutant background.

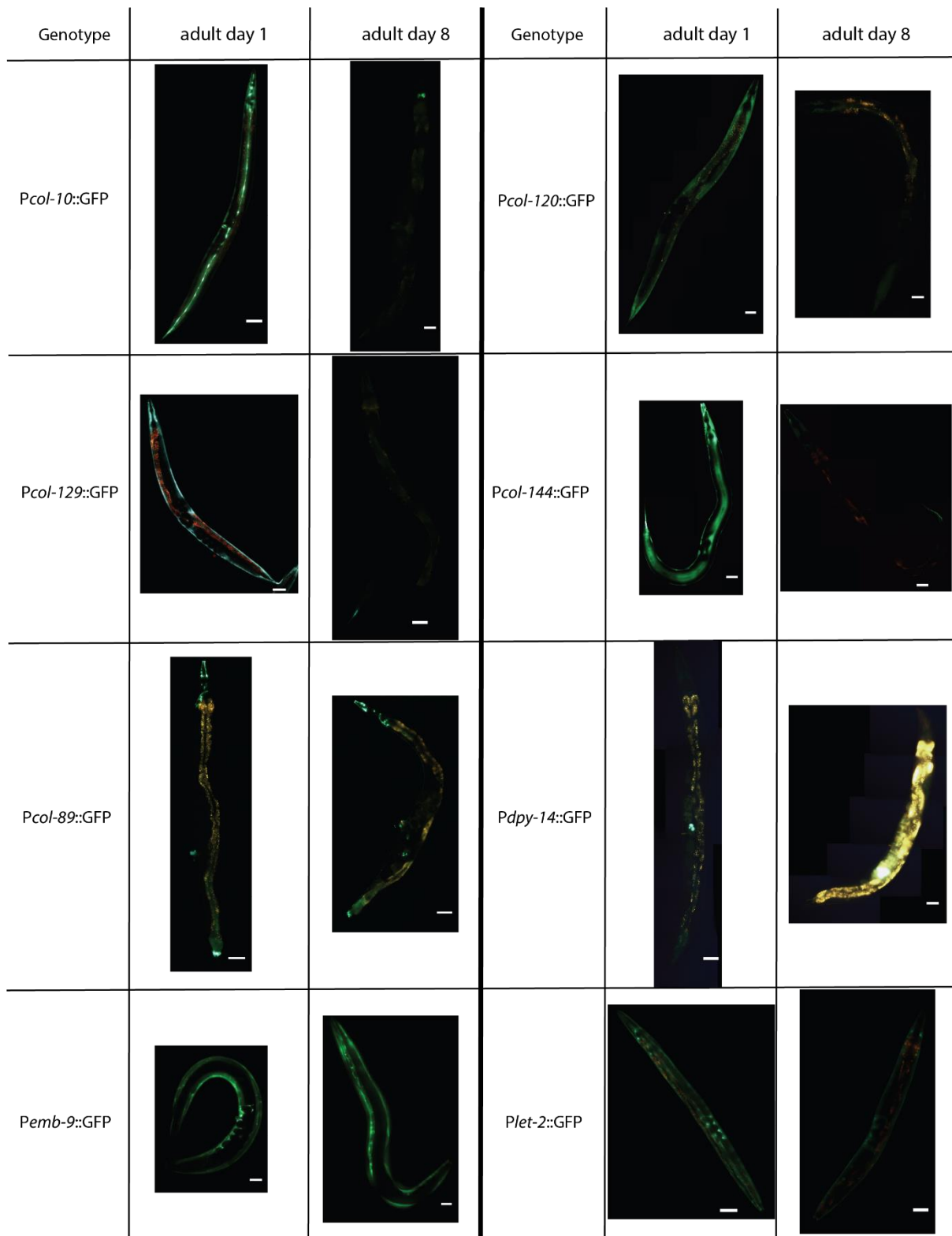
In order to gain more knowledge about the role of integrin signaling during aging, it would be informative to use a FRET sensor or FRET-based molecular tension sensors (MTSs) for the integrin heterodimer to measure conformation and force changes during aging. Another possibility could be immunoprecipitation to check for changing binding partners during aging.

Mechanotransduction is a signaling mechanism of vital importance for *C. elegans*. A complete removal of the key proteins leads to larval or adult lethality (Suman et al., 2019; Williams and Waterston, 1994). A better maintenance or regulation of mechanotransduction, specifically during aging, could be a strong pro-longevity factor. Therefore, it would be interesting to investigate potential longevity-specific “maintenance” genes. Especially genes that are differently regulated in long-lived animals compared to normal-lived ones but do not display a strong phenotype. We could test if they are required explicitly for longevity by treating long-lived *C. elegans* with RNAi or cross them with the respective mutants. Later, they could be examined for their effect on the mechanotransduction system.

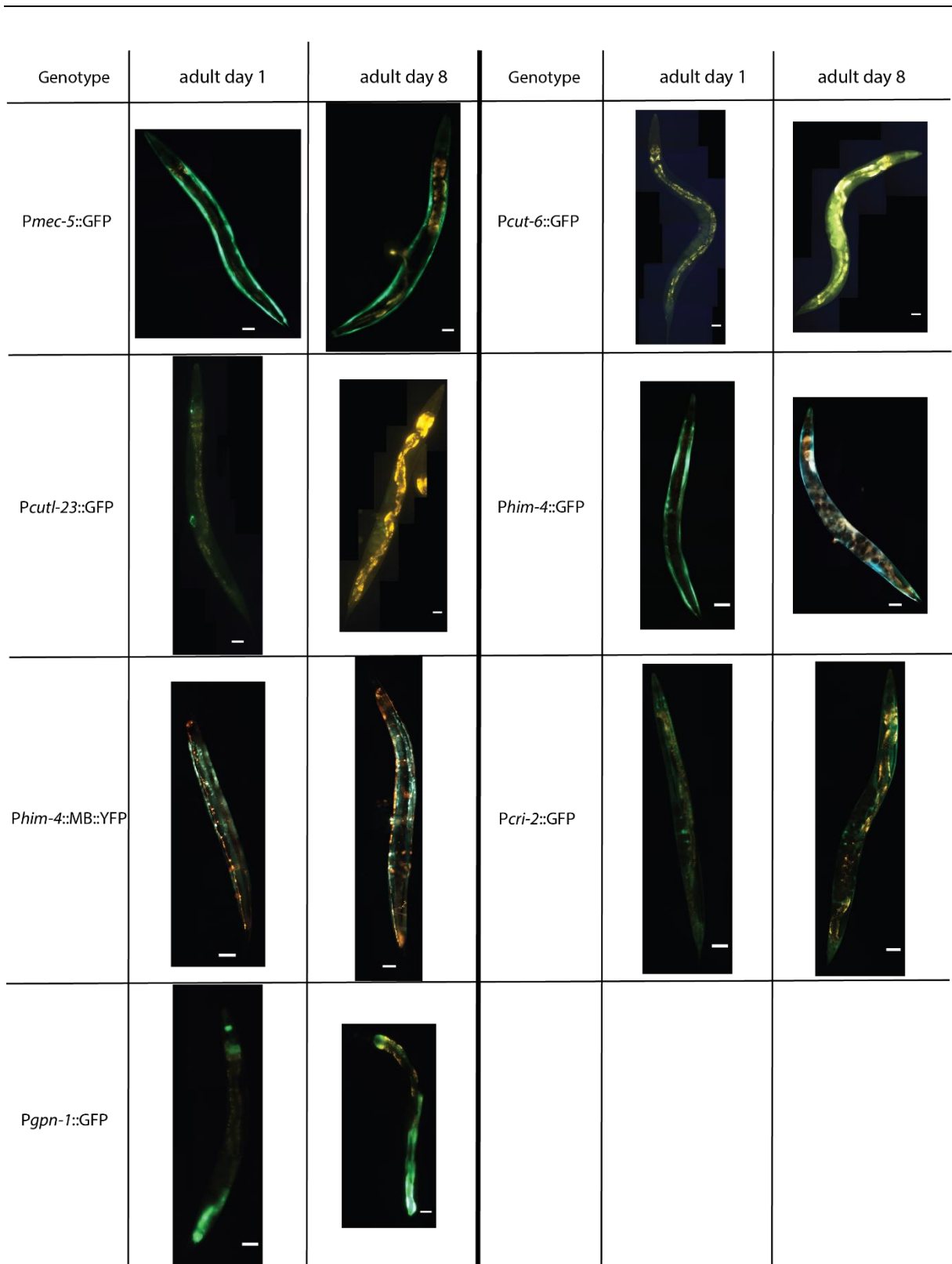
Furthermore, we could show that the *daf-7* and especially the *dbl-1* TGF beta pathways are interesting candidates for collagen regulation parallel or in combination with mechanotransduction. The same applies to STA-2 and probably ELT-3 signaling at the hemidesmosome-like junction level. Additional experiments could reveal more about the relationship of these pathways with mechanotransduction and collagen regulation.

In summary, during my studies, I contributed to the development of several useful tools for the examination of the ECM in aging *C. elegans*. I helped to define the *C. elegans* Matrisome, developing a filter set facilitating the distinction between GFP and autofluorescence in old animals, and the introduction of the Herovici staining into *C. elegans* research. We could provide more information about the expression and behavior of several ECM and adhesion genes during aging by generating an atlas of transcriptional and translational reporter strains. Finally, we elucidated the importance of mechanotransduction for the regulation of collagens during aging and its role in longevity.

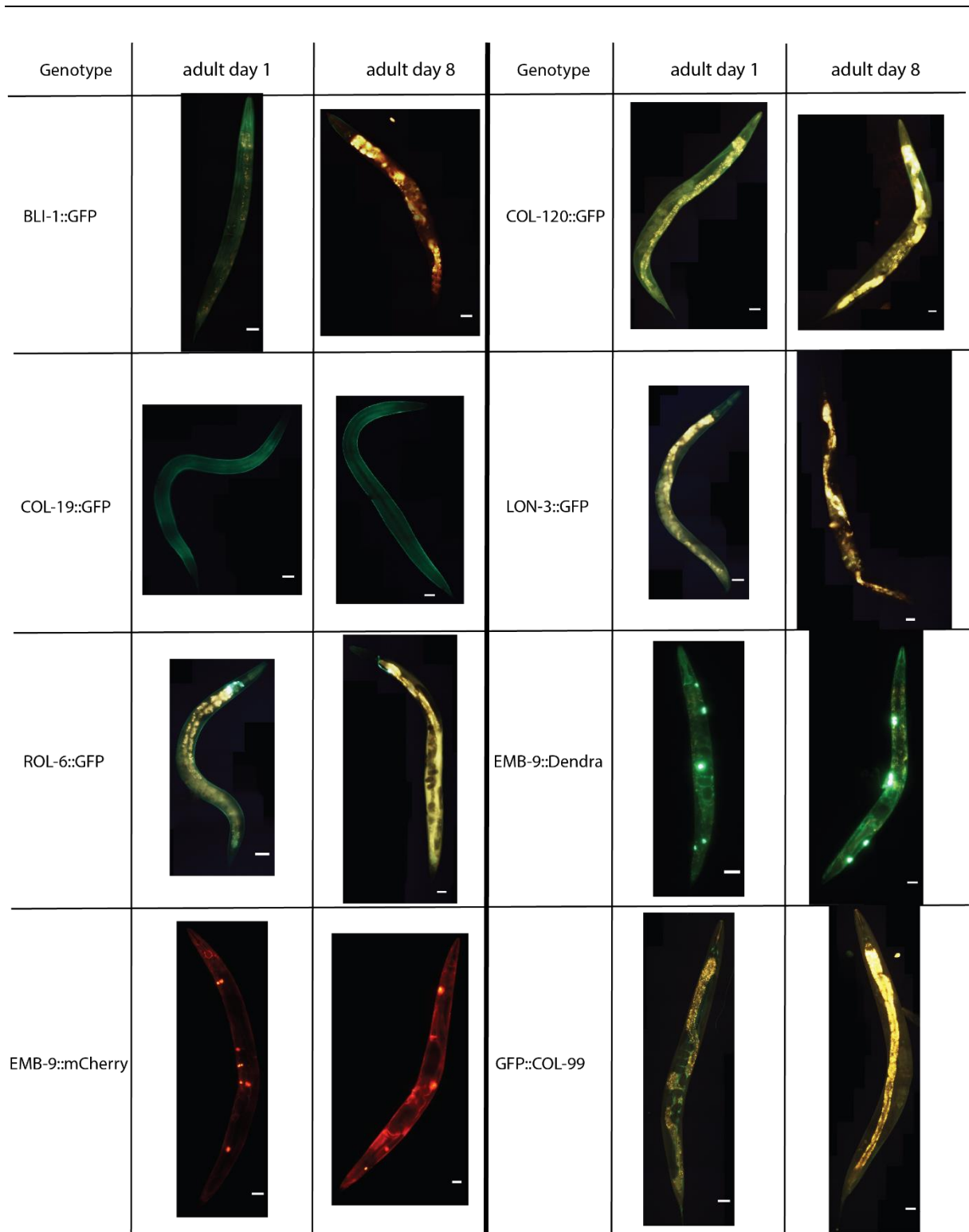
8. Supplements



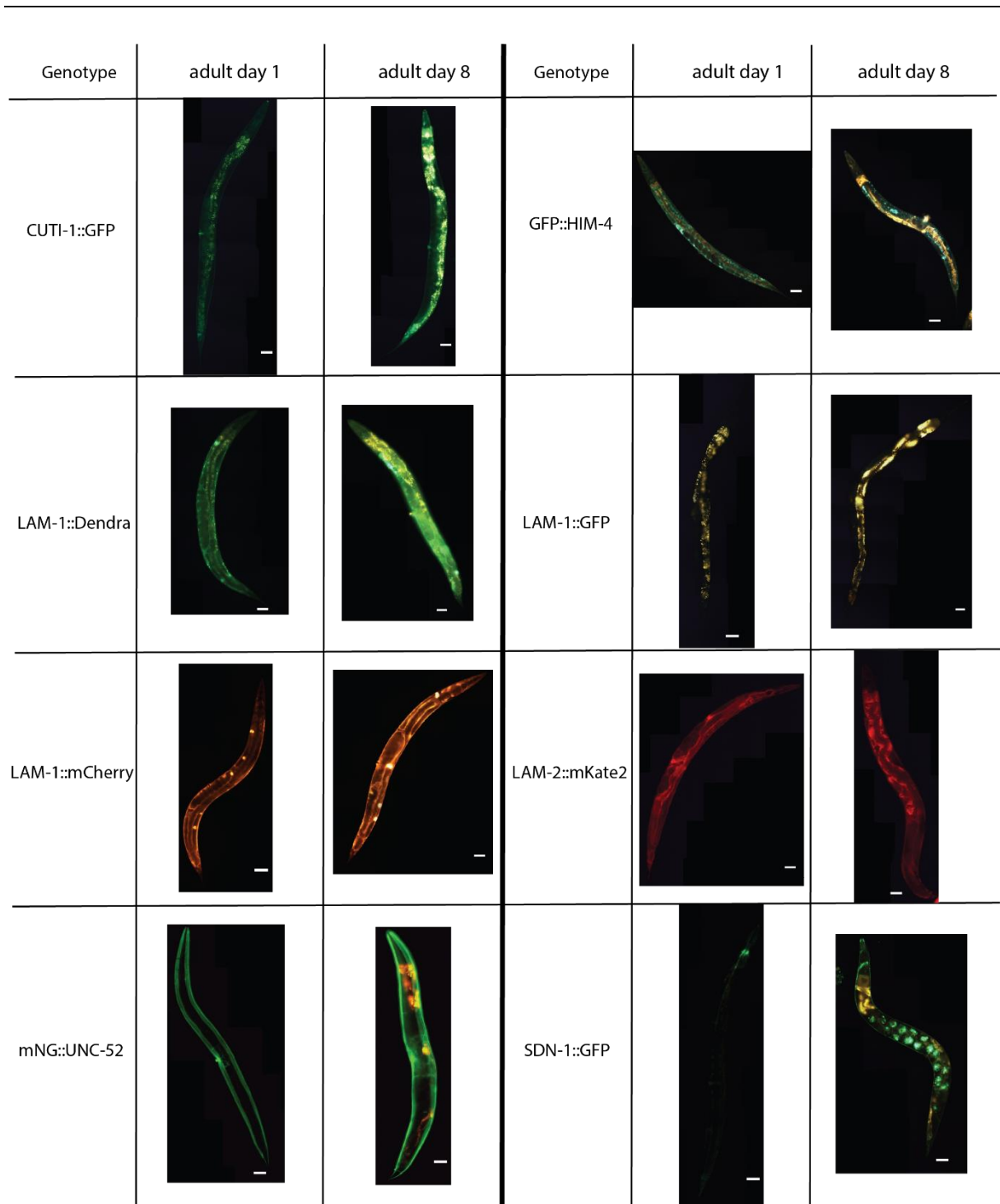
Supplemental Figure 1: Adulthood day 1 and day 8 images of the transcriptional strains of the *in-vivo* atlas of the matrisome and adhesome. Part I



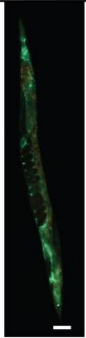
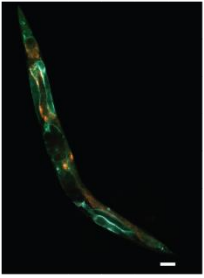

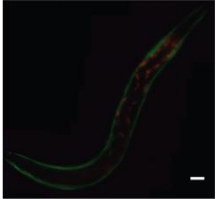
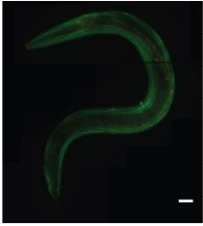
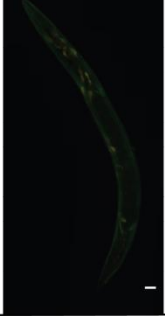
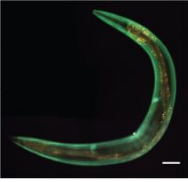
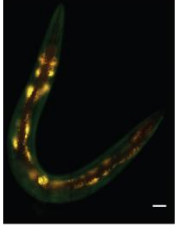
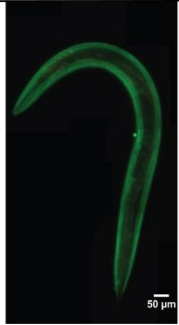
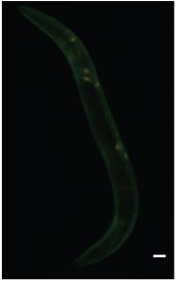
Supplemental Figure 2: Adulthood day 1 and day 8 images of the transcriptional strains of the *in-vivo* atlas of the matrisome and adhesome. Part II



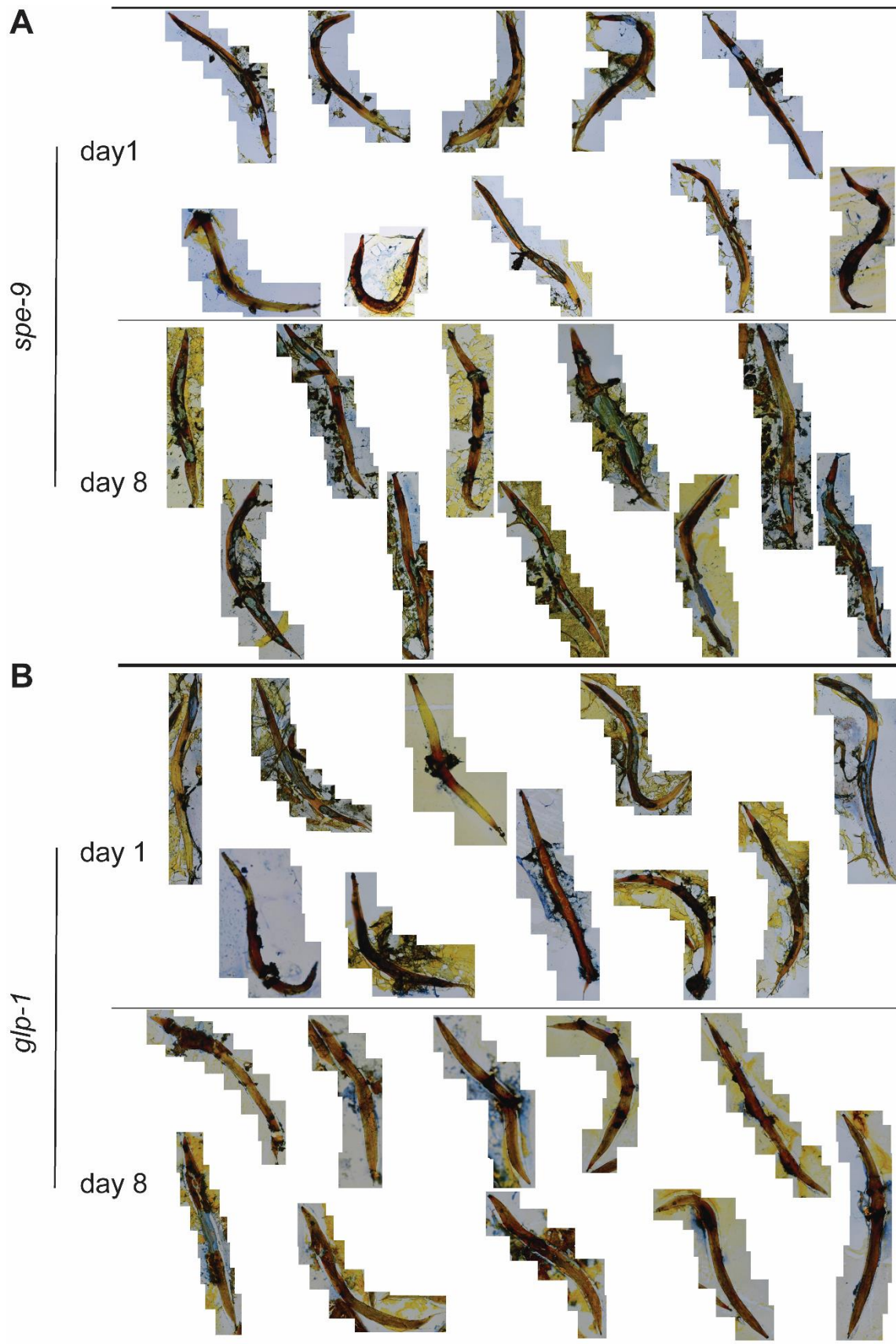
Supplemental Figure 3: Adulthood day 1 and day 8 images of the translational strains of the *in-vivo* atlas of the matrisome and adhesome. Part I



Supplemental Figure 4: Adulthood day 1 and day 8 images of the translational strains of the *in-vivo* atlas of the matrisome and adhesome. Part II

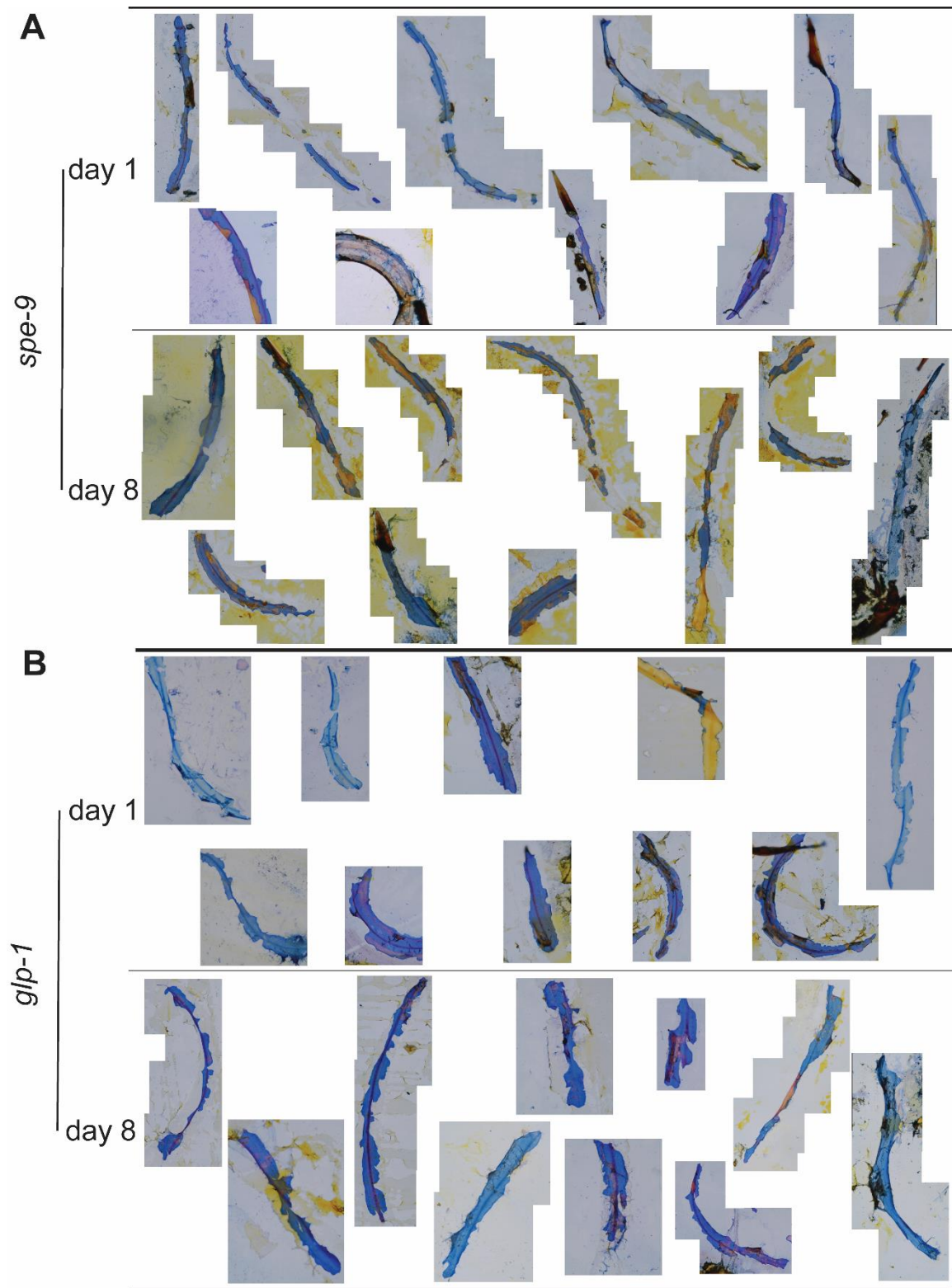
Genotype	adult day 1	adult day 8	Genotype	adult day 1	adult day 8
INA-1::GFP			PAT-2::GFP		
PAT-3::GFP AH4617			PAT-3::GFP NK358		
GFP::TLN-1					

Supplemental Figure 5: Adulthood day 1 and day 8 images of the translational strains of the *in-vivo* atlas of the matrisome and adhesome. Part III



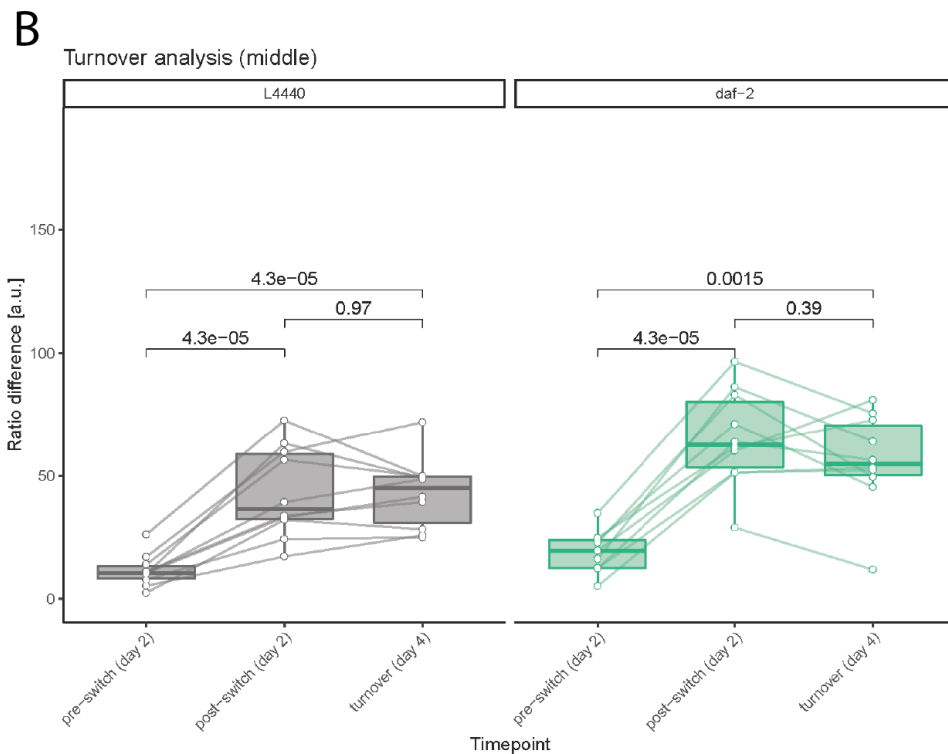
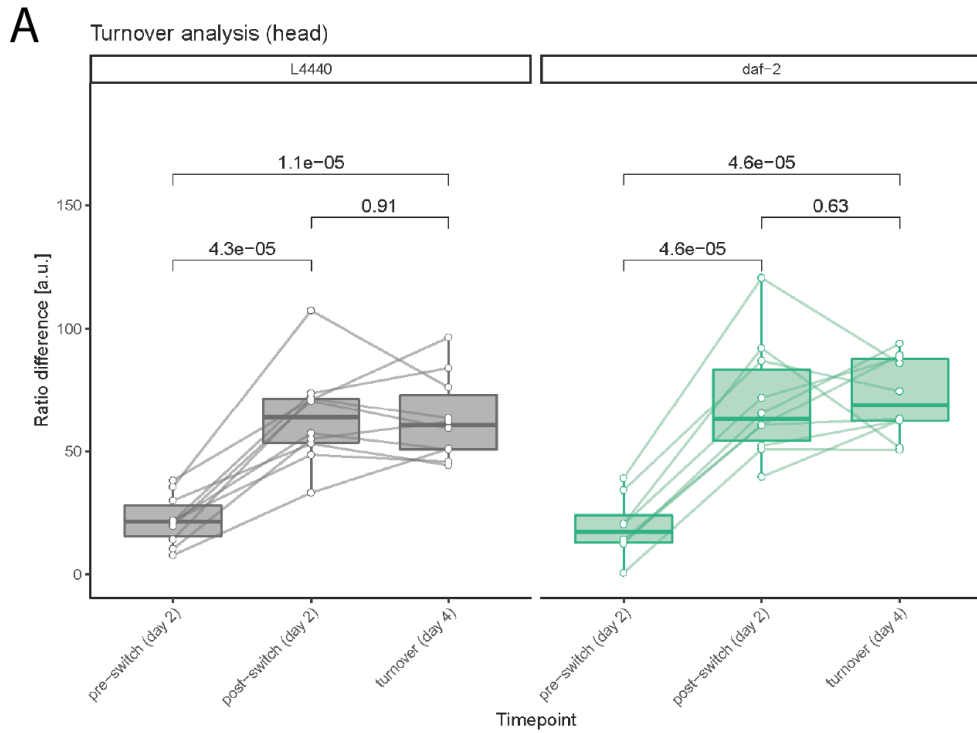
Supplemental Figure 6: Herovici Staining of whole *C. elegans* after freeze crack

Microscope images of Herovici stained *C. elegans* with two different mutant backgrounds and at different ages. (A) *spe-9(hc88)* with normal lifespan. Upper row adults day 1. Lower row adults day 8. (B) *glp-1(e2141)* animals with long lifespan. Upper row adults day 1. Lower row adults day 8.



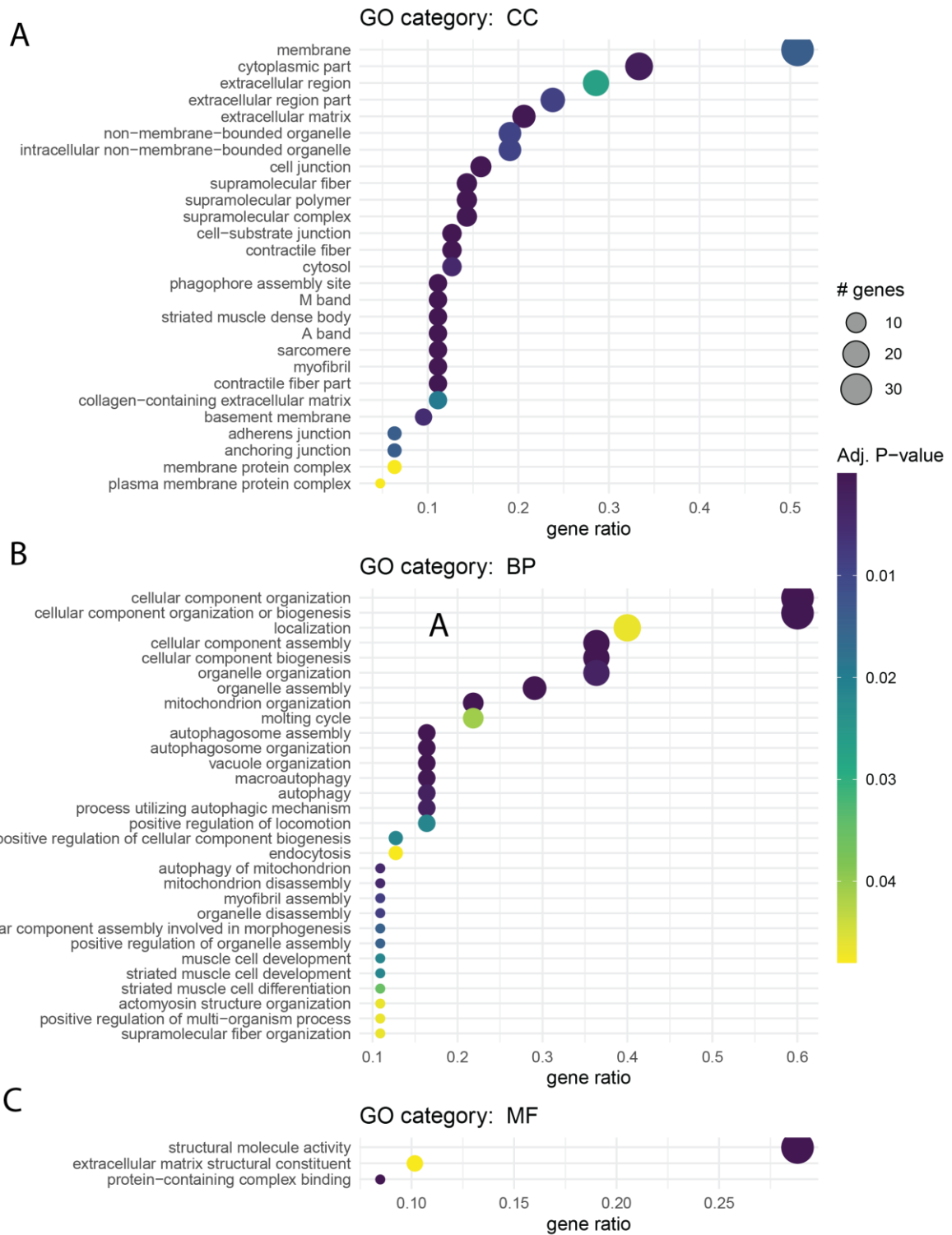
Supplemental Figure 7: Herovici Staining *C. elegans* cuticle after freeze crack

Microscope images of Herovici stained *C. elegans* cuticle from animals with two different mutant backgrounds and at different age. (A) Cuticles from *spe-9(hc88)* with normal lifespan. Upper row adults day 1. Lower row adults day 8. (B) Cuticles from *glp-1(e2141)* animals with long lifespan. Upper row adult days 1. Lower row adults day 8.



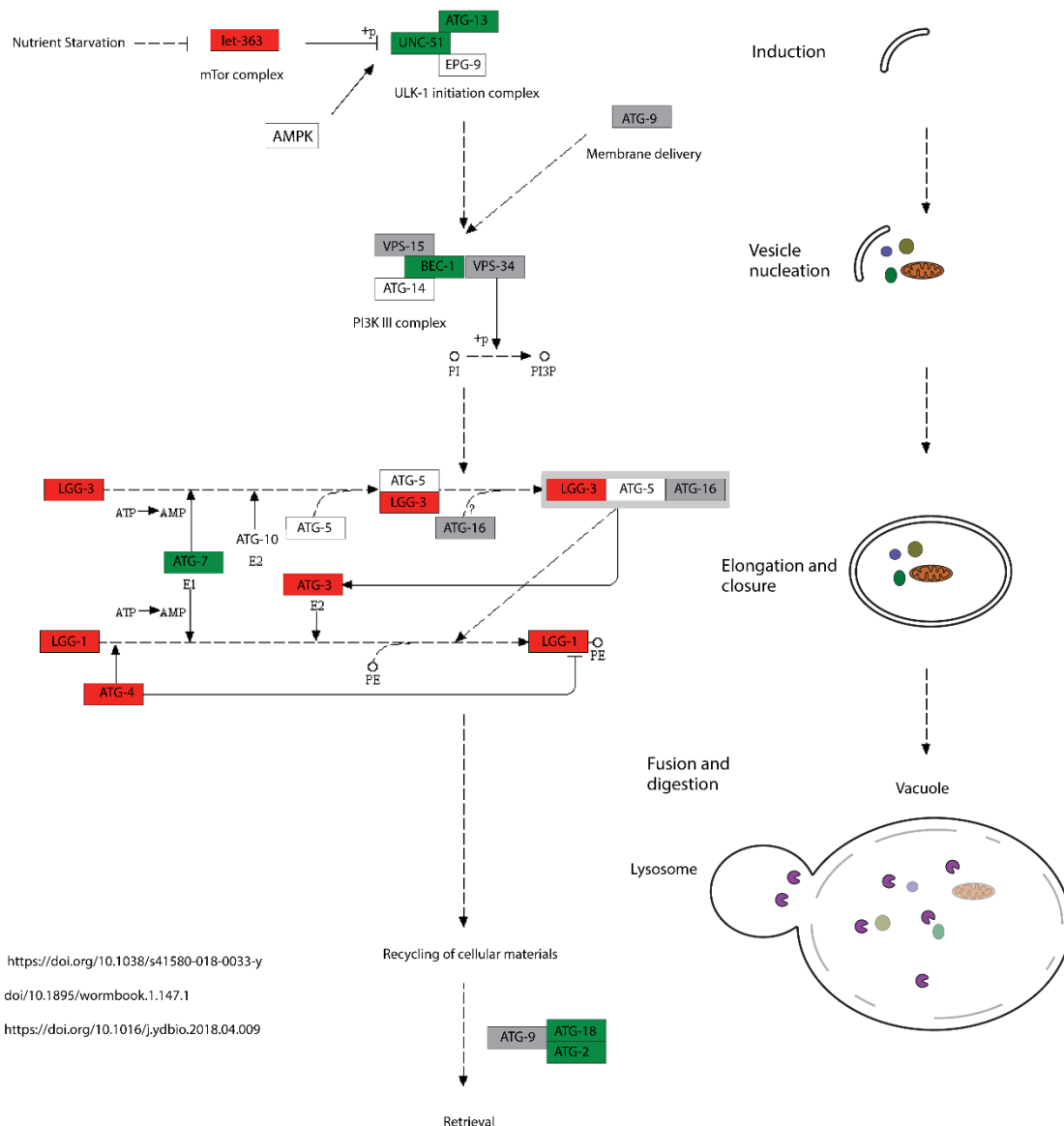
Supplemental Figure 8: Alternative visualization of the image analysis for a potential turnover of COL-120::Dendra2.

The data points shown represent the relative difference of the photoconverted area to the surrounding non-treated area in percentage. The error bars show the SD. N=10 per strain. (A) shows the data for the head region (B) for the middle region around the vulva. Graphs were done by Cyril Statzer.



Supplemental Figure 9: GO term enrichment analysis of genes associated with *glp-1*-dependent *col-144* promoter activation

Significantly enriched GO terms are displayed by their location (A), biological process (B) and molecular function (C). The individual GO terms are shown on the y-axis and the number of genes observed compared to the overall size of each GO term displayed on the x-axis. The color of each point reflects the P-value of the one-sided Fisher's exact test and its size corresponds to the absolute number of genes enriched within each term. Analysis by Cyril Statzer.



Supplemental Figure 10: Overview of screen hits in the *C. elegans* macroautophagy pathway

On the right side is a diagram of the different autophagy steps. Starting with the induction of the isolation membrane or phagophore, followed by the engulfment of cellular material. The elongation and closure finishing the creation of the autophagosome. After the fusion with a lysosome, the engulfed material is degraded in the so-called autophagolysosome and gets recycled. On the left side is a diagram of the molecular autophagy pathway, starting with the mainly by mTOR and AMP-activated kinase (AMPK) controlled ULK-1 initiation complex. The class III phosphatidylinositol 3-kinase (PI3K) lipid kinase enzymatic complex is involved in the vesicle nucleation, while ATG-9 is recruiting membrane to the growing phagophore. The LGG-1 system is involved in the earlier steps of autophagy, while LGG-2 is needed in the maturation of the autophagosome. Together they are required for the elongation and formation to a mature autophagosome. After fusion with a lysosome and degradation for the cellular material inside the autophagolysosome, ATG-2 and ATG-18 retrieve the integral membrane protein ATG-9 from the phagophore assembly site. RNAi against the mRNA of the green marked proteins led to an upregulation of our *Pcol-144::GFP* reporter signal (potential suppressors/inhibitors) in at least one of the three screened strains, while RNAi against the red ones led to an downregulation (potential activators). The RNAi against the mRNA of the grey marked proteins was also tested, but did not show a significant regulation, while the white ones were not included in the screen. Arrows indicate a direct molecular interaction, while dashed arrows symbolize an indirect interaction. Figure was adapted from the *Autophagy - other - Caenorhabditis elegans (nematode)* KEGG-pathway webpage (Kanehisa).

Supplement Table 1: Short overview of *Pcol-144::GFP* RNAi screen hits at day 1 of adulthood.

Results on the right represent the average relative fluorescence in percentage from the last validation screening rounds. Results in red show a downregulation of *col-144* compared to control. Results in green show a upregulation of *col-144* compared to control.

Promoter *col-144::GFP* expression at day 1 of adulthood.

WormBase Gene ID	Gene Name	Gene Type	Human Ortholog	Control (<i>spe-9(hc88)</i>)	Long-lived (<i>glp-1(e2142)</i>)	Long-lived (<i>daf-2(e1370)</i>)
Control						
L4440	empty control			83.33%	100%	100%
GFP	neg.control			0%	15%	0%
<i>daf-2</i>	pos. control			87.5%	100%	100%
Adhesiosome						
WBGene00006876	<i>vab-10</i>	two spectraplakins	DST	33.3%	33.3%	33.3%
WBGene00012489	<i>Y19D2B.1</i>	tubulin	AC092143.1\;TUBB6/TUBG2	83.3%	100%	66.7%
Matrisome						
WBGene00000039	<i>acn-1</i>	ACE-like	ACE2	83.3%	100%	66.7%
WBGene00000659	<i>col-84</i>	cuticular collagen	COLQ	72.2%	100%	22%
WBGene00001065	<i>dpy-3</i>	cuticular collagen	-	83.3%	100%	66.7%
WBGene00001263	<i>emb-9</i>	α -chain type IV collagen	COL4A6	-	100%	33.3%
WBGene00001328	<i>epi-1</i>	laminin α -chain	LAMA5	72.20%	66.70%	100%
WBGene00002915	<i>let-805</i>	myotactin	FN1	66.70%	100%	22.20%
WBGene00003029	<i>lin-44</i>	Wnt signaling ligand	WNT2B/WNT3A/WNT8B	8%	50%	0%
WBGene00022743	<i>mlt-7</i>	heme peroxidase	EPX	22.20%	100%	100% L4
WBGene00003497	<i>mup-4</i>	transmembrane protein	MATN4	-	77.8%	11.1%
WBGene00016422	<i>noah-1</i>	PAN and ZP domain-containing	-	61.1%	100%	33%
WBGene00009926	<i>noah-2</i>	PAN and ZP domain-containing	-	44.4%	100%	100%
WBGene00003915	<i>pan-1</i>	leucine-rich repeats transmembrane	LRRTM4	11.1%	77.8%	0%
WBGene00004257	<i>pxn-2</i>	peroxidasin family	PXDN	55.60%	100%	100%

WBGene00020554	<i>T19A5.3</i>	-	-	22.2%	88.9%	33%
WBGene00019212	<i>zmp-2</i>	matrix metalloproteinase	MMP1/20/24	0%	100%	100% L4

Metabolism

WBGene00003906	<i>paf-1</i>	acetylglycerophosphocholine esterase	PAFAH2/PLA2G7	17%	100%	0%
WBGene00004978	<i>spg-7</i>	metalloprotease	AFG3L2	66.7%	100%	55.6%

Molting related

WBGene00022591	<i>cuti-1</i>	membrane tetraspan	-	55.60%	100%	66.7%
WBGene00022042	<i>icd-2</i>	NAC A\B domain superfamily	NACA	83.3%	91.7%	50.0%

Signaling

WBGene00000548	<i>clr-1</i>	tyrosine phosphatase	PTPRC	50%	88.90%	94.40%
WBGene00009921	<i>F52B5.2</i>	serine\threonine kinase	MOK	16.7%	33.3%	0%
WBGene00010776	<i>pix-1</i>	GTPase/kinase	ARHGEF6/ β -PIX	-	-	66.7%
WBGene00004210	<i>ptc-3</i>	sterol sensing domain/hedgehog receptor activity	PTCH1	66.7%	100%	0%
WBGene00004219	<i>ptr-4</i>	sterol sensing domain	PTCHD1	72.2%	100%	16.7%

Transcription factors

WBGene00009133	<i>bed-3</i>	zinc finger BED-type containing TF	ZBED1/4/6	-	-	0%
WBGene00001250	<i>elt-2</i>	GATA TF	GATA4/5	61.1%	100.0%	100.0%
WBGene00006652	<i>ttx-1</i>	OTD\OTX TF	OTX1	-	-	0%

Supplement Table 2: Short overview of *Pcol-144::GFP* RNAi screen hits at day 8 of adulthood.

Results on the right represent the average relative fluorescence in percentage from the last validation screening rounds. Results in red show a downregulation of *col-144* compared to control. Results in green show a upregulation of *col-144* compared to control.

Promoter_ *col-144::GFP* expression at day 8 of adulthood.

WormBase ID	Gene Name	Gene Type	Human Ortholog	Control (spe-9(hc88))	Long-lived (glp-1(e2142))	Long-lived (daf-2(e1370))
Control						
L4440	L4440			1.0%	17.7%	28.4%
GFP	GFP			0.0%	0.0%	0.0%
WBGene00000898	daf-2			72.2%	71.4%	70.8%
Adhesiosome						
WBGene00002135	<i>inx-13</i>	integral transmembrane channel	-	22.0%	25.0%	39.0%
WBGene00003934	<i>pat-10</i>	muscle troponin C	CABP2/4/7	0.0%	55.6%	55.6%
WBGene00003929	<i>pat-2</i>	α -integrin subunit	ITGA5/8	6.0%	50.0%	28.0%
WBGene00003931	<i>pat-4</i>	serine/threonine kinase	ILK	0.0%	39.0%	46.0%
WBGene00016197	<i>pxl-1</i>	paxillin	LPXN	0.0%	42.0%	28.0%
WBGene00006836	<i>unc-112</i>	pleckstrin homology domain	FERMT1/2	0.0%	44.0%	50.0%
WBGene00006824	<i>unc-95</i>	LIM domain-containing/paxilin	AL928654.3\; CRIP2/ZFHX4	22.0%	50.0%	22.0%
Autophagy						
WBGene00017045	<i>atg-13</i>	adaptor protein	ATG13	50.0%	17.0%	83.0%
WBGene00018294	<i>atg-18</i>	phosphatidylinositol phosphate binding activity	WIPI2	61.0%	39.0%	44.0%

WBGene00019748	<i>atg-2</i>	autophagosome assembly	ATG2A/B	33.0%	44.0%	56.0%
WBGene00021922	<i>atg-3</i>	ligase activity	ATG3	8.3%	0.0%	16.7%
WBGene00013595	<i>atg-4.1</i>	putative cysteine protease	ATG4A/B	0.0%	0.0%	22.2%
WBGene00010882	<i>atg-7</i>	E1 ubiquitin-activating-like enzyme	ATG7	25.0%	-	39.0%
WBGene00000247	<i>bec-1</i>	core subunit of the PI3K complex	BECN1	28.0%	44.0%	50.0%
WBGene00002980	<i>lgg-1</i>	GABA receptor binding activit	GABARAP/GABARAP	0.0%	-	0.0%
WBGene00002982	<i>lgg-3</i>	modifier protein	ATG12	11.1%	0.0%	27.8%
WBGene00006786	<i>unc-51</i>	serine\threonine kinase	ULK2	44.0%	33.0%	33.0%

Chaperone

WBGene00000802	<i>crt-1</i>	calreticulin	CALR	0.0%	22.2%	11.1%
----------------	--------------	--------------	------	------	-------	-------

Matrisome

WBGene00007170	<i>B0393.5</i>	calcium ion binding activity	SNED1	11.0%	17.0%	50.0%
WBGene00010460	<i>clcc-142</i>	c-type lectin-like domain	-	0.0%	16.7%	50.0%
WBGene00000690	<i>col-116</i>	cuticular collagen	SFTPD	38.9%	8.3%	16.7%
WBGene00000694	<i>col-120</i>	cuticular collagen	-	0.0%	0.0%	22.2%
WBGene00000695	<i>col-121</i>	cuticular collagen	-	0.0%	0.0%	16.7%
WBGene00000703	<i>col-129</i>	cuticular collagen	SFTPD	8.3%	8.3%	11.1%
WBGene00000602	<i>col-13</i>	cuticular collagen	-	-	100% (1)	-
WBGene00000721	<i>col-148</i>	cuticular collagen	SFTPD	0.0%	0.0%	22.2%
WBGene00000727	<i>col-154</i>	cuticular collagen	-	0.0%	16.7%	0.0%
WBGene00000731	<i>col-158</i>	cuticular collagen	COLQ	16.7%	0.0%	16.7%
WBGene00000733	<i>col-160</i>	cuticular collagen	-	0.0%	0.0%	27.8%
WBGene00000638	<i>col-62</i>	cuticular collagen	SFTPD	-	50.0%	0.0%
WBGene00000649	<i>col-73</i>	cuticular collagen	-	0.0%	11.1%	50.0%
WBGene00000597	<i>col-8</i>	cuticular collagen	SFTPD	0.0%	0.0%	22.2%

WBGene00000659	<i>col-84</i>	cuticular collagen	COLQ	56.0%	67%	-
WBGene00000673	<i>col-98</i>	cuticular collagen	-	0.0%	22.2%	55.6%
WBGene00001072	<i>dpy-10</i>	cuticular collagen	-	0.0%	0.0%	5.6%
WBGene00001066	<i>dpy-4</i>	cuticular collagen	-	0.0%	75.0%	72.2%
WBGene00001263	<i>emb-9</i>	α -chain type IV collagen	COL4A6	-	16.7%	0.0%
WBGene00001328	<i>epi-1</i>	laminin α -chain	LAMA5	0.0%	0.0%	11.1%
WBGene00017937	<i>F30H5.3</i>	endopeptidase inhibitor activity	AMBP/ LRP11/ SPINT1	0.0%	16.7%	50.0%
WBGene00016913	<i>lam-2</i>	laminin γ -chain	LAMC1	0.0%	0.0%	16.7%
WBGene00002273	<i>lec-10</i>	galectin	LGALS3	0.0%	16.7%	50.0%
WBGene00002265	<i>lec-2</i>	galectin	LGALS9	67.0%	58.0%	-
WBGene00002915	<i>let-805</i>	myotactin	FN1	27.8%	66.6% (1)	0% (1)
WBGene00003169	<i>mec-5</i>	nematode specific collagen	COL1A2	22.2%	8.3%	16.7%
WBGene00009671	<i>mfap-1</i>	microfibrillar-associated	MFAP1	5.6%	38.9%	5.6%
WBGene00003242	<i>mig-6</i>	papilin/lacunin-like	PAPLN	-	0.0%	38.9%
WBGene00003497	<i>mup-4</i>	transmembrane protein	MATN4	-	66.7%	0.0%
WBGene00003544	<i>nas-25</i>	astacin-like metalloprotease	-	0.0%	0.0%	16.7%
WBGene00003545	<i>nas-27</i>	astacin-like metalloprotease	-	67.0%	17.0%	17.0%
WBGene00003523	<i>nas-4</i>	astacin-like metalloprotease	ASTL	0.0%	16.7%	11.1%
WBGene00003528	<i>nas-9</i>	astacin-like metalloprotease	-	0.0%	0.0%	33.3%
WBGene00003588	<i>nex-1</i>	annexin	ANXA13	0.0%	16.7%	50.0%
WBGene00016422	<i>noah-1</i>	PAN and ZP domain-containing	-	33.0%	0.0%	0.0%
WBGene00009926	<i>noah-2</i>	PAN and ZP domain-containing	-	0.0%	0.0%	22.2%
WBGene00003915	<i>pan-1</i>	leucine-rich repeats transmembrane	LRRTM4	0.0%	50.0%	0.0%
WBGene00004257	<i>pxn-2</i>	peroxidasin family	PXDN	0.0%	16.7%	0.0%
WBGene00004889	<i>smp-1</i>	semaphorin	SEMA6A	0.0%	22.2%	50.0%
WBGene00006787	<i>unc-52</i>	perlecan	HSPG2	0.0%	0.0%	28.0%
WBGene00006947	<i>wrt-1</i>	hedgehog signaling	DHH/IHH/SHH	5.6%	16.7%	50.0%
WBGene00012782	<i>Y43C5A.2</i>	Fibrinogen C-terminal domain	-	0.0%	16.7%	55.6%
WBGene00021171	<i>Y8A9A.2</i>	ADAM metallopeptidase	ADAMTS3/13/16	0.0%	16.7%	50.0%

WBGene00019212	<i>zmp-2</i>	matrix metallopeptidase	MMP1/20/24	42.0%	33.0%	-
----------------	--------------	-------------------------	------------	-------	-------	---

Metabolism

WBGene00003906	<i>paf-1</i>	acetyl glycerophosphocholine esterase	PAFAH2/PLA2G7	-	6%	0.0%
WBGene00008205	<i>sams-1</i>	S-adenosyl methionine synthetase	MAT1A/ MAT2A	22.2%	16.7%	75.0%
WBGene00020258	<i>T05E7.1</i>	acyl-CoA hydrolase	ACOT1/4/BAAT	0.0%	16.67% (1)	50.0%
WBGene00007210	<i>agmo-1</i>	glyceryl-ether monooxygenase	AGMO	0.0%	5.6%	11.1%
WBGene00010425	<i>lpin-1</i>	phosphatidic acid phosphatase	LPIN1/3	-	-	0.0%
WBGene00004978	<i>spg-7</i>	metalloprotease	AFG3L2	0.0%	0.0%	0.0%
WBGene00020596	<i>oga-1</i>	N-acetyl-beta-D-glucosaminidase	OGA/MGEA5	-	11.1%	11.1%

Molting related

WBGene00022591	<i>cuti-1</i>	membrane tetraspan	-	0.0%	5.6%	8.3%
WBGene00001089	<i>dre-1</i>	ubiquitin-protein transferase	FBXO11/PRMT9	-	-	0.0%
WBGene00022042	<i>icd-2</i>	NAC A/B domain superfamily	NACA	0.0%	16.7%	0.0%
WBGene00015205	<i>moa-2</i>	-	SF3B5	17.0%	22.0%	50.0%

Pathogen related

WBGene00002187	<i>kgb-1</i>	serine/threonine kinase	MAPK10	25.0%	25.0%	17.0%
WBGene00077712	<i>nipi-4</i>	Pseudokinase		39.0%	17.0%	28.0%
WBGene00006578	<i>tli-1</i>	ubiquitin binding activity	TOLLIP	33.3%	5.6%	0.0%

Signaling

WBGene00016059	<i>hir-1</i>	transmembrane receptor tyrosine kinase	STYK1	0.0%	22.2%	11.1%
WBGene00000548	<i>clr-1</i>	tyrosine phosphatase	PTPRC	-	11.0%	5.6%
WBGene00022631	<i>nekl-2</i>	serine/threonine kinase	NEK8	5.6%	0.0%	0.0%
WBGene00009921	<i>F52B5.2</i>	serine/threonine kinase	MOK	0.0%	100.0%	0.0%

WBGene00001184	<i>egl-15</i>	fibroblast growth factor receptor	FGFR1/3/4	0.0%	16.7%	58.3%
WBGene00004219	<i>ptr-4</i>	sterol sensing domain	PTCHD1	-	50.0%	0.0%
WBGene00010556	<i>rack-1</i>	kinase C and ribosome binding	RACK1	11.0%	44.0%	61.0%
WBGene00002583	<i>let-363</i>	serine\threonine kinase	MTOR	0.0%	11.1%	0.0%
WBGene00001455	<i>flp-12</i>	neurotransmitter	-	0.0%	16.7%	58.3%

Trascription Factors

WBGene00014193	<i>nhr-247</i>	Nuclear Hormone Receptor	-	27.8%	44.4%	5.6%
WBGene00003847	<i>blmp-1</i>	TF	PRDM1	0.0%	27.8%	8.3%
WBGene00009133	<i>bed-3</i>	zinc finger BED-type containing TF	ZBED1/4/6	-	-	0.0%
WBGene00006652	<i>ttx-1</i>	OTD\OTX TF	OTX1	-	-	0.0%
WBGene00003015	<i>lin-29</i>	zinc finger TF	ZNF362	50.0%	16.7%	61.1%
WBGene00017535	<i>atf-8</i>	BZIP domain-containing TF	TEF	5.6%	16.7%	55.6%
WBGene00000912	<i>daf-16</i>	FOXO TF	FOXO1/3/4	0.0%	16.7%	5.6%
WBGene00004096	<i>pqm-1</i>	C2H2-type TF	-	0.0%	0.0%	22.2%
WBGene00006986	<i>zip-1</i>	TF	-	44.0%	22.0%	8.0%
WBGene00006959	<i>xbp-1</i>	bZIP TF	XBP1	0.0%	33.3%	5.6%

Supplement Table 3: Summary table of L4 screen of hit in the mechanotransduction model in *spe-9* mutants

The average was calculated from three rounds of screening. The fluorescence of the animals was graded on a scale from 0-3 in 0.5 steps

Pcol-144::GFP; spe-9

	Clone	Average	Median	%	SD	P-value: Wilcox (in R)
1	<i>nekl-2</i>	1.00	1.00	33.3%	12%	0.001578
2	<i>dpy-10</i>	0.89	1.00	29.6%	20%	0.03021
3	<i>col-120</i>	1.28	1.00	42.6%	17%	0.000514
4	<i>let-805</i>	0.50	0.50	16.7%	12%	0.4237
5	<i>noah-1</i>	0.78	1.00	25.9%	9%	0.009954
6	<i>emb-9</i>	0.22	0.00	7.4%	9%	0.2771
7	<i>mup-4</i>	0.17	0.00	5.6%	8%	0.1277
8	<i>vab-10</i>	0.56	0.50	18.5%	10%	0.2028
9	<i>unc-52</i>	0.67	0.50	22.2%	19%	0.2428
10	<i>tln-1</i>	1.17	1.00	38.9%	17%	0.003452
11	<i>epi-1</i>	0.56	0.50	18.5%	10%	0.2028
12	<i>lam-2</i>	0.78	1.00	25.9%	12%	0.01656
13	<i>unc-112</i>	0.61	0.50	20.4%	11%	0.1201
14	<i>unc-95</i>	0.83	1.00	27.8%	12%	0.009289
15	<i>spg-7</i>	0.67	0.50	22.2%	12%	0.06697
16	L4440	0.38	0.50	12.5%	11%	control

Supplement Table 4: Summary table of L4 screen of hit in the mechanotransduction model in *glp-1* mutants

The average was calculated from three rounds of screening. The fluorescence of the animals was graded on a scale from 0-3 in 0.5 steps

<i>Pcol-144::GFP; glp-1</i>					
Clone	Average	Median	%	STDEV	P-value: Wilcox (in R)
<i>nekl-2</i>	1.22	1.5	40.7%	22.2%	0.02374
<i>dpy-10</i>	1.00	1	33.3%	23.6%	0.2373
<i>col-120</i>	1.11	1	37.0%	16.2%	0.01991
<i>let-805</i>	1.11	1	37.0%	16.2%	0.01991
<i>noah-1</i>	1.00	1	33.3%	18.6%	0.1291
<i>emb-9</i>	0.56	0.5	18.5%	13.0%	0.7237
<i>mup-4</i>	0.33	0	11.1%	14.4%	0.09494
<i>vab-10</i>	0.61	0.5	20.4%	13.9%	0.7427
<i>unc-52</i>	0.72	0.5	24.1%	12.1%	0.7102
<i>tln-1</i>	0.83	1	27.8%	17.2%	0.2874
<i>epi-1</i>	0.72	0.5	24.1%	14.7%	0.6378
<i>lam-2</i>	0.78	1	25.9%	14.7%	0.3719
<i>unc-112</i>	1.39	1.5	46.3%	27.4%	0.0279
<i>unc-95</i>	0.72	0.5	24.1%	14.7%	0.6378
<i>spg-7</i>	0.72	0.5	24.1%	14.7%	0.6378
L4440	0.63	0.5	20.8%	11.1%	control

9. Curriculum vitae

Name: Alina Teuscher
Date of birth: 09.06.1991
in Bergisch-Gladbach
email: alincaro@web.de
phone: +41 78 657 58 59



Education

September 2016 – exp. Januar 2021

Doctorate in molecular biology and genetics of aging

Ewald lab, Department of Health Sciences and Technology, ETH Zurich, Switzerland

April 2014 - August 2016

Master in Biological Science

Faculty of Mathematics and Natural Sciences University of Cologne, Germany. Major: Genetics and Cell Biology. Master thesis: Remote hypoxia signalling in *C. elegans* (Kidney Research Center)

October 2010 – October 2013

Bachelor of Science in Biology, Faculty of Mathematics and Natural Sciences University of Cologne, Germany. Thesis: Analyses of Signals in Ossification of the Axial and the Head Skeleton in *Danio rerio* (Hammerschmidt lab)

Work experience

August 2015 – September. 2015

Research assistant, Max Planck Institute of plant breeding research, Cologne, Germany. AG Soppe, Project: Monitoring protein redox state in *Arabidopsis thaliana*

November 2013 – February 2014

Research assistant, Institute for Developmental Biology, University of Cologne, Germany. AG Hammerschmidt, Project: Analysis of pathways involved in ossification in *Danio rerio*

Internships

October 2015 - November 2015

Internship (during Master), Cluster of Excellence in Cellular Stress Response in Aging-associated Diseases, University of Cologne, Germany. Project: Expression analysis of candidate genes in *C. elegans*' response to stress

June 2015 – July. 2015

Internship (during Master), Max Planck Institute of plant breeding research, Cologne, Germany. Soppe lab, Project: Monitoring protein redox state in *Arabidopsis thaliana*

April 2015 – Mai 2015

Internship (during Master), Max Planck Institute of plant breeding research, Cologne, Germany. Coupland lab, Project: Generation of mutants in *Arabidopsis thaliana* and *Arabis alpine* using the CRISPR/Cas system

June 2014 – July 2014

Internship (during Master), Cluster of Excellence in Cellular Stress Response in Aging-associated Diseases, Kidney Research Center Cologne, Germany.
Project: Protein glutathionylation induced by ROS (in cell culture)

March 2012 – April 2012

Internship (during Bachelor), Life & Medical Sciences Institute for Developmental Biology, University of Bonn, Germany.
Hoch lab, Project: Chitinases in the development of trachea in *Drosophila melanogaster*

Research skills

Molecular Biology

- CRISPR/Cas9 in *Arabidopsis thaliana*
- Immunofluorescence staining, *in situ* hybridisation (fluorescent and non- fluorescent)
- PCR, RT-qPCR, cloning, genotyping, sequencing, DNA/RNA extraction

Microscopy

- Confocal laser scanning microscopy
- Epifluorescence Microscopy

Proteomics

- Western blots

Microbiology

- Transformation of bacteria with plasmids
- Standard culturing and maintenance (OP50, PA14)

Nematode-related work

- All basic methods for nematodes' maintenance and culturing
- Functional genetic analysis with mutants and RNAi
- Generation of transgenic worms via micro-injection
- Survival assays under different stress conditions

Language skills

German	Native language
English	Very good knowledge

EDP skills

Office	Good knowledge in Microsoft Excel, Word and PowerPoint
Fuji/ImageJ	Good knowledge

Hobbies

Violin
Board Games and Escape Rooms

References

Prof. Dr. Collin Y. Ewald (Doctoral Thesis Supervisor)
Institute of Translational Medicine, Schorenstr. 16, 8603, Switzerland
Phone: +41 44 655 74 07
Email: collin-ewald@ethz.ch

PD Dr. Roman-Ulrich Müller (Master Thesis Supervisor)
Klinik II für Innere Medizin, Kerpener Str. 62, 50937 Cologne, Germany
Phone: +49 221 478 84449
Email: roman-ulrich.mueller@uk-koeln.de

Prof. Dr. Matthias Hammerschmidt (Bachelor Thesis Supervisor)
Cologne Biocenter, Zülpicher Str. 47b, D-50674 Cologne
Phone: +49 221-470-5665
Email: mhammers@uni-koeln.de